UNIVERSITÀ
DI PARMA

UNIVERSITA' DEGLI STUDI DI PARMA

DOTTORATO DI RICERCA IN

Scienze Chimiche

CICLO XXXVI

Advances in Organometallic Chemistry: from Ligand Design to Cascade Reactivity

Coordinatore: Chiar.ma Prof. Bacchi Alessia

Tutore: Prof. Giovanni Maestri

Dottorando: Ruggeri Davide

Anni Accademici 2020/2021 – 2022/2023

Index

Diastereoselective Synthesis of Tetrahydropyranes via Ag(I) initiated dimerization of Cinnamyl Ethers

From this chapter:

Davide Ruggeri, Elena Motti, Nicola Della Ca', Giovanni Maestri, Org. Biomol. Chem., 2022,20, 9287-9291, DOI: https://doi.org/10.1039/D2OB01876D

1.1 Introduction: Recent developments of Silver catalysis in organic synthesis

The conventional belief held for a long time was that silver, among various transition metals, had limited utility as a catalyst in synthetic transformations. However, this perspective has evolved significantly over the past two decades. Today, silver catalysts stand as a formidable tool in organic chemistry, thanks to their remarkable efficiency and versatility.[1]

This progression has been driven by several factors. Silver's tendency to engage in various coordination modes and its exceptional catalytic efficiency have been pivotal. Additionally, the ecological and economic advantages of silver catalysts have further fuelled their adoption. In fact, compared to other transition metals, silver is non-toxic, relatively more abundant and inexpensive, making it an attractive option for sustainable and cost-efficient chemical synthesis.

A quick overview on some of the most interesting silver catalysis applications in the last decade is reported hereafter. Song and Li recently reviewed the literature regarding silver-mediated intermolecular radical 1,2-difunctionalization of alkenes[2]. These transformations are generally initiated by different radicals, such as carbon-, oxygen-, sulfur-, phosphinyl-, and halogen-center radicals, and terminated with nucleophiles to form two new bonds in a single reaction. In the context of alkenes di-functionalization, Ag(I) salts are particularly efficient catalysts due to their ability to mediate the formation of a radical, which then adds across the C=C bond of alkenes. Afterwards, the sequential single electron oxidation/nucleophilic attack lead to a cascade in which two functional groups are incorporated and two new bonds are simultaneously formed, giving the functionalized product.

Anilkumar instead reviewed various silver catalyzed methods for the synthesis of six-membered heterocyclic scaffolds[3]. The mechanism involves the initial coordination of silver to the substrate, followed by a 6-endo-dig cyclization yielding the desired products. For example, various α-aminopyrones and iminoisocoumarins were synthesized by treatment of *o*-(1-Alkynyl)benzamides and and (*Z*)-Alk-2-en-4-ynamides with 5 mol% of AgOTf in 1,2-dichloroethane under nitrogen atmosphere (Scheme 1).

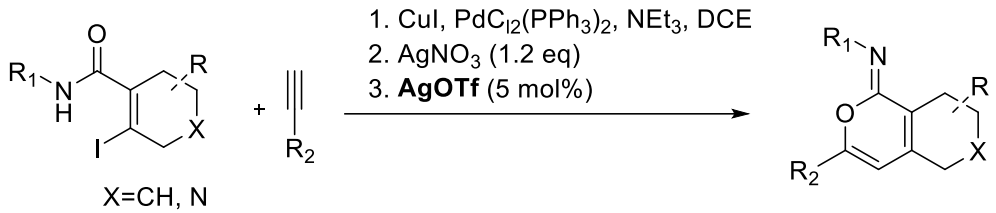

Scheme 1: Preparation of Iminoisocoumarins and α-iminopyrones via Sonogashira coupling and AgOTf-catalyzed 6-endo-dig cyclization.

Ma's group reported in 2020 the approach towards various Coumarin-Decorated Tetrazoles through a Silver catalyzed [3+2] cycloaddition (Scheme 2).[4] The reaction, which involves the coupling of aromatic diazonium salts with a specific aromatic diazo reagent is simple, scalable, efficient and regioselective. The combined use of silver salt and a base was found to be essential for the success of this transformation. The suggested mechanism consists of diazo activation to form a silver-diazo intermediate, cycloaddition with aryldiazonium species to give the cyclized intermediate, and release of silver catalyst to generate the final tetrazole.

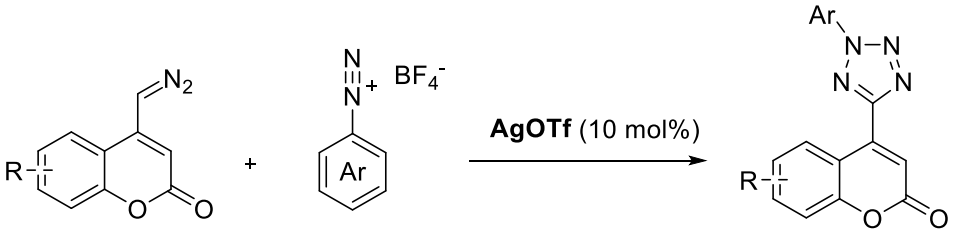

Scheme 2: Intermolecular cycloaddition reaction of coumarin-diazo reagents.

Jiang and Wu, on the other hand, recently reviewed the advances in Silver-Catalyzed Transformations of Electronically Unbiased Alkenes and Alkynes.[5] This study includes hydro-functionalizations, di-functionalizations, C-C and C-X formation through cross-coupling reactions, and, finally, cyclization protocols. One example of cyclization is that described in 2012 by Zhu and consists of a [4+2] cycloaddition reaction of 2-alkylbenzaldehydes with simple alkenes, providing diverse polysubstituted tetrahydronaphthols in excellent yields and high stereoselectivity (Scheme 3).[6]

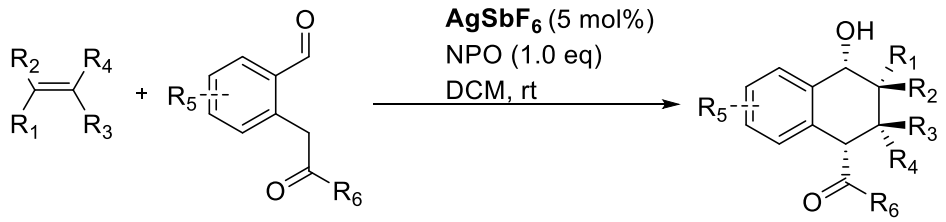

Scheme 3: [4+2] cycloaddition reaction of 2-alkylbenzaldehydes with simple alkenes.

Another example of Silver-catalyzed transformation of electronically unbiased alkenes or alkynes (specifically a C-C bond formation through cross-coupling) can be found in Wen's research work.[7] Indeed, in 2015, Wen and co-workers proposed the Silver-catalyzed Glaser coupling of alkynes. Using the homocoupling of phenylacetylene as model reaction, they found the reaction's optimal conditions to be: 5 mol% of $AgNO_3$, PPh_3, KOAc as the base and DMF as the solvent (Scheme 4).

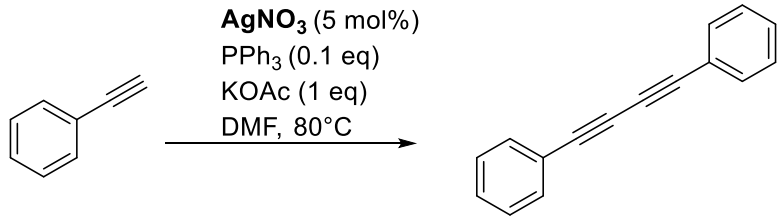

Scheme 4: Silver-catalyzed Glaser coupling of alkynes.

1.2 Introduction: Synthesis of tetrahydropyranes

The tetrahydropyrane unit (THP), sometimes referred to as oxane, is a widely recognized molecular framework, frequently encountered in nature, as well as in various synthetic drugs. Indeed, this chemical scaffold serves as a fundamental building block for a diverse range of pharmaceutical compounds. The tetrahydropyrane is a typical substructure for glycomimetics aiming to inhibit carbohydrate-protein interactions. Glycomimetics are synthetic compounds engineered to mimic the three-dimensional structure and functional groups of natural carbohydrates. Beside this application, Bryostatin, Eribulin and (+)-Neopeltolide are other examples of THP-containing pharmaceutically active compounds. These marine macrolides exhibit cytotoxicity against several cancer cell lines. Lasalocid instead is a potent and widespread antibacterial agent featuring the tetrahydropyrane building block. It is primarily used as a veterinary drug in the treatment of infections caused by Gram-positive bacteria, especially in poultry and livestock. Another instance in which the tetrahydropyrane unit can be found is Omarigliptin, a potent and highly selective dipeptidyl peptidase-4 (DPP-4) inhibitor, which is a class of drugs used in the treatment of type 2 diabetes mellitus. Finally, (-)-Centrolobine is a THP-containing alkaloid isolated in the amazon forest which exhibits antibiotic activity (Figure 1).[8–11]

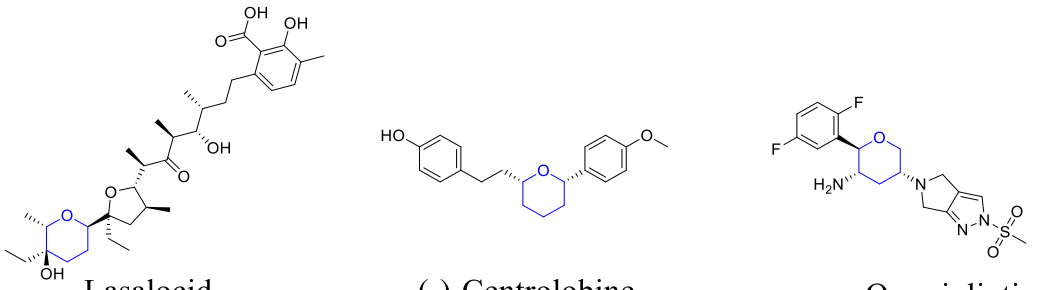

Figure 1: Chemical structure of some THP-containing drugs.

Due to their broad and at times impressive biological activity, the synthesis of these six-membered rings has attracted the attention of the scientific community in the last decades. The versatility of these substrates potentially allows for the introduction of various modifications, leading to the creation of structurally diverse analogs with possibly enhanced pharmacological properties. Indeed, researchers continually strive to develop efficient and sustainable synthetic routes to access these compounds and, at the same time, to resolve the intricate relationships between the structure and the function of these six-membered rings.

A first possible strategy for the synthesis of these building blocks involves the intramolecular addition of an alkene to an oxocarbenium ion. The Prins reaction and its variants are examples of this concept. This reaction offers a concise and selective method for constructing macrocyclic rings containing tetrahydropyran moieties of different sizes. The benefit of this approach lies in its ability to accommodate a wide range of functional groups within the macrocycle, while consistently achieving good to excellent yields. Interestingly, the concept of the Prins macrocyclization reaction was first reported back in 1979. However, it did not regain attention until 2008, when renewed interest and extensive exploration of its applications in organic synthesis took place. The mechanism involves the condensation of an alcohol onto an activated aldehyde to give an oxocarbenium intermediate. Then, this intermediate is attacked by the alkene to give a tetrahydropyranal carbocation. The resulting chair conformer has the hydrogen adjacent to the carbocation in a pseudo-axial position. For this reason, the empty p orbital is confined to the equatorial position, orientating the attack by the nucleophile to afford the THP product (Scheme 5). [12,13]

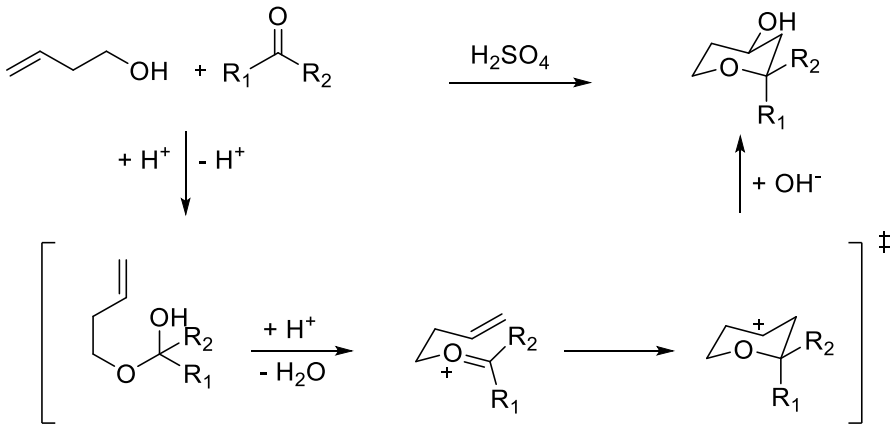

Scheme 5: Mechanism of the synthesis of THP rings by the Prins reaction.

Illustrious examples of THP formation via oxocarbenium ion can be observed in the Total Synthesis of (+)-Exiguolide described by Lee[14] and in the Total Synthesis of (-)-Apicularen A reported by Panek[15].

A second noteworthy chemical route for the synthesis of tetrahydropyranes is the well-known Hetero-Diels-Alder cycloaddition, which usually occurs with the assistance of a Lewis acid catalyst. An example of this reactivity is reported in the synthesis of cyto-toxic agent (+)-Neopeltolide by Dawson[16]. There, the THP ring within the macrocycle is synthesized through an oxa-Diels–Alder reaction between a silyloxydiene and an aldehyde, in the presence of a Cr(III) catalyst, with good diastereoselectivity (Scheme 6).

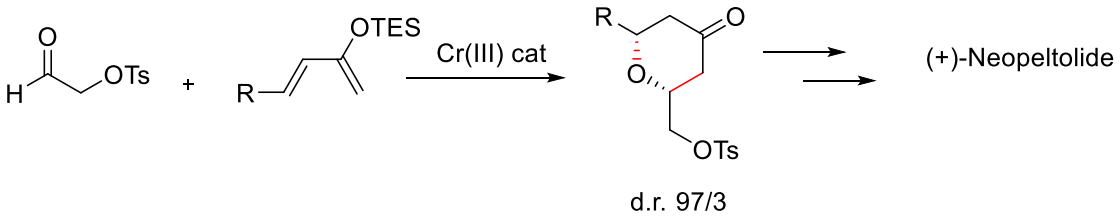

Scheme 6: Example of oxa-Diels–Alder reaction in the synthesis of THP ring for the preparation of (+)-Neopeltolide by Dawson Group.[16]

A third interesting alternative for the preparation of oxanes exploits Bismuth salts to catalyze the cross-coupling reaction of homoallyl alcohols with aldehydes, generating in this way poly-substituted tetrahydropyrans. Moreover, Bismuth tribromide catalyzes the reaction of δ-trialkylsilyloxy aldehydes and ketones, using various trialkylsilyl nucleophiles for the construction of cis- and trans-2,6-di- and trisubstituted tetrahydropyrans. The bismuth salt acts as a Brønsted acid source in the process. The hydrolysis of bismuth(III) bromide is known to afford two equivalents of hydrogen bromide and insoluble bismuth oxybromide: the former is responsible for the observed catalysis. (Scheme 7)[17]

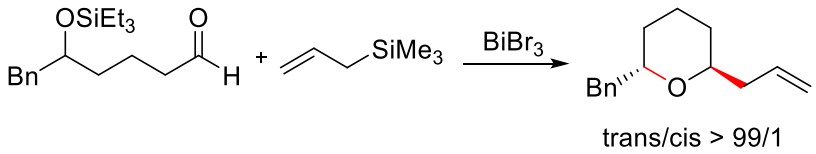

Scheme 7: Example of $BiBr_3$ catalyzed preparation of di-substituted tetrahydropyranes.[17]

Another possibility consists in the notorious ring-closing metathesis process (RCM).[18] RCM is a powerful and versatile chemical reaction, catalyzed by transition metals, which involves the rearrangement of two carbon-carbon double bonds within a molecule to form a new ring. One of the most representative examples of this synthetic route applied to the synthesis of oxanes can be found in the Total Synthesis of (+)-Neopeltolide by Fuwa and Sasaki (Scheme 8).[11]

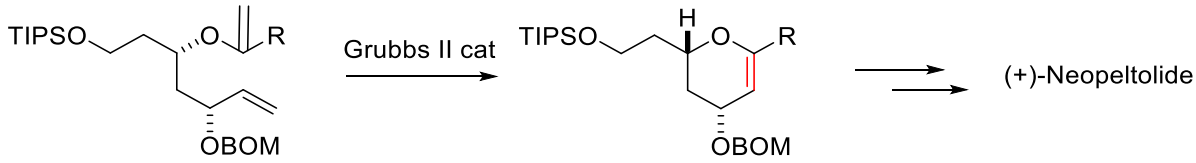

Scheme 8: Example of RCM in the synthesis of THP ring for the preparation of (+)-Neopeltolide by Sasaki Group.[11]

The oxa-Michael Reaction is a valid alternative for the formation of THP rings. Addition reactions of oxygen nucleophiles to acceptor conjugated systems have received few attention from the scientific community compared to the addition of carbon nucleophiles. However, in

the last two decades, there has been a remarkable increase in publications focusing on the development of the method as well as on applications to natural product synthesis.[19] In 2010 Menche's group reported a novel route for the synthesis of substituted tetrahydropyrans based on a three-step sequential process involving an oxa-Michael addition and a Tsuji–Trost coupling (Scheme 9).[20]

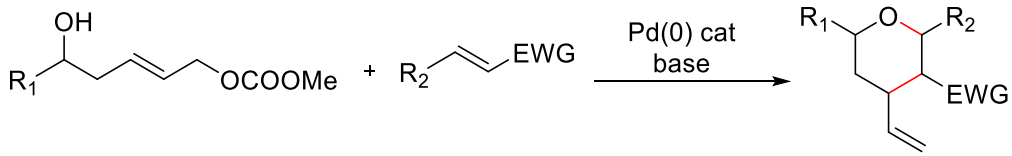

Scheme 9: Example of Oxa-Michael Reaction for the synthesis of THP ring.

Before concluding this overview on the synthesis of oxanes, it is worth to mention the intramolecular alkoxy-carbonylation of hydroxy alkenes promoted by Pd(II). The addition of the hydroxy group on the alkene lead to an alkyl-palladium intermediate which undergoes CO insertion and cleavage with MeOH. The cis-2,6 arrangement of the substituents on the tetrahydropyran product has been rationalized with a pseudo-chair conformation of the hydroxy-alkene while approaching the transition state for nucleophilic addition (Scheme 10).[21]

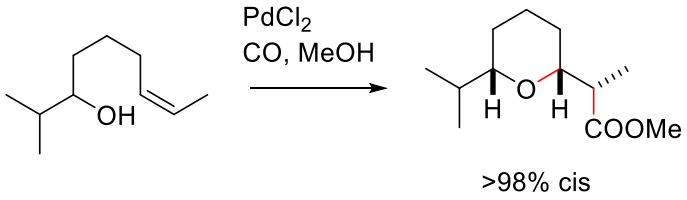

Scheme 10: Example of intramolecular alkoxy-carbonylation of hydroxy alkenes for the synthesis of THP ring.[21]

1.3 Results and Discussion

In this chapter I will present an unprecedent approach for the synthesis of substituted tetrahydropyrans, initiated by Silver (I) salts. The reaction involves the dimerization of readily available cinnamyl ethers, leading to the formation of sophisticated tetrahydropyran rings. This transformation is particularly significant because it involves the creation of three new covalent bonds and the establishment of four stereocenters, as illustrated in Scheme 11. In this study, we have unlocked a novel and efficient pathway for the construction of THP-containing compounds with a high degree of stereocontrol. These tetrahydropyranes hold great promise as key building blocks for the preparation of bioactive molecules, natural product analogues and potential pharmaceutical candidates.

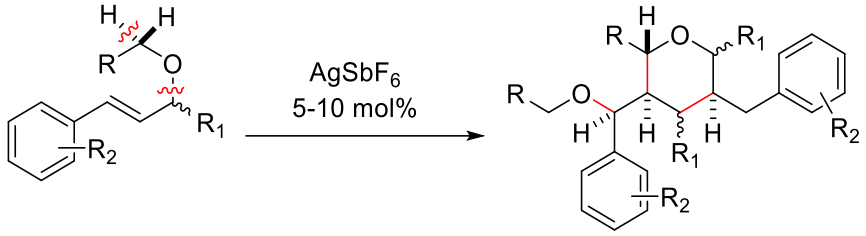

Scheme 11: General scheme of the developed dimerization cascade of cinnamyl ethers.

The method involves a C(sp^3)-O bond cleavage followed by a C(sp^3)-H bond functionalization, which is an original reactivity in the field of Ag-promoted processes.[22–24] This reaction afforded us a class of polysubstituted tetrahydropyrans, with great diastereocontrol and moderate to good yields, using a catalytic loading of a silver(I) salt in an apolar, aprotic solvent.

The genesis of this work is a serendipitous discovery. In fact, as part of an ongoing interest on synthetic cascades,[25,26] we treated diendiyne **1** with a Ru-based catalytic system (originally developed by Mori)[27] and a Ag(I) salt and, unexpectedly, we observed the formation of macrocycle **2** (Scheme 12). After few additional experiments, we realized that the ruthenium catalyst was actually inert in the process and that the Ag(I) salt used to trigger the chloride abstraction was in fact the real active species for the conversion of **1** into **2**.

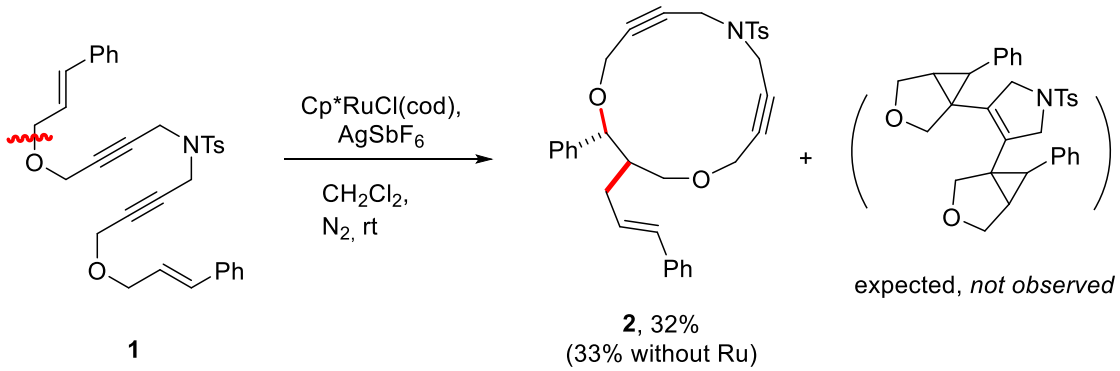

Scheme 12: The serendipitous discovery of the present reactivity.

Inspired by the formation of macrocycle **2**, which inevitably implies that an unexpected C(sp^3)-O bond cleavage took place, we decided to try to improve and expand this reactivity. However, during our optimization experiments, we noticed that significant substrate decomposition constantly occurred, preventing the formation of **2** with reasonable efficiency (maximum 33% yield). Therefore, we decided to take a step back and focus on better understanding the reactivity using a simpler substrate. This idea led us to investigate the behavior of the simpler cinnamyl ether **3a** as a model system, in order to gain insights into the underlying factors contributing to the observed C(sp^3)-O bond cleavage. Surprisingly, the reactivity of **3a** did not stop with the cleavage of the C-O bond, but led instead, through a subsequent C-H functionalization, to the formation of dimeric product **4a**. This surprising result pushed us to try the optimization of the newly observed reactivity (Table 1).

Table 1: Optimization of reaction conditions.

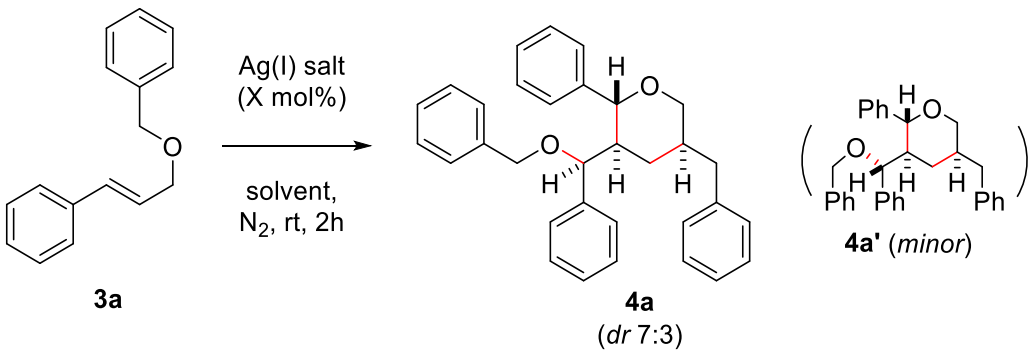

Entry[a]	Ag(I) salt (mol%)	Solvent	Yield of 4 [%]
1	$AgSbF_6$ (10)	CH_2Cl_2	46

2	$AgNTf_2$ (10)	CH_2Cl_2	31
3[b]	$AgBF_4$ (10)	CH_2Cl_2	--
4[b]	$AgNO_3$ (10)	CH_2Cl_2	--
5[b]	AgOTf (10)	CH_2Cl_2	--
6	$AgSbF_6$ (10)	DCE	48
7	$AgSbF_6$ (10)	CH_3Cl	--
8	$AgSbF_6$ (10)	C_7H_8	27
9[b]	$AgSbF_6$ (10)	THF	--
10[b]	$AgSbF_6$ (10)	EtOAc	--
11	$AgSbF_6$ (5)	CH_2Cl_2	60
12	$Sc(OTf)_3$ (20)	CH_2Cl_2	--
13	$AlCl_3$ (100)	CH_2Cl_2	22
14	$Cu(OTf)_2$ (10)	CH_2Cl_2	--
15	JohnPhos-Au(MeCN)SbF_6 (5)	CH_2Cl_2	36

[a] Reaction conditions: 0.3 mmol of 3a, 4 mL of solvent, N_2 atmosphere, r.t., 2h; [b] no conversion by TLC; isolated yields.

We conducted experiments with various silver salts (as shown in Table 1) and we observed that only weakly coordinating anions, such as SbF_6^- and NTf_2^-, were tolerated. Interestingly, no formation of **4a** was observed when using Ag(I) salts with more coordinating anions, such as TfO^-, NO_3^-, and BF_4^-. Among the solvents tested, dichloromethane and dichloroethane (DCE) yielded the best results, with CH_2Cl_2 being preferred due to its lower toxicity and environmental impact. On the contrary, chloroform did not lead to any reaction, likely because traces of hydrochloric acid deactivated the silver salt by forming insoluble AgCl. In addition to strongly coordinating anions, coordinating solvents were also found to inhibit the reactivity, possibly due to the interaction with Ag(I), making it unable to activate the substrate through interaction with its ethereal oxygen.

To further investigate this hypothesis, we poisoned the reactivity by adding acetonitrile (ACN), a strongly coordinating molecule. As expected, the reaction rate decreased with the

addition of 10 mol% of ACN (resulting in a 39% yield after 24 hours), and larger amounts of ACN completely inhibited the process. Similarly, the addition of ligands, such as tertiary phosphines, phosphites, or *N*-heterocyclic carbenes, inhibited the conversion of **4a**.

Both heating and cooling the system did not lead to significant improvements, and the reaction was therefore performed at room temperature. In the same way, varying the substrate dilution did not alter the outcome of the reaction significantly: a concentration of 0.1M was chosen as standard condition.

After that, we tested several different Lewis acids to explore their potential to promote substrate dimerization. For example, when using 1 equiv. of $AlCl_3$, product **4a** formed in low yield (22%), accompanied by extensive substrate decomposition. Additionally, various species based on transition metals, such as Ti(IV), Fe(III), and Sc(III) derivatives, proved ineffective in promoting the desired reaction. No traces of the target compound were observed in the presence of Cu(I) and Cu(II) Lewis acids (CuCl, CuI, and Cu(OTf)(C_7H_8)). Cationic Au(I) complexes instead successfully promoted the formation of **4a**. The best result was obtained using Echavarren's catalyst JohnPhos Au(MeCN)SbF_6 (36% yield), which, nevertheless, proved to be less performing than the appropriate Ag(I) salt.

The resulting product is obtained as a mixture of two diastereoisomers in a 7:3 ratio. This result reveals a significant degree of stereocontrol in the dimerization process, considering the presence of four stereocenters within the product. Unfortunately, the viscous nature of compounds **4** posed insurmountable challenges in growing suitable crystals for X-ray diffraction analysis. For this reason, the determination of the relative configuration of the four stereocenters was achieved through extensive NMR correlation experiments (among which the NOESY experiment reported in Figure 2). The red circle indicate the spatial relationship between proton H_B and H_C, which point to the same quadrant. Violet and Green circles instead show the 3D proximity of protons H_G and $H_{G'}$ with H_D and H_A respectively. All this information, taken together, confirms the assignment of the proposed diastereoisomer.

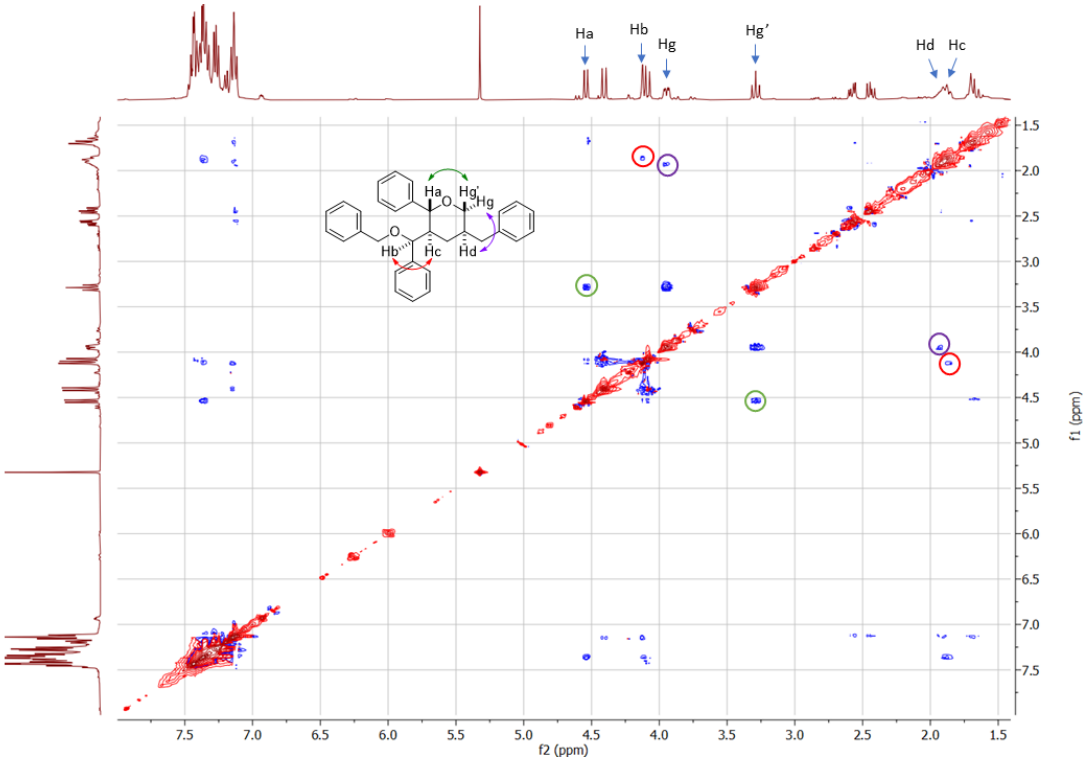

Figure 2: NOESY NMR experiment (400 MHz, $CDCl_3$), 4a, Cross peaks indicating the interaction between spatially close protons are circled with different colours.

Once we concluded the optimization of the reaction, our focus shifted to the investigation of the scope and limitations of the reaction, as reported in Figure 3. Substituting the benzyl arm of the model substrate with an alkyl chain resulted in comparable yields of the corresponding products (**4a-b**, 73% and 65%, respectively) with a high degree of diastereocontrol (dr > 8:2). Introducing a 4-methylbenzyl arm did not significantly affect the diastereoselectivity (dr = 86:14), although it led to a considerable increase in decomposition, yielding **4d** in 26%. Improved results were achieved using a 4-chloro substituent on the aryl group of the cinnamyl arm (**4e**, 60%). On the other hand, utilizing substrate **3f**, which features the same unsaturated arm combined with a propyl chain, we observed a better diastereoselectivity, associated with a lower yield (38%). On the contrary, a substrate with a donating group on the cinnamyl arm displayed higher efficacy when coupled with an alkyl chain rather than a benzyl side unit (**4g-h**, 22% and 52%, respectively). The synthetically valuable C(sp^3)-Br function was successfully incorporated into both ether fragments, yielding dibrominated tetrahydropyrane products (**4i-j**, 38% and 60%, respectively). Substituents on the allylic position were tolerated by the reaction. The reaction of racemic substrate **3k**

yielded a mixture of four main diastereoisomers of **4k**, which possess six contiguous stereocenters, achieving a moderate combined yield of 40%.

With regard to limitations of the method (Figure 3, unsuccessful substrates), substrates adorned with strongly electron-withdrawing groups, such as $-CF_3$, $-NO_2$, and -CN, did not undergo conversion under the current experimental conditions. A similar outcome was noted when functionalities capable of coordinating more strongly with the Ag^+ cation compared to the dialkyl ether were present. This included esters, other carbonyl-containing derivatives and amines. We attribute these limitations to the higher coordinating ability of these functional groups compared to dialkyl ethers, which might quench the Lewis acidity of the Ag(I) cation, thus impeding the pivotal substrate activation process. The disubstituted cinnamyl arm was also fundamental, as the utilization of distinct allyl fragments, including tri- and tetrasubstituted ones, proved to be ineffective. In these instances, extensive decomposition was readily observed via TLC. Additionally, employing a simple methyl group as substituent of the ether yielded no dimerization. This outcome potentially suggest that the C-H functionalization likely involves a cationic species, since this substrate would require a highly unstable primary cation intermediate, which, in fact, resulted in complete degradation.

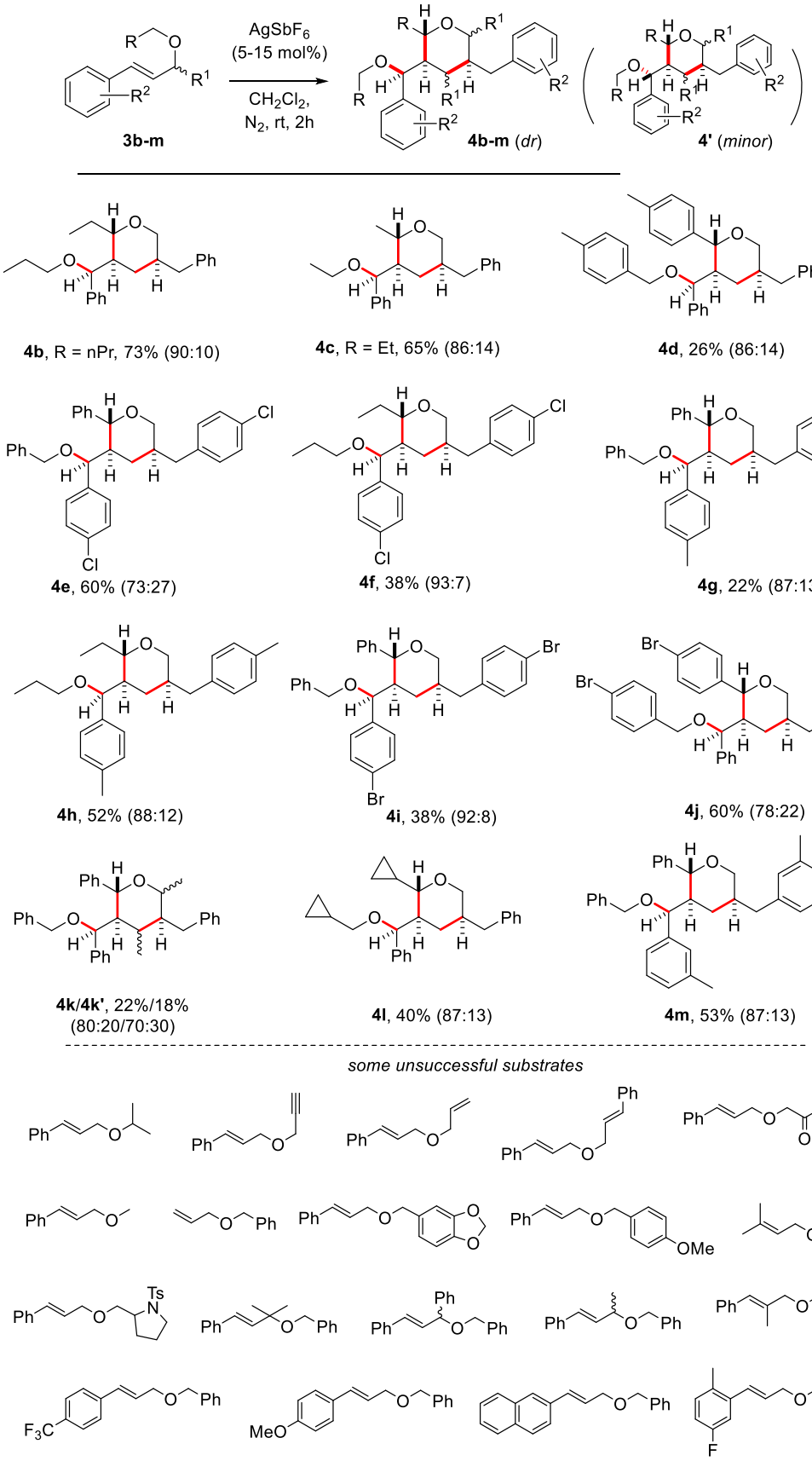

Figure 3: Scope and limitations of the reaction.

Then, to investigate the mechanistic nature of the C-H functionalization step, we designed a substrate featuring an α-cyclopropyl ring, **3l**. Interestingly, no ring opening products were observed treating **3l** with standard conditions, but compound **4l** was isolated in 40% yield, with satisfactory diastereocontrol (Figure 3). This outcome confirmed that the C-H functionalization proceeds via a closed shell mechanism rather than a radical mechanism, since cyclopropylmethyl radicals would undergo a very rapid ring opening rearrangement in order to relieve the ring strain (Scheme 13).[28]

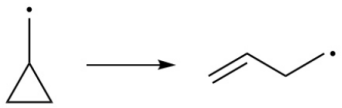

Scheme 13: Cyclopropyl radical opening.

Hypothesizing that the reaction might involve cationic species, we synthesized compound **3m**, which features a methyl substituent in the meta-position of the aryl ring. This arrangement results in a decreased donating ability, leading to a reduced electronic density on the alkene in comparison to compound **3g**. When subjected to the catalytic reaction, **3m** yielded product **4m** with a significantly improved yield (53%, Figure 3). This observation suggests that species that are excessively electron rich are more susceptible to decomposition under the current conditions. Subsequent research involving substrates with methoxy-substituted arenes consistently resulted in complete conversion and extensive decomposition within a matter of minutes.

Likely, the apolar solvent, which enhances the Lewis acidic character of the Ag(I) catalyst, appears to be unable to stabilize cationic intermediates. Consequently, these highly reactive intermediates are incapable to undergo selective dimerization. This deduction aligns with the notion that the solvent's polarity plays a crucial role in influencing the behavior of cationic reaction intermediates and consequently impacting the reaction's outcome.

The experiments depicted in Figure 3 were conducted utilizing 5 mol% of Ag(I) catalyst, with the sole exception being substrates featuring halogen substituents (**3e-f-i-j**). For these particular cases, a higher quantity of silver salt, specifically 15 mol%, was necessary to achieve complete conversion of the substrate.

In order to gain insights into the mechanistic intricacies of this cascade reaction, we conducted the experiment using **d7-3a**, which featured a deuterated benzyl arm, as illustrated in Scheme 14. Product **d14-4a** was obtained in 58% yield, a result closely comparable to that of its unlabeled counterpart. The deuterium on the C(sp^3) that underwent the C-H functionalization was selectively retrieved on the benzyl fragment on the pyrane 5- position.

This observation led us to propose a rationale wherein the Ag^+ cation initiates substrate activation by cleaving the C-O bond, yielding silver alcolate **I** and cinnamyl cation **II**. The latter could then participate in an addition to the double bond of another substrate molecule in a regiocontrolled manner, culminating in the formation of benzylic cation **III**. A favorable 1,5-hydride shift would then pave the way for the formation of the more stable carbocation **IV**, which resonate with the corresponding oxonium form **IV'**. This rearrangement sets the stage for an intramolecular 6-exo-trig cyclization, which likely occurs in a highly diastereocontrolled fashion and ensures the creation of the second and the third stereocenters of the final product. Intermediate **V** can ultimately be quenched by **I**, releasing the product and regenerating the Lewis acid catalyst. However, this intermolecular step is accountable for the formation of the minor diastereoisomer of the product. This arises from the fact that the attack of the carbocation from its most hindered face cannot be entirely suppressed.

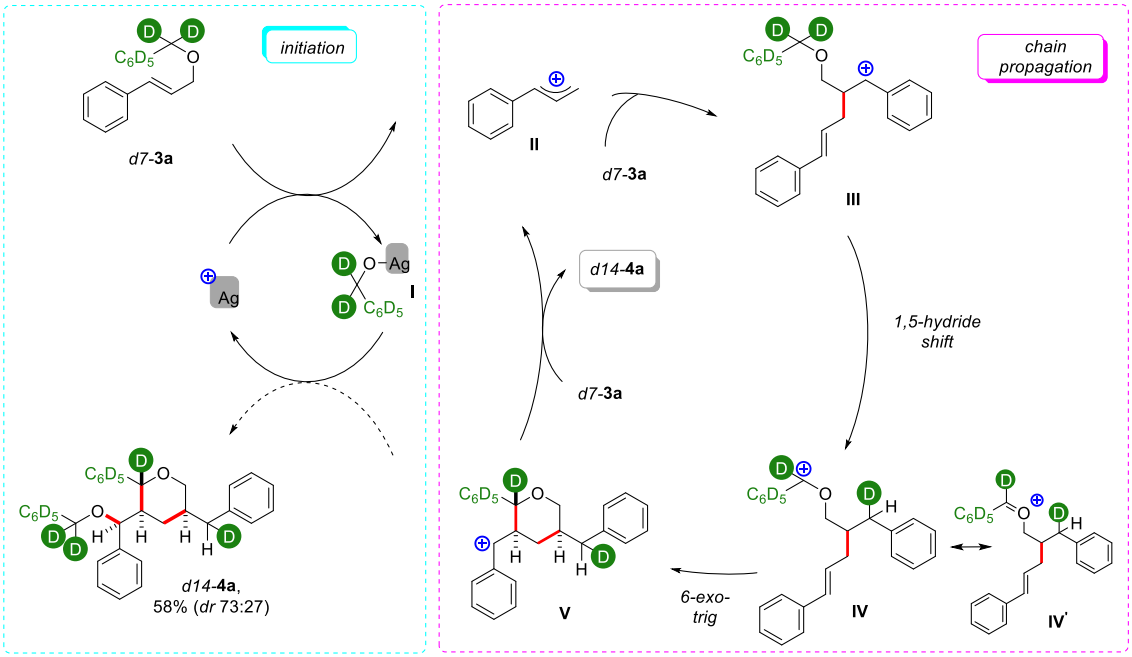

Scheme 14: Deuterium-labelling experiment and proposed mechanistic rationale.

In order to test these hypotheses, DFT modelling studies were carried out at the M06/Def2-svp level, using CH_2Cl_2 as implicit solvent. The reaction was tested on substrate **3c**. The investigation suggested that the most favourable route for product formation involves a cationic chain process as opposed to a catalytic cycle. These two pathways evenly overlap throughout their progression up to their conclusion. Indeed, the activation of the substrate could commence with the coordination of the Ag(I) cation, leading to the generation of the highly reactive cinnamyl cation **II**. This species could then evolve through a series of low-energy transition states (with delta energy ranging between +3.1 and +10.1 kcal/mol) to

culminate in intermediate **V.** The formation of this intermediate occurs with good diastereocontrol, likely to minimize the unfavorable syn-pentane-like strain within the corresponding transition state.

Despite many attempts to identify a convergent transition state for the reaction between **V** and **I**, no fruitful results were achieved. Yet, a significantly simpler route emerged. An additional molecule of the substrate could effectively engage with **V**, thereby generating oxonium cation **VI**. The latter could then readily release the product while regenerating **II**. In this context, the silver salt functions as the initiator of a cationic chain process, wherein the propagation step plays a pivotal role in the formation of the targeted product. The higher concentration in solution of **3** compared to **I** further suggests that the chain mechanism is likely faster than a purely catalytic one (Scheme 15).

It is worth noting that, in contrast to free-radical chains which are well-established, ionic ones are underdeveloped, but are increasingly captivating the attention of synthetic chemists.

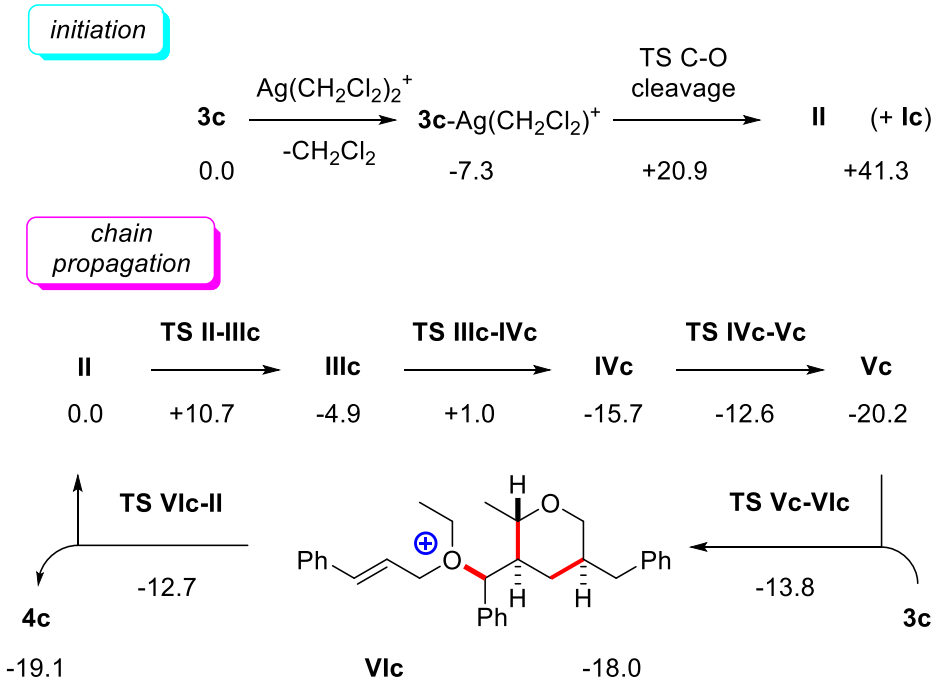

M06/Def2-svp, CPCM =CH_2Cl_2, ΔG values @ 298.15 K

Scheme 15: DFT modelling studies.

This rationale is able to explain the unselective reactions observed using substrates with a tri- or tetra-substituted alkene group, as discussed above. In these instances, the initial cleavage of the C(sp^3)-O bond is facilitated due to the higher stability of the corresponding

carbocation. However, the enhanced steric hindrance around the C-C double bond blocks the intermolecular step of the cascade, ultimately leading to the experimentally observed extensive decomposition of the starting material.

While the use of a more polar solvent could potentially moderate the reactivity of cationic intermediates, such an option is precluded in the current scenario because the heteroatoms within the solvent would likely quench the essential Lewis acidity of the Ag(I) catalyst, as indicated in Table 1. Moreover, the presence of strongly nucleophilic functions would most likely hinder the smooth propagation of the cationic chain itself.

1.4 Conclusions

In summary, we have introduced a novel cascade reaction initiated by Ag(I) that pivots on the cleavage of a C(sp^3)-O bond. This reactivity showcases an exciting potential, as it offers the possibility to generate either functionally enriched macrocycles or, following an additional C(sp^3)-H functionalization, decorated tetrahydropyrans. Insights into the mechanistic intricacies of this sequence indicate that the Lewis acid salt can initiate this cationic chain process.

Our findings represent a significant advancement in the field of tetrahydropyran synthesis and highlight the potential of Silver(I)-initiated reactions in promoting complex transformations with remarkable efficiency and stereocontrol.

This work opens up exciting opportunities for further investigations and applications of this novel synthetic strategy in organic synthesis and drug discovery.

1.4 Experimental Section

General Remarks

All chemicals were purchased from commercial sources and used as received. Solvents were dried passing through alumina columns using an Inert® system and were stored under nitrogen. Chromatographic purifications were performed under gradient or isocratic regimes using a Combiflash system and prepacked disposable silica cartridges. ^{1}H NMR and ^{13}C NMR spectra were recorded at 300 K on Bruker 400 MHz spectrometer using the solvent as internal standard (7.26 ppm for ^{1}H NMR and 77.00 ppm for ^{13}CNMR for $CDCl_3$). Reported assignments are based on decoupling, COSY, NOESY, HSQC, and HMBC correlation experiments. The terms m, s, d, t, q, and quint represent multiplet, singlet, doublet, triplet, quadruplet, and quintuplet, respectively, and the term br means a broad signal. Exact masses were recorded on an LTQ ORBITRAP XL Thermo Mass Spectrometer (electrospray source). Cinnamyl ethers **3a**-**m** were synthesized according to literature procedures.[29–32] Spectroscopic data of **3a-c**,**e**,**g**,**i-l** correspond to those described in the literature. Calculations were performed at the DFT level using Gaussian16 as described in the published paper.[33]

Synthesis of substrates

Synthesis of Diendiyne 1

To a stirred solution of 4-methylbenzenesulfonamide (260 mg, 1.52 mmol, 1 eq.) in acetone (16 mL) was added (E)-(3-((4-bromobut-2-yn-1-yl)oxy)prop-1-en-1-yl)benzene (807 mg, 3.04 mmol, 2.0 eq.) and K_2CO_3 (630 mg, 4.56 mmol, 3.0 eq.). The reaction mixture was stirred overnight under reflux. The mixture was quenched by addition of water and extracted with ethyl acetate. The combined organic layers were dried over anhydrous Na_2SO_4 and concentrated under reduced pressure. The crude was purified by column chromatography on silica gel (*n*-hexane/ EtOAc, gradient).

General Procedure I for the Synthesis of Cynnamyl Ethers 3a-b, j

A solution of cinnamyl alcohol (387 μL, 3 mmol, 1 equiv) in THF (5 mL) was added to a suspension of NaH (60% in mineral oil, 160 mg, 4 mmol, 1.3 equiv) in THF (10 mL). The resulting mixture was stirred for 30 min prior to the addition of the corresponding halide (4 mmol, 1.3 equiv). The mixture was then stirred at r.T. overnight. After completion, the reaction was quenched with NH_4Cl acqueous solution. The mixture was extracted with diethyl ether. The combined organic layers were washed with brine, dried over Na_2SO_4, and concentrated under reduced pressure. The resulting crude was purified by chromatography on silica gel (*n*-hexane/ EtOAc, gradient).

General Procedure II for the Synthesis of Cynnamyl Ethers 3c-d, l

A solution of the desired alcohol (2.6 mmol, 1 equiv) in THF (4 mL) was added to a suspension of NaH (60% in mineral oil, 136 mg, 3.4 mmol, 1.3 equiv) in THF (8 mL). The resulting mixture was stirred for 30 min prior to the addition of cinnamyl bromide (3.4 mmol, 1.3 equiv). The mixture was then stirred at r.T. overnight. After completion, the reaction was quenched with NH_4Cl acqueous solution. The mixture was extracted with diethyl ether. The combined organic layers were washed with brine, dried over Na_2SO_4, and concentrated under reduced pressure. The resulting crude was purified by chromatography on silica gel (*n*-hexane/ EtOAc, gradient).

General Procedure III for the Synthesis of Cynnamyl Ethers 3e, g, i, k, m

A solution of the desired alcohol (0.82 mmol, 1 equiv) in THF (4 mL) was added to a suspension of NaH (60% in mineral oil, 43 mg, 1.1 mmol, 1.3 equiv) in DMF (1 mL). The

resulting mixture was stirred for 30 min prior to the addition of benzyl bromide (0.96 mmol, 1.1 equiv). The mixture was then stirred at r.T. overnight. After completion, the reaction was quenched with NH_4Cl acqueous solution. The mixture was extracted with diethyl ether. The combined organic layers were washed with water and brine, dried over Na_2SO_4, and concentrated under reduced pressure. The resulting crude was purified by chromatography on silica gel (*n*-hexane/ EtOAc, gradient).

General Procedure IV for the Synthesis of Cynnamyl Ethers 3h, f

A solution of the desired alcohol (1.32 mmol, 1 equiv) in THF (4 mL) was added to a suspension of NaH (60% in mineral oil, 79 mg, 1.97 mmol, 1.5 equiv) in DMF (4 mL). The resulting mixture was stirred for 30 min prior to the addition of 1-iodo propane (335 mg, 1.97 mmol, 1.5 equiv). The mixture was then stirred at r.T. overnight. After completion, the reaction was quenched with NH_4Cl acqueous solution. The mixture was extracted with diethyl ether. The combined organic layers were washed with water and brine, dried over Na_2SO_4, and concentrated under reduced pressure. The resulting crude was purified by chromatography on silica gel (*n*-hexane/ EtOAc, gradient).

Carachterization of substrates

N,N-bis(4-(cinnamyloxy)but-2-yn-1-yl)-4-methylbenzenesulfonamide (1)

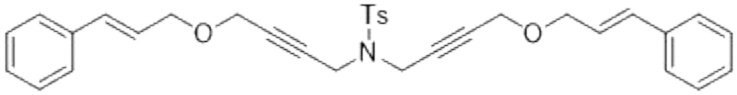

Diendiyne 1 was isolated (silica gel, *n*-hexane/EtOAc, gradient) as a transparent oil (552 mg, 1.02 mmol, 67%). The NMR data was consistent with previously reported spectra.[34] ^{1}H NMR (400 MHz, $CDCl_3$) δ 7.73 (d, J = 8.3 Hz, 2H), 7.40 – 7.23 (m, 12H), 6.59 (d, J = 16.0 Hz, 2H), 6.22 (dt, J = 15.9, 6.2 Hz, 2H), 4.24 – 4.21 (m, 4H), 4.10 (dd, J = 6.2, 1.4 Hz, 4H), 4.06 – 4.03 (m, 4H), 2.37 (s, 3H).

(E)-(3-(benzyloxy)prop-1-en-1-yl)benzene (3a)

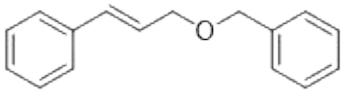

Following general procedure I, **3a** was isolated (silica gel, *n*-hexane/EtOAc, gradient) as a transparent oil (656 mg, 2.92 mmol, 78%). The NMR data was consistent with previously reported spectra.[32] ^{1}H NMR (400 MHz, $CDCl_3$) δ 7.42 – 7.36 (m, 6H), 7.36 – 7.30 (m, 3H), 7.27 – 7.22 (m, 1H), 6.64 (d, J = 15.9 Hz, 1H), 6.34 (dt, J = 15.9, 6.0 Hz, 1H), 4.59 (s, 2H), 4.21 (dd, J = 6.0, 1.5 Hz, 2H).

(E)-(3-propoxyprop-1-en-1-yl)benzene (3b)

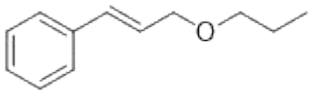

Following general procedure I, **3b** was isolated (silica gel, *n*-hexane/EtOAc, gradient) as a transparent oil (129 mg, 0.73 mmol, 33%). The NMR data was consistent with previously reported spectra.[31] ^{1}H NMR (400 MHz, $CDCl_3$) δ 7.42 – 7.37 (m, 2H), 7.34 – 7.29 (m, 2H), 7.27 – 7.21 (m, 1H), 6.61 (d, J = 15.9 Hz, 1H), 6.31 (dt, J = 15.9, 6.0 Hz, 1H), 4.14 (dd, J = 6.0, 1.5 Hz, 2H), 3.45 (t, J = 6.7 Hz, 2H), 1.71 – 1.58 (m, 2H), 0.95 (t, J = 7.4 Hz, 3H).

(E)-(3-ethoxyprop-1-en-1-yl)benzene (3c)

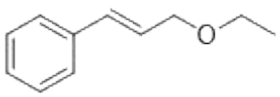

Following general procedure II, **3c** was isolated (silica gel, *n*-hexane/EtOAc, gradient) as a transparent oil (377 mg, 2.32 mmol, 70%). The NMR data was consistent with previously reported spectra.[30] ^{1}H NMR (400 MHz, $CDCl_3$) δ 7.42 – 7.37 (m, 2H), 7.34 – 7.29 (m, 2H), 7.26 – 7.21 (m, 1H), 6.61 (d, J = 15.9 Hz, 1H), 6.31 (dt, J = 15.9, 6.0 Hz, 1H), 4.15 (dd, J = 6.0, 1.5 Hz, 2H), 3.56 (q, J = 7.0 Hz, 2H), 1.25 (t, J = 7.0 Hz, 3H).

1-((cinnamyloxy)methyl)-4-methylbenzene) (3d)

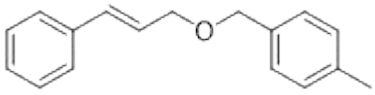

Following general procedure II, **3d** was isolated (silica gel, *n*-hexane/EtOAc, gradient) as a transparent oil (563 mg, 2.36 mmol, 91%). ^{1}H NMR (400 MHz, $CDCl_3$) δ 7.44 – 7.38 (m, 2H), 7.36 – 7.23 (m, 5H), 7.21 – 7.15 (m, 2H), 6.64 (d, J = 16.0 Hz, 1H), 6.34 (dt, J = 15.9, 6.0 Hz, 1H), 4.55 (s, 2H), 4.19 (dd, J = 6.0, 1.5 Hz, 2H), 2.37 (s, 3H). ^{13}C NMR (101 MHz, $CDCl_3$) δ 137.5 (Cq), 136.9 (Cq), 135.4 (Cq), 132.6 (CH), 129.2 (2CH), 128.7 (2CH), 128.1 (2CH), 127.8 (CH), 126.6 (2CH), 126.3 (CH), 72.2 (CH_2), 70.7 (CH_2), 21.3 (CH_3). (ESI)-HRMS calcd for $C_{17}H_{18}O$ $[M + Na]^+$ 261.1256, found 261.1249.

(E)-1-(3-(benzyloxy)prop-1-en-1-yl)-4-chlorobenzene (3e)

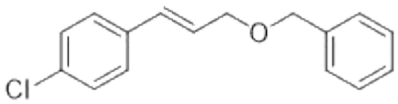

Following general procedure III, **3e** was isolated (silica gel, *n*-hexane/EtOAc, gradient) as a transparent oil (185 mg, 0.71 mmol, 87%). The NMR data was consistent with previously reported spectra.[29] ^{1}H NMR (400 MHz, $CDCl_3$) δ 7.39 – 7.34 (m, 4H), 7.33 – 7.26 (m, 5H), 6.59 (d, J = 15.9 Hz, 1H), 6.30 (dt, J = 15.9, 5.9 Hz, 1H), 4.58 (s, 2H), 4.19 (dd, J = 5.9, 1.5 Hz, 2H).

(E)-1-chloro-4-(3-propoxyprop-1-en-1-yl)benzene (3f)

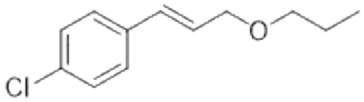

Following general procedure IV, **3f** was isolated (silica gel, *n*-hexane/EtOAc, gradient) as a transparent oil (105 mg, 0.50 mmol, 38%). ^{1}H NMR (400 MHz, $CDCl_3$) δ 7.36 – 7.22 (m, 4H), 6.56 (d, J = 15.9 Hz, 1H), 6.28 (dt, J = 15.9, 5.9 Hz, 1H), 4.12 (dd, J = 5.9, 1.5 Hz, 2H), 3.44 (t, J = 6.7 Hz, 2H), 1.64 (h, J = 7.2 Hz, 2H), 0.95 (t, J = 7.4 Hz, 3H). ^{13}C NMR (101

MHz, $CDCl_3$) δ 135.5 (Cq), 133.3 (Cq), 130.8 (CH), 128.8 (2CH), 127.8 (2CH), 127.3 (CH), 72.5 (CH_2), 71.3 (CH_2), 23.1 (CH_2), 10.8 (CH_3). (ESI)-HRMS calcd for $C_{12}H_{15}ClO$ $[M + Na]^+$ 233.0709, found 233.0711.

(E)-1-(3-(benzyloxy)prop-1-en-1-yl)-4-methylbenzene (3g)

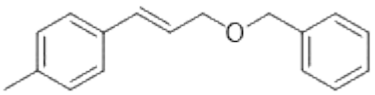

Following general procedure III, **3g** was isolated (silica gel, *n*-hexane/EtOAc, gradient) as a transparent oil (144 mg, 0.60 mmol, 90%). The NMR data was consistent with previously reported spectra.[29] ^{1}H NMR (400 MHz, $CDCl_3$) δ 7.40 – 7.32 (m, 4H), 7.33 – 7.28 (m, 3H), 7.14 (d, J = 7.9 Hz, 2H), 6.61 (d, J = 15.9 Hz, 1H), 6.29 (dt, J = 15.9, 6.1 Hz, 1H), 4.58 (s, 2H), 4.20 (dd, J = 6.2, 1.4 Hz, 2H), 2.35 (s, 3H).

(E)-1-methyl-4-(3-propoxyprop-1-en-1-yl)benzene (3h)

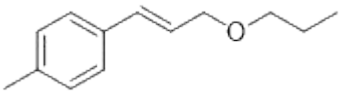

Following general procedure IV, **3h** was isolated (silica gel, *n*-hexane/EtOAc, gradient) as a transparent oil (53 mg, 0.28 mmol, 28%). ^{1}H NMR (400 MHz, $CDCl_3$) δ 7.31 (d, J = 8.2 Hz, 2H), 7.14 (d, J = 7.9 Hz, 2H), 6.60 (d, J = 15.9 Hz, 1H), 6.27 (dt, J = 15.9, 6.0 Hz, 1H), 4.15 (dd, J = 6.0, 1.5 Hz, 2H), 3.47 (t, J = 6.7 Hz, 2H), 2.36 (s, 3H), 1.74 – 1.60 (m, 2H), 0.99 (t, J = 7.4 Hz, 3H). ^{13}C NMR (101 MHz, $CDCl_3$) δ 137.4 (Cq), 134.3 (Cq), 132.1 (CH), 129.3 (2CH), 126.5 (2CH), 125.7 (CH), 72.2 (CH_2), 71.6 (CH_2), 23.1 (CH_2), 21.2 (CH_3), 10.7 (CH_3). (ESI)-HRMS calcd for $C_{13}H_{18}O$ $[M + Na]^+$ 213.1256, found 213.1250.

(E)-1-(3-(benzyloxy)prop-1-en-1-yl)-4-bromobenzene (3i)

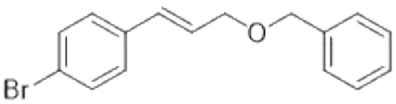

Following general procedure III, **3i** was isolated (silica gel, *n*-hexane/EtOAc, gradient) as a transparent oil (132 mg, 0.44 mmol, 87%). The NMR data was consistent with previously reported spectra.[29] ^{1}H NMR (400 MHz, $CDCl_3$) δ 7.44 (d, J = 8.5 Hz, 2H), 7.39 – 7.28 (m, 5H), 7.27 – 7.23 (m, 2H), 6.58 (d, J = 15.9 Hz, 1H), 6.32 (dt, J = 15.9, 5.9 Hz, 1H), 4.58 (s, 2H), 4.19 (dd, J = 5.9, 1.5 Hz, 2H).

1-bromo-4-((cinnamyloxy)methyl)benzene (3j)

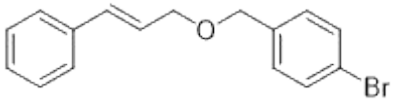

Following general procedure I, **3j** was isolated (silica gel, *n*-hexane/EtOAc, gradient) as a transparent oil (681 mg, 2.25 mmol, 75%). ^{1}H NMR (400 MHz, $CDCl_3$) δ 7.53 – 7.46 (m, 2H), 7.43 – 7.38 (m, 2H), 7.37 – 7.31 (m, 2H), 7.30 – 7.23 (m, 3H), 6.64 (d, J = 15.9 Hz, 1H), 6.33 (dt, J = 15.9, 6.0 Hz, 1H), 4.53 (s, 2H), 4.20 (dd, J = 6.1, 1.5 Hz, 2H). ^{13}C NMR (101 MHz, $CDCl_3$) δ 137.5 (Cq), 136.7 (Cq), 132.9 (CH), 131.6 (2CH), 129.5 (2CH), 128.7 (2CH), 127.9 (CH), 126.6 (2CH), 125.9 (CH), 121.6 (Cq), 71.5 (CH_2), 71.0 (CH_2). (ESI)-HRMS calcd for $C_{16}H_{15}BrO$ $[M + Na]^+$ 325.0204, found 325.0201.

(E)-(3-(benzyloxy)but-1-en-1-yl)benzene (3k)

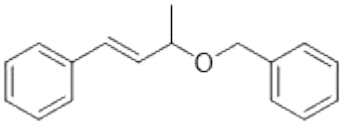

Following general procedure III, **3k** was isolated (silica gel, *n*-hexane/EtOAc, gradient) as a transparent oil (432 mg, 1.81 mmol, 60%). The NMR data was consistent with previously reported spectra.[29] ^{1}H NMR (400 MHz, $CDCl_3$) δ 7.44 – 7.40 (m, 2H), 7.39 – 7.32 (m, 6H), 7.31 – 7.24 (m, 2H), 6.56 (d, J = 16.0 Hz, 1H), 6.19 (dd, J = 15.9, 7.7 Hz, 1H), 4.63 (d, J = 11.9 Hz, 1H), 4.46 (d, J = 12.1 Hz, 1H), 4.12 (p, J = 6.4 Hz, 1H), 1.40 (d, J = 6.4 Hz, 3H).

(E)-(3-(cyclopropylmethoxy)prop-1-en-1-yl)benzene (3l)

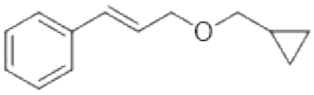

Following general procedure II, **3l** was isolated (silica gel, *n*-hexane/EtOAc, gradient) as a transparent oil (360 mg, 1.91 mmol, 64%). ^{1}H NMR (400 MHz, $CDCl_3$) δ 7.42 – 7.36 (m, 2H), 7.34 – 7.28 (m, 2H), 7.26 – 7.21 (m, 1H), 6.61 (d, J = 15.9 Hz, 1H), 6.31 (dt, J = 15.9, 6.1 Hz, 1H), 4.17 (dd, J = 6.1, 1.5 Hz, 2H), 3.33 (d, J = 6.9 Hz, 2H), 1.16 – 1.05 (m, 1H), 0.61 – 0.51 (m, 2H), 0.26 – 0.19 (m, 2H). ^{13}C NMR (101 MHz, $CDCl_3$) δ 136.9 (Cq), 132.4 (CH), 128.7 (2CH), 127.8 (CH), 126.6 (2CH), 126.5 (CH), 75.2 (CH_2), 71.3 (CH_2), 10.8 (CH), 3.2 ($2CH_2$). (ESI)-HRMS calcd for $C_{13}H_{16}O$ $[M + Na]^+$ 211.1100, found 211.1105.

(E)-1-(3-(benzyloxy)prop-1-en-1-yl)-3-methylbenzene (3m)

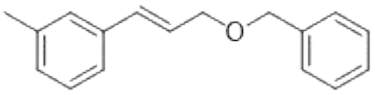

Following general procedure III, **3m** was isolated (silica gel, *n*-hexane/EtOAc, gradient) as a transparent oil (263 mg, 1.10 mmol, 89%). ^{1}H NMR (400 MHz, $CDCl_3$) δ 7.42 – 7.27 (m, 5H), 7.21 (dd, J = 4.7, 1.7 Hz, 3H), 7.11 – 7.04 (m, 1H), 6.61 (d, J = 15.9 Hz, 1H), 6.33 (dt, J = 15.9, 6.0 Hz, 1H), 4.58 (s, 2H), 4.21 (dd, J = 6.1, 1.5 Hz, 2H), 2.35 (s, 3H). ^{13}C NMR (101 MHz, $CDCl_3$) δ 138.4 (Cq), 138.2 (Cq), 136.8 (Cq), 132.8 (CH), 128.62 (CH), 128.59 (CH), 128.56 (2CH), 127.9 (2CH), 127.8 (CH), 127.4 (CH), 126.0 (CH), 123.8 (CH), 72.2 (CH_2), 70.9 (CH_2), 21.5 (CH_3). (ESI)-HRMS calcd for $C_{17}H_{18}O$ $[M + Na]^+$ 261.1256, found 261.1258.

1-((cinnamyloxy)methyl-d2)benzene-2,3,4,5,6-d5 (7d-3a)

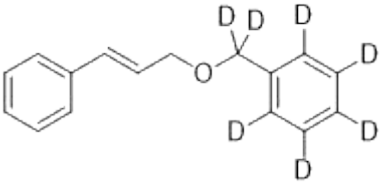

Following general procedure I, **7d-3a** was isolated (silica gel, *n*-hexane/EtOAc, gradient) as a transparent oil (522 mg, 2.26 mmol, 80%). ^{1}H NMR (400 MHz, $CDCl_3$) δ 7.43 – 7.38 (m, 2H), 7.35 – 7.29 (m, 2H), 7.27 – 7.22 (m, 1H), 6.64 (d, J = 15.9 Hz, 1H), 6.34 (dt, J = 15.9, 6.0 Hz, 1H), 4.21 (dd, J = 6.0, 1.5 Hz, 2H). ^{13}C NMR (101 MHz, $CDCl_3$) δ 138.1 (Cq), 136.9 (Cq), 132.7 (CH), 128.7 (2CH), 127.8 (CH), 126.6 (2CH), 126.2 (CH), 70.8 (CH_2). (ESI)-HRMS calcd for $C_{16}H_9D_7O$ [M + Na]+ 254.1538, found 254.1535.

Synthesis of products

Catalytic Synthesis of 2

A solution of 1 (81.0 mg, 0.15 mmol, 1 equiv) in DCM (45 mL) was stirred under nitrogen in a Schlenk-type flask equipped with a magnetic stirring bar and a septum. $AgSbF_6$ (5.2 mg, 0.015 mmol, 10 mol %) was added and the reaction's conversion was monitored by TLC. Upon complete conversion of the substrate, the mixture was directly purified by chromatography on silica gel (*n*-hexane/EtOAc, gradient).

Catalytic Synthesis I (4a-d, f-h, j-m, d14-4a)

A solution of the desired substrate (0.4 mmol, 1 equiv) in DCM (4 mL) was stirred under nitrogen in a Schlenk-type flask equipped with a magnetic stirring bar and a septum. $AgSbF_6$ (6.9 mg, 0.02 mmol, 5 mol %) was added and the reaction's conversion was monitored by TLC. Upon complete conversion of the substrate, the mixture was directly purified by chromatography on silica gel (*n*-exane/EtOAc, gradient).

Catalytic Synthesis II (4e, i)

A solution of the desired substrate (0.4 mmol, 1 equiv) in DCM (4 mL) was stirred under nitrogen in a Schlenk-type flask equipped with a magnetic stirring bar and a septum. $AgSbF_6$ (20.6 mg, 0.06 mmol, 15 mol %) was added in three different batches (5 mol % each). The reaction's conversion was monitored by TLC. Upon complete conversion of the substrate, the mixture was directly purified by chromatography on silica gel (*n*-hexane/EtOAc, gradient).

Carachterization of products

3-cinnamyl-2-phenyl-10-tosyl-1,5-dioxa-10-azacyclotetradeca-7,12-diyne (2)

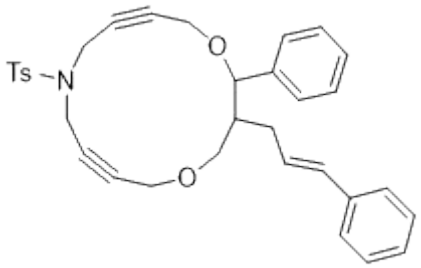

Macrocycle **2** was isolated (silica gel, *n*-hexane/EtOAc, gradient) as a white solid (26.8 mg, 0.050 mmol, 33% yield) from starting material **1** (81 mg, 0.15 mmol). ^{1}H NMR (400 MHz, $CDCl_3$) δ 7.78 – 7.74 (m, 2H), 7.39 – 7.14 (m, 12H), 6.18 (d, J = 15.8 Hz, 1H), 5.93 (ddd, J = 15.8, 7.8, 6.2 Hz, 1H), 4.48 (d, J = 8.9 Hz, 1H), 4.36 (dd, J = 17.6, 6.5 Hz, 2H), 4.30 – 4.23 (m, 1H), 4.19 – 4.10 (m, 2H), 4.04 (dd, J = 8.7, 1.7 Hz, 1H), 3.95 (dd, J = 16.5, 1.3 Hz, 1H), 3.78 (d, J = 16.4, 1H), 3.59 (d, J = 16.5, 1H), 3.31 (dd, J = 8.7, 3.4 Hz, 1H), 2.43 (s, 3H), 2.04 – 1.88 (m, 2H), 1.70 – 1.60 (m, 1H). ^{13}C NMR (101 MHz, $CDCl_3$) δ 144.0 (Cq), 139.7 (Cq), 137.8 (Cq), 134.9 (Cq), 131.5 (CH), 129.6 (2CH), 128.62 (2CH), 128.57 (2CH), 128.46 (CH), 128.29 (CH), 128.25 (2CH), 128.0 (2CH), 127.1 (CH), 126.0 (2CH), 83.9 (Cq), 83.6 (Cq), 80.1 (CH), 79.3 (Cq), 79.0 (Cq), 67.6 (CH_2), 58.3 (CH_2), 55.5 (CH_2), 45.4 (CH), 38.03 (CH_2), 37.99 (CH_2), 31.0 (CH_2), 21.7 (CH_3). (ESI)-HRMS calcd for $C_{33}H_{33}NO_4S$ [M + Na]$^+$ 562.2130, found 562.2137.

(±)(2R,3R,5R)-5-benzyl-3-((S)-(benzyloxy)(phenyl)methyl)-2-phenyltetrahydro-2H-pyran (4a)

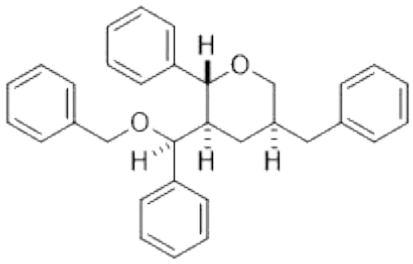

Following catalytic synthesis I, **4a** was isolated (silica gel, *n*-hexane/EtOAc, gradient) as a white solid (40.0 mg, 0.178 mmol, 60% yield, *dr* 73:27 based on ^{1}H NMR integration) from starting material **3a** (100 mg, 0.45 mmol). ^{1}H NMR (400 MHz, $CDCl_3$) δ 7.46 – 7.31 (m, 13H), 7.29 – 7.22 (m, 3H), 7.20 – 7.10 (m, 4H), 4.54 (d, J = 10.0 Hz, 1H), 4.40 (d, J = 11.5 Hz, 1H), 4.14 – 4.11 (m, 1H), 4.11 – 4.06 (m, 1H), 3.94 (ddd, J = 11.1, 4.3, 1.7 Hz, 1H), 3.28

(t, J = 11.1 Hz, 1H), 2.57 (dd, J = 13.7, 5.9 Hz, 1H), 2.43 (dd, J = 13.7, 8.5 Hz, 1H), 1.99 – 1.81 (m, 2H), 1.73 – 1.63 (m, 2H). ^{13}C NMR (101 MHz, $CDCl_3$) δ 141.3 (Cq), 140.3 (Cq), 139.9 (Cq), 138.7 (Cq), 128.9 (2CH), 128.7 (2CH), 128.5 (2CH), 128.34 (2CH), 128.27 (2CH), 128.1 (CH), 127.71 (2CH), 127.69 (CH), 127.62 (2CH), 127.2 (CH), 126.7 (2CH), 126.1 (CH), 83.2 (CH), 80.2 (CH), 73.2 (CH_2), 71.0 (CH_2), 49.9 (CH), 39.6 (CH_2), 38.3 (CH), 29.1 (CH_2). (ESI)-HRMS calcd for $C_{32}H_{32}O_2$ $[M + Na]^+$ 471.2300, found 471.2309.

(±)(2S,3R,5R)-5-benzyl-2-ethyl-3-((S)-phenyl(propoxy)methyl)tetrahydro-2H-pyran (4b)

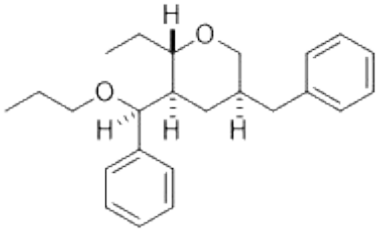

Following catalytic synthesis I, **4b** was isolated (silica gel, n-hexane/EtOAc, gradient) as a white solid (32.1 mg, 0.182 mmol, 73% yield, *dr* 90:10 based on ^{1}H NMR integration) from starting material **3b** (44 mg, 0.25 mmol). ^{1}H NMR (400 MHz, $CDCl_3$) δ 7.37 – 7.29 (m, 2H), 7.25 – 7.16 (m, 5H), 7.16 – 7.08 (m, 1H), 7.03 (d, J = 7.4 Hz, 2H), 4.48 (br s, 1H), 3.76 (dd, J = 11.2, 4.5 Hz, 1H), 3.45 – 3.34 (m, 2H), 3.15 – 3.07 (m, 1H), 3.02 (t, J = 11.1 Hz, 1H), 2.46 (dd, J = 13.6, 5.8 Hz, 1H), 2.30 (dd, J = 13.6, 8.6 Hz, 1H), 1.97 – 1.84 (m, 1H), 1.68 – 1.48 (m, 5H), 1.46 – 1.38 (m, 1H), 1.37 – 1.28 (m, 1H), 1.02 (t, J = 7.3 Hz, 3H), 0.95 (t, J = 7.4 Hz, 3H). ^{13}C NMR (101 MHz, $CDCl_3$) δ 141.1 (Cq), 140.1 (Cq), 128.9 (2CH), 128.3 (2CH), 128.2 (2CH), 127.0 (CH), 126.8 (2CH), 125.9 (CH), 80.9 (CH), 80.0 (CH), 72.7 (CH_2), 71.5 (CH_2), 46.8 (CH), 39.6 (CH_2), 38.4 (CH), 29.4 (CH_2), 25.8 (CH_2), 23.3 (CH_2), 11.0 (CH_3), 9.7 (CH_3). (ESI)-HRMS calcd for $C_{24}H_{32}O_2$ $[M + Na]^+$ 375.2300, found 375.2298.

(±)(2S,3R,5R)-5-benzyl-3-((S)-ethoxy(phenyl)methyl)-2-methyltetrahydro-2H-pyran (4c)

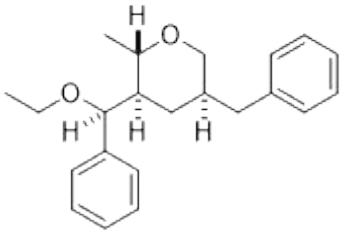

Following catalytic synthesis I, **4c** was isolated (silica gel, *n*-hexane/EtOAc, gradient) as a white solid (42.2 mg, 0.260 mmol, 65% yield, *dr* 86:14 based on ^{1}H NMR integration) from starting material **3c** (65 mg, 0.40 mmol). ^{1}H NMR (400 MHz, $CDCl_3$) δ 7.38 – 7.31 (m, 2H), 7.25 – 7.17 (m, 5H), 7.15 – 7.07 (m, 1H), 7.06 – 7.01 (m, 2H), 4.49 (d, J = 2.3 Hz, 1H), 3.73 (ddd, J = 11.0, 4.3, 1.9 Hz, 1H), 3.62 – 3.53 (m, 1H), 3.51 – 3.43 (m, 1H), 3.31 – 3.20 (m, 1H), 3.06 (t, J = 11.1 Hz, 1H), 2.45 (dd, J = 13.6, 5.9 Hz, 1H), 2.31 (dd, J = 13.7, 8.6 Hz, 1H), 1.76 – 1.65 (m, 1H), 1.44 – 1.38 (m, 2H), 1.35 (d, J = 6.1 Hz, 3H), 1.32 – 1.25 (m, 1H), 1.20 (t, J = 7.0 Hz, 3H). ^{13}C NMR (101 MHz, $CDCl_3$) δ 141.0 (Cq), 140.0 (Cq), 128.9 (2CH), 128.3 (2CH), 128.2 (2CH), 127.1 (CH), 126.7 (2CH), 126.0 (CH), 81.0 (CH), 75.4 (CH), 72.6 (CH_2), 65.1 (CH_2), 49.5 (CH), 39.6 (CH_2), 38.3 (CH), 29.3 (CH_2), 19.8 (CH_3), 15.5 (CH_3). (ESI)-HRMS calcd for $C_{22}H_{28}O_2$ $[M + Na]^+$ 347.1987, found 347.1981.

(±)(2R,3R,5R)-5-benzyl-3-((S)-((4-methylbenzyl)oxy)(phenyl)methyl)-2-(p-tolyl)tetrahydro-2H-pyran (4d)

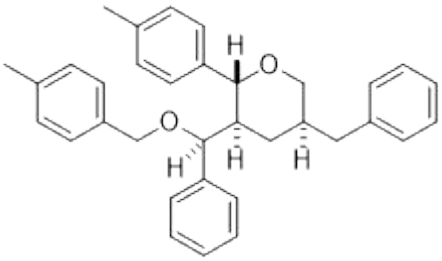

Following catalytic synthesis I, **4d** was isolated (silica gel, *n*-hexane/EtOAc, gradient) as a white solid (24.4 mg, 0.102 mmol, 26% yield, *dr* 86:14 based on ^{1}H NMR integration) from starting material **3d** (95 mg, 0.40 mmol). ^{1}H NMR (400 MHz, $CDCl_3$) δ 7.35 – 7.01 (m, 18H), 4.45 (d, J = 9.9 Hz, 1H), 4.30 (d, J = 11.2 Hz, 1H), 4.08 (d, J = 2.2 Hz, 1H), 3.99 (d, J = 11.3 Hz, 1H), 3.92 – 3.83 (m, 1H), 3.21 (t, J = 11.1 Hz, 1H), 2.51 (dd, J = 13.7, 5.8 Hz, 1H), 2.41 (s, 3H), 2.40 – 2.36 (m, 1H), 2.36 (s, 3H), 1.91 – 1.76 (m, 2H), 1.66 – 1.58 (m, 2H). ^{13}C NMR (101 MHz, $CDCl_3$) δ 140.5 (Cq), 140.0 (Cq), 138.3 (Cq), 137.7 (Cq), 137.4 (Cq), 135.7 (Cq), 129.3 (2CH), 129.2 (2CH), 128.9 (2CH), 128.3 (2CH), 128.2 (2CH), 127.9 (2CH), 127.5 (2CH), 127.1 (CH), 126.7 (2CH), 126.0 (CH), 83.0 (CH), 80.2 (CH), 73.2 (CH_2), 71.0 (CH_2), 49.8 (CH), 39.6 (CH_2), 38.3 (CH), 29.1 (CH_2), 21.4 ($2CH_3$). (ESI)-HRMS calcd for $C_{34}H_{36}O_2$ $[M + Na]^+$ 499.2613, found 499.2611.

(±)(2R,3R,5R)-3-((S)-(benzyloxy)(4-chlorophenyl)methyl)-5-(4-chlorobenzyl)-2-phenyltetrahydro-2H-pyran (4e)

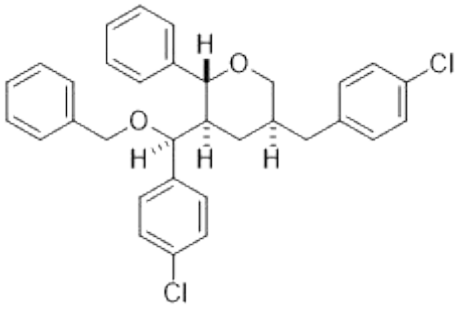

Following catalytic synthesis II, **4e** was isolated (silica gel, *n*-hexane/EtOAc, gradient) as a white solid (50.3 mg, 0.194 mmol, 50% yield, *dr* 90:10 based on ^{1}H NMR integration) from starting material **3e** (101 mg, 0.39 mmol). ^{1}H NMR (400 MHz, $CDCl_3$) δ 7.45 – 7.26 (m, 12H), 7.24 – 7.19 (m, 2H), 7.07 – 7.00 (m, 4H), 4.47 (d, J = 10.0 Hz, 1H), 4.33 (d, J = 11.3 Hz, 1H), 4.10 – 4.01 (m, 2H), 3.93 – 3.86 (m, 1H), 3.23 (t, J = 11.1 Hz, 1H), 2.50 (dd, J = 13.8, 5.9 Hz, 1H), 2.39 (dd, J = 13.8, 8.4 Hz, 1H), 1.92 – 1.73 (m, 2H), 1.64 – 1.55 (m, 2H). ^{13}C NMR (101 MHz, $CDCl_3$) δ 141.0 (Cq), 138.8 (Cq), 138.3 (Cq), 138.2 (Cq), 133.0 (Cq), 131.9 (Cq), 130.2 (2CH), 128.8 (2CH), 128.6 (2CH), 128.53 (2CH), 128.51 (2CH), 128.3 (CH), 128.0 (2CH), 127.9 (CH), 127.7 (2CH), 127.6 (2CH), 83.1 (CH), 79.6 (CH), 73.0 (CH_2), 71.2 (CH_2), 49.8 (CH), 38.8 (CH_2), 38.1 (CH), 29.0 (CH_2). (ESI)-HRMS calcd for $C_{32}H_{30}Cl_2O_2$ $[M + Na]^+$ 539.1521, found 539.1515.

(±)(2S,3R,5R)-5-(4-chlorobenzyl)-3-((S)-(4-chlorophenyl)(propoxy)methyl)-2-ethyltetrahydro-2H-pyran (4f)

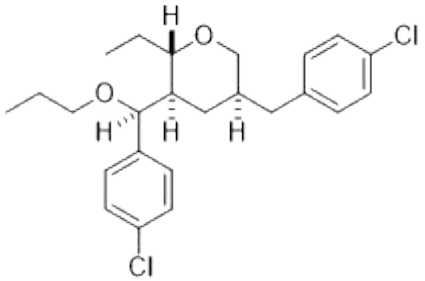

Following catalytic synthesis I, **4f** was isolated (silica gel, *n*-hexane/EtOAc, gradient) as a white solid (20.1 mg, 0.095 mmol, 38% yield, *dr* 93:7 based on ^{1}H NMR integration) from starting material **3f** (52 mg, 0.25 mmol). ^{1}H NMR (400 MHz, $CDCl_3$) δ 7.33 – 7.29 (m, 2H), 7.20 – 7.11 (m, 4H), 6.99 – 6.94 (m, 2H), 4.45 (d, J = 2.6 Hz, 1H), 3.74 (ddd, J = 11.1, 4.4, 2.0 Hz, 1H), 3.42 – 3.32 (m, 2H), 3.15 – 3.06 (m, 1H), 3.00 (t, J = 11.1 Hz, 1H), 2.41 (dd, J = 13.7, 5.9 Hz, 1H), 2.28 (dd, J = 13.8, 8.6 Hz, 1H), 1.94 – 1.82 (m, 1H), 1.65 – 1.43 (m, 5H), 1.34 – 1.23 (m, 2H), 1.01 (t, J = 7.4 Hz, 3H), 0.94 (t, J = 7.4 Hz, 3H). ^{13}C NMR (101 MHz, $CDCl_3$) δ 139.6 (Cq), 138.4 (Cq), 132.7 (Cq), 131.8 (Cq), 130.2 (2CH), 128.4 (4CH), 128.0

(2CH), 80.3 (CH), 79.9 (CH), 72.5 (CH_2), 71.6 (CH_2), 46.7 (CH), 38.9 (CH_2), 38.3 (CH), 29.2 (CH_2), 25.7 (CH_2), 23.3 (CH_2), 11.0 (CH_3), 9.7 (CH_3). (ESI)-HRMS calcd for $C_{24}H_{30}Cl_2O_2$ $[M + Na]^+$ 443.1521, found 443.1522.

(±)(2R,3R,5R)-3-((S)-(benzyloxy)(p-tolyl)methyl)-5-(4-methylbenzyl)-2-phenyltetrahydro-2H-pyran (4g)

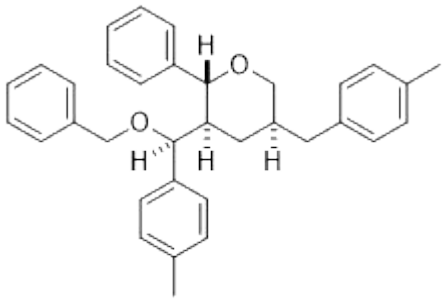

Following catalytic synthesis I, **4g** was isolated (silica gel, *n*-hexane/EtOAc, gradient) as a white solid (29.0 mg, 0.122 mmol, 22% yield, *dr* 87:13 based on ^{1}H NMR integration) from starting material **3g** (129 mg, 0.54 mmol). ^{1}H NMR (400 MHz, $CDCl_3$) δ 7.43 – 7.28 (m, 10H), 7.11 (d, J = 7.9 Hz, 2H), 7.07 – 6.95 (m, 6H), 4.48 (d, J = 9.9 Hz, 1H), 4.35 (d, J = 11.6 Hz, 1H), 4.07 – 3.98 (m, 2H), 3.93 – 3.85 (m, 1H), 3.22 (t, J = 11.1 Hz, 1H), 2.51 (dd, J = 13.7, 5.5 Hz, 1H), 2.39 – 2.32 (m, 1H), 2.33 (s, 3H), 2.29 (s, 3H), 1.89 – 1.76 (m, 2H), 1.73 – 1.61 (m, 2H). ^{13}C NMR (101 MHz, $CDCl_3$) δ 141.4 (Cq), 138.9 (Cq), 137.3 (Cq), 136.88 (Cq), 136.84 (Cq), 135.5 (Cq), 129.04 (2CH), 128.99 (2CH), 128.8 (2CH), 128.7 (2CH), 128.5 (2CH), 128.1 (CH), 127.71 (2CH), 127.65 (3CH), 126.7 (2CH), 83.2 (CH), 80.1 (CH), 73.3 (CH_2), 70.9 (CH_2), 49.9 (CH), 39.2 (CH_2), 38.3 (CH), 29.2 (CH_2), 21.2 (CH_3), 21.1 (CH_3). (ESI)-HRMS calcd for $C_{34}H_{36}O_2$ $[M + Na]^+$ 499.2613, found 499.2618.

(±)(2S,3R,5R)-2-ethyl-5-(4-methylbenzyl)-3-((S)-propoxy(p-tolyl)methyl)tetrahydro-2H-pyran (4h)

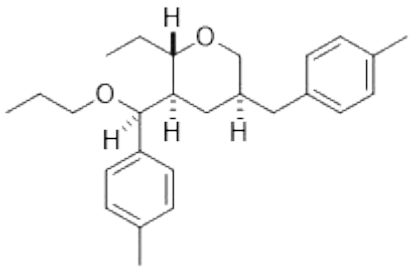

Following catalytic synthesis I, **4h** was isolated (silica gel, *n*-hexane/EtOAc, gradient) as a white solid (25.5 mg, 0.134 mmol, 52% yield, *dr* 88:12 based on ^{1}H NMR integration) from

starting material **3h** (50 mg, 0.26 mmol). ^{1}H NMR (400 MHz, $CDCl_3$) δ 7.18 – 7.07 (m, 4H), 7.03 – 6.98 (m, 2H), 6.95 – 6.89 (m, 2H), 4.45 (d, J = 2.5 Hz, 1H), 3.76 (ddd, J = 11.0, 4.3, 2.0 Hz, 1H), 3.46 – 3.33 (m, 2H), 3.14 – 3.06 (m, 1H), 3.00 (t, J = 11.1 Hz, 1H), 2.43 (dd, J = 13.7, 5.5 Hz, 1H), 2.35 (s, 3H), 2.27 (s, 3H), 2.27 – 2.18 (m, 1H), 1.90 (ddd, J = 14.2, 7.4, 2.8 Hz, 1H), 1.65 – 1.49 (m, 4H), 1.49 – 1.41 (m, 2H), 1.36 – 1.27 (m, 1H), 1.01 (t, J = 7.5 Hz, 3H), 0.94 (t, J = 7.4 Hz, 3H). ^{13}C NMR (101 MHz, $CDCl_3$) δ 138.0 (Cq), 137.0 (Cq), 136.6 (Cq), 135.3 (Cq), 128.94 (2CH), 128.87 (2CH), 128.78 (2CH), 126.8 (2CH), 80.9 (CH), 80.0 (CH), 72.8 (CH_2), 71.4 (CH_2), 46.8 (CH), 39.2 (CH_2), 38.5 (CH), 29.5 (CH_2), 25.8 (CH_2), 23.3 (CH_2), 21.3 (CH_3), 21.1 (CH_3), 11.0 (CH_3), 9.7 (CH_3). (ESI)-HRMS calcd for $C_{26}H_{36}O_2$ $[M + Na]^+$ 403.2613, found 403.2608.

(±)(2S,3R,5S)-3-((R)-(benzyloxy)(4-bromophenyl)methyl)-5-(4-bromobenzyl)-3-methyl-2-phenyltetrahydro-2H-pyran (4i)

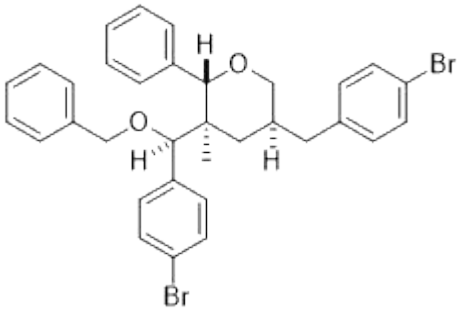

Following catalytic synthesis II, **4i** was isolated (silica gel, *n*-hexane/EtOAc, gradient) as a white solid (45.2 mg, 0.149 mmol, 38% yield, *dr* 92:8 based on ^{1}H NMR integration) from starting material **3i** (118 mg, 0.39 mmol). ^{1}H NMR (400 MHz, $CDCl_3$) δ 7.46 – 7.28 (m, 14H), 6.97 (dd, J = 8.4, 3.1 Hz, 4H), 4.46 (d, J = 9.9 Hz, 1H), 4.32 (d, J = 11.3 Hz, 1H), 4.07 – 4.02 (m, 2H), 3.92 – 3.85 (m, 1H), 3.22 (t, J = 11.1 Hz, 1H), 2.49 (dd, J = 13.8, 5.9 Hz, 1H), 2.37 (dd, J = 13.8, 8.4 Hz, 1H), 1.90 – 1.74 (m, 2H), 1.63 – 1.56 (m, 2H). ^{13}C NMR (101 MHz, $CDCl_3$) δ 140.9 (Cq), 139.3 (Cq), 138.7 (Cq), 138.3 (Cq), 131.5 (4CH), 130.6 (2CH), 128.8 (2CH), 128.6 (2CH), 128.35 (2CH), 128.27 (CH), 127.9 (CH), 127.7 (2CH), 127.6 (2CH), 83.1 (CH), 79.6 (CH), 73.0 (CH_2), 71.2 (CH_2), 49.7 (CH), 38.9 (CH_2), 38.1 (CH), 29.0 (CH_2). (ESI)-HRMS calcd for $C_{33}H_{32}Br_2O_2$ $[M + Na]^+$ 641.0667, found 641.0664.

(±)(2R,3R,5R)-5-benzyl-3-((S)-((4-bromobenzyl)oxy)(phenyl)methyl)-2-(4-bromophenyl)tetrahydro-2H-pyran (4j/4j')

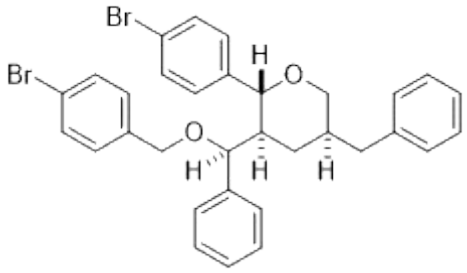

Following catalytic synthesis I, **4j** (50.1 mg, 0.165 mmol, 41% yield) and 4j' (14.8 mg, 0.049 mmol, 12% yield) were isolated (silica gel, *n*-hexane/EtOAc, gradient) as white solids from starting material **3j** (121 mg, 0.40 mmol). **4j**: ^{1}H NMR (400 MHz, $CDCl_3$) δ 7.52 (d, J = 8.3 Hz, 2H), 7.46 (d, J = 8.4 Hz, 2H), 7.33 – 7.28 (m, 2H), 7.25 – 7.11 (m, 8H), 7.09 – 7.05 (m, 4H), 4.39 (d, J = 9.9 Hz, 1H), 4.33 (d, J = 11.8 Hz, 1H), 4.02 (d, J = 2.3 Hz, 1H), 3.96 (d, J = 11.9 Hz, 1H), 3.88 (ddd, J = 11.2, 4.3, 1.9 Hz, 1H), 3.21 (t, J = 11.2 Hz, 1H), 2.53 (dd, J = 13.7, 5.9 Hz, 1H), 2.40 (dd, J = 13.6, 8.5 Hz, 1H), 1.90 – 1.82 (m, 1H), 1.80 – 1.72 (m, 1H), 1.70 – 1.63 (m, 1H), 1.63 – 1.54 (m, 1H). ^{13}C NMR (101 MHz, $CDCl_3$) δ 140.2 (Cq), 139.7 (Cq), 139.7 (Cq), 137.4 (Cq), 131.8 (2CH), 131.7 (2CH), 129.5 (2CH), 129.3 (2CH), 128.9 (2CH), 128.4 (4CH), 127.5 (CH), 126.7 (2CH), 126.1 (CH), 122.0 (Cq), 121.7 (Cq), 82.4 (CH), 80.1 (CH), 73.2 (CH_2), 70.2 (CH_2), 49.7 (CH), 39.5 (CH_2), 38.2 (CH), 29.1 (CH_2). (ESI)-HRMS calcd for $C_{32}H_{30}Br_2O_2$ $[M + Na]^+$ 627.0511, found 627.0514. **4j'**: ^{1}H NMR (400 MHz, $CDCl_3$) δ 7.42 (d, J = 8.4 Hz, 2H), 7.37 (d, J = 8.3 Hz, 2H), 7.34 – 7.28 (m, 4H), 7.22 – 7.16 (m, 4H), 7.12 – 7.06 (m, 4H), 6.84 (d, J = 8.4 Hz, 2H), 4.13 (d, J = 11.8 Hz, 1H), 4.02 (d, J = 4.7 Hz, 1H), 3.90 – 3.80 (m, 3H), 3.03 (t, J = 11.1 Hz, 1H), 2.46 (dd, J = 13.7, 6.5 Hz, 1H), 2.40 – 2.33 (m, 1H), 2.09 – 1.99 (m, 1H), 1.97 – 1.90 (m, 1H), 1.66 – 1.49 (m, 2H). ^{13}C NMR (101 MHz, $CDCl_3$) δ 140.0 (Cq), 139.5 (Cq), 138.8 (Cq), 137.2 (Cq), 131.7 (2CH), 131.4 (2CH), 129.9 (2CH), 129.2 (2CH), 129.0 (2CH), 128.4 (2CH), 128.3 (2CH), 127.9 (CH), 127.8 (2CH), 126.2 (CH), 122.1 (Cq), 121.4 (Cq), 82.9 (CH), 81.5 (CH), 73.4 (CH_2), 69.6 (CH_2), 46.9 (CH), 39.3 (CH_2), 37.9 (CH), 32.7 (CH_2). (ESI)-HRMS calcd for $C_{32}H_{30}Br_2O_2$ $[M + Na]^+$ 627.0511, found 627.0515.

(±)(3S,5S,6R)-3-benzyl-5-((S)-(benzyloxy)(phenyl)methyl)-2,4-dimethyl-6-phenyltetrahydro-2H-pyran (4k/4k')

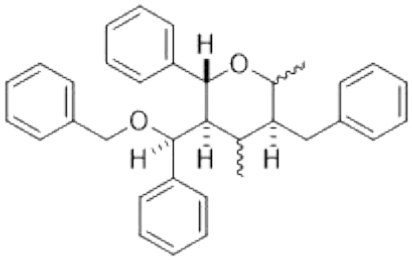

Following catalytic synthesis I, **4k** (26.1 mg, 0.110 mmol, 22% yield, *dr* 80:20 based on ^{1}H NMR integration) and **4k'** (21.8 mg, 0.091 mmol, 18% yield, *dr* 70:30 based on ^{1}H NMR integration) were isolated (silica gel, *n*-hexane/EtOAc, gradient) as white solids from starting material 3k (119 mg, 0.50 mmol). **4k**: ^{1}H NMR (400 MHz, $CDCl_3$) δ 7.52 – 7.45 (m, 2H), 7.42 – 7.28 (m, 10H), 7.25 – 7.18 (m, 4H), 7.15 – 7.09 (m, 2H), 7.06 – 6.98 (m, 4H), 6.81 – 6.75 (m, 2H), 5.00 (d, J = 10.4 Hz, 1H), 4.33 – 4.24 (m, 2H), 4.07 (d, J = 3.5 Hz, 1H), 3.84 (d, J = 11.7 Hz, 1H), 2.91 (dd, J = 13.8, 4.1 Hz, 1H), 2.70 – 2.56 (m, 1H), 2.31 (dt, J = 10.4, 3.7 Hz, 1H), 1.32 (d, J = 7.1 Hz, 2H), 1.26 (d, J = 6.5 Hz, 2H). ^{13}C NMR (101 MHz, $CDCl_3$) δ 141.8 (Cq), 141.2 (Cq), 140.0 (Cq), 139.2 (Cq), 129.1 (2CH), 128.7 (2CH), 128.4 (2CH), 128.3 (2CH), 128.2 (2CH), 128.1(CH), 127.6 (2CH), 127.2 (CH), 127.0 (CH), 126.6 (2CH), 126.1 (2CH), 125.5 (CH), 82.3 (CH), 78.4 (CH), 71.4 (CH_2), 70.3 (CH), 48.9 (CH), 47.6 (CH), 32.3 (CH_2), 28.0 (CH), 19.5 (CH_3), 17.3 (CH_3). (ESI)-HRMS calcd for $C_{34}H_{36}O_2$ [M + Na]$^+$ 499.2613, found 499.2617. **4k'**: ^{1}H NMR (400 MHz, $CDCl_3$) δ 7.37 – 7.27 (m, 5H), 7.22 – 7.14 (m, 9H), 7.09 – 7.06 (m, 2H), 6.89 – 6.85 (m, 2H), 6.80 – 6.75 (m, 2H), 4.76 (d, J = 10.3 Hz, 1H), 4.23 – 4.17 (m, 1H), 4.07 (d, J = 6.0 Hz, 1H), 3.94 (d, J = 11.1 Hz, 1H), 3.79 (d, J = 11.2 Hz, 1H), 3.02 (dd, J = 14.1, 4.7 Hz, 1H), 2.86 (dd, J = 14.1, 11.2 Hz, 1H), 2.71 – 2.63 (m, 1H), 1.70 – 1.63 (m, 1H), 1.61 – 1.55 (m, 1H), 1.23 (d, J = 6.5 Hz, 3H), 1.03 (d, J = 7.2 Hz, 3H). ^{13}C NMR (101 MHz, $CDCl_3$) δ 142.8 (Cq), 141.4 (Cq), 140.6 (Cq), 138.4 (Cq), 129.3 (2CH), 128.5 (2CH), 128.1 (2CH), 128.0 (2CH), 127.9 (2CH), 127.8 (2CH), 127.46 (2CH), 127.43 (CH), 127.37 (2CH), 127.1 (CH), 126.9 (CH), 125.9 (CH), 83.1 (CH), 79.4 (CH), 70.08 (CH), 70.05 (CH_2), 47.4 (CH), 45.1 (CH), 32.4 (CH), 32.2 (CH_2), 19.4 (CH_3), 14.8 (CH_3). (ESI)-HRMS calcd for $C_{34}H_{36}O_2$ [M + Na]$^+$ 499.2613, found 499.2619.

(±)(2S,3R,5R)-5-benzyl-2-cyclopropyl-3-((S)-(cyclopropylmethoxy)(phenyl)methyl)tetrahydro-2H-pyran (4l)

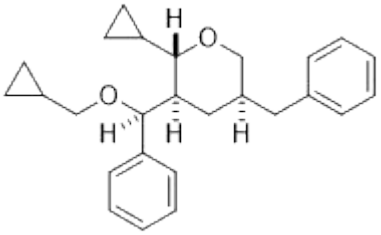

Following catalytic synthesis I, **4l** was isolated (silica gel, n-hexane/EtOAc, gradient) as a white solid (45.5 mg, 0.242 mmol, 40% yield, *dr* 87:13 based on ^{1}H NMR integration) from starting material **3l** (115 mg, 0.61 mmol). ^{1}H NMR (400 MHz, $CDCl_3$) δ 7.36 – 7.28 (m, 2H), 7.27 – 7.15 (m, 5H), 7.12 (d, J = 7.3 Hz, 1H), 7.06 – 6.99 (m, 2H), 4.87 (d, J = 2.3 Hz, 1H), 3.77 (ddd, J = 11.1, 4.4, 2.1 Hz, 1H), 3.20 – 3.07 (m, 2H), 3.02 (t, J = 11.1 Hz, 1H), 2.78 (t, J = 9.1 Hz, 1H), 2.46 (dd, J = 13.7, 5.9 Hz, 1H), 2.31 (dd, J = 13.7, 8.5 Hz, 1H), 1.72 – 1.61 (m, 1H), 1.62 – 1.58 (m, 1H), 1.50 – 1.45 (m, 1H), 1.38 (t, J = 12.3 Hz, 1H), 1.07 – 1.00 (m, 1H), 0.99 – 0.92 (m, 1H), 0.73 – 0.64 (m, 1H), 0.63 – 0.55 (m, 1H), 0.55 – 0.46 (m, 2H), 0.47 – 0.38 (m, 2H), 0.18 – 0.11 (m, 2H). ^{13}C NMR (101 MHz, $CDCl_3$) δ 141.1 (Cq), 140.0 (Cq), 128.9 (2CH), 128.3 (2CH), 128.2 (2CH), 127.0 (CH), 126.9 (2CH), 126.0 (CH), 83.8 (CH), 80.3 (CH), 73.6 (CH_2), 72.9 (CH_2), 49.5 (CH), 39.5 (CH_2), 38.2 (CH), 28.8 (CH_2), 14.9 (CH), 11.0 (CH), 4.5 (CH_2), 3.2 (CH_2), 3.1 (CH_2), 1.9 (CH_2). (ESI)-HRMS calcd for $C_{26}H_{32}O_2$ [M + Na]$^+$ 399.2300, found 399.2307.

(±)(2R,3R,5R)-3-((S)-(benzyloxy)(m-tolyl)methyl)-5-(3-methylbenzyl)-2-phenyltetrahydro-2H-pyran (4m)

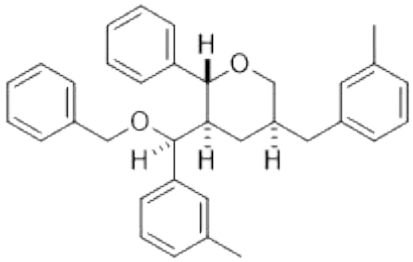

Following catalytic synthesis I, **4m** was isolated (silica gel, *n*-hexane/EtOAc, gradient) as a white solid (50.4 mg, 0.211 mmol, 53% yield, *dr* 87:13 based on ^{1}H NMR integration) from starting material **3m** (95 mg, 0.40 mmol). ^{1}H NMR (400 MHz, $CDCl_3$) δ 7.47 – 7.30 (m, 10H), 7.24 – 7.18 (m, 1H), 7.17 – 7.11 (m, 1H), 7.08 – 7.03 (m, 1H), 7.00 – 6.88 (m, 5H), 4.52 (d, J = 9.9 Hz, 1H), 4.39 (d, J = 11.4 Hz, 1H), 4.10 – 4.02 (m, 2H), 3.98 – 3.90 (m, 1H), 3.26 (t, J = 11.1 Hz, 1H), 2.51 (dd, J = 13.8, 5.8 Hz, 1H), 2.44 – 2.36 (m, 1H), 2.34 (s, 3H), 2.31 (s, 3H), 1.94 – 1.79 (m, 2H), 1.76 – 1.54 (m, 2H). ^{13}C NMR (101 MHz, $CDCl_3$) δ 141.3

(Cq), 140.3(Cq), 139.9 (Cq), 138.9 (Cq), 137.87 (Cq), 137.84 (Cq), 129.8 (CH), 128.7 (2CH), 128.5 (2CH), 128.2 (CH), 128.12 (CH), 128.06 (CH), 127.99 (CH), 127.70 (2CH), 127.66 (CH), 127.64 (2CH), 127.4 (CH), 126.7 (CH), 126.0 (CH), 123.8 (CH), 83.2 (CH), 80.3 (CH), 73.4 (CH_2), 71.0 (CH_2), 49.8 (CH), 39.5 (CH_2), 38.3 (CH), 29.2 (CH_2), 21.6 (CH_3), 21.5 (CH_3). (ESI)-HRMS calcd for $C_{34}H_{36}O_2$ $[M + Na]^+$ 499.2613, found 499.2609.

(±)(2R,3S,5R)-2-(phenyl-d5)-3-((S)-phenyl((phenyl-d5)methoxy-d2)methyl)-5-(phenylmethyl-d)tetrahydro-2H-pyran-2-d (d14-4a)

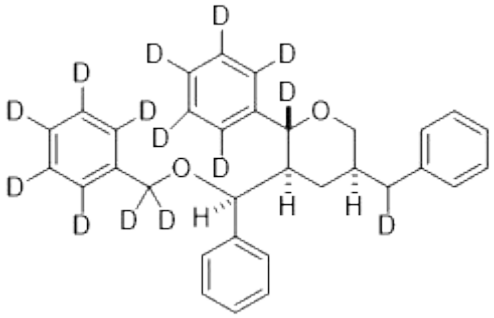

Following catalytic synthesis I, **d14-4a** was isolated (silica gel, *n*-hexane/EtOAc, gradient) as a white solid (58.5 mg, 0.25 mmol, 58% yield, *dr* 83:17 based on ^{1}H NMR integration) from starting material **d7-3a** (100 mg, 0.43 mmol). ^{1}H NMR (400 MHz, $CDCl_3$) δ 7.36 – 7.11 (m, 10H), 4.11 (d, J = 2.2 Hz, 1H), 3.94 (ddd, J = 11.2, 4.3, 1.7 Hz, 1H), 3.28 (t, J = 11.1 Hz, 1H), 2.55 (d, J = 5.7 Hz, 1H), 1.95 – 1.84 (m, 1H), 1.74 – 1.60 (m, 1H). ^{13}C NMR (101 MHz, $CDCl_3$) δ 141.0 (Cq), 140.3 (Cq), 139.9 (Cq), 138.4 (Cq), 128.9 (2CH), 128.3 (2CH), 128.3 (2CH), 127.2 (CH), 126.7 (2CH), 126.0 (CH), 80.1 (CH), 73.2 (CH2), 49.7 (CH), 39.2 (CHD, t, 19.8), 38.2 (CH), 29.1 (CH_2). (ESI)-HRMS calcd for $C_{32}H_{18}D_{14}O_2$ $[M + Na]^+$ 485.3179, found 485.3170.

Comprehensive table in AU

M06/Def2-svp CPCM = CH_2Cl_2

	H (hartrees)	S (cal/K*mol)	imaginary freq. (cm-1)
CH_2Cl_2	-959.291172	65.937	
$Ag(CH_2Cl_2)_2^+$	-2065.451193	113.472	
3c	-501.829144	112.155	
$Ag(CH_2Cl_2)(3c)^+$	-1608.005336	150.085	
TS C-O cleavage	-1607.961310	148.238	-342.6528
$Ag(CH_2Cl_2)(OEt)$	-1260.451686	111.117	
Cinnamyl cation (II)	-347.453425	86.884	
TS II-IIIc	-849.285091	157.534	-204.6774
IIIc	-849.310607	155.746	
TS IIIc-IVc	-849.306473	145.416	-368.1151
IVc	-849.332457	146.745	
TS IVc-Vc	-849.329977	141.433	-271.8465
Vc	-849.341535	142.687	
TS Vc-VIc	-1351.185333	202.517	-168.5970
VIc	-1351.193065	200.259	
TS VIc-II	-1351.184646	200.335	-241.8321
4c + II	-1351.191185	207.894	
4c	-1003.732271	164.272	

The effect of visible light intensity on the two-photon promoted Intermolecular cascades of 1,6-enynes and alkenes

2.1 Introduction: Visible light catalysis

Visible light catalysis has emerged as a groundbreaking field at the intersection of chemistry and materials science, revolutionizing the way chemical reactions are initiated and controlled. Traditional catalytic processes predominantly relied on thermal or chemical activation, often requiring harsh conditions and resulting in undesirable side reactions. The advent of visible light catalysis, however, has introduced a more sustainable and efficient approach to trigger catalytic reactions. This development has not only expanded the scope of synthetic possibilities, but has also contributed significantly to the pursuit of environmentally greener processes.

Giacomo Ciamician was the pioneering chemist who initially recognized that visible light could promote organic reactions (Figure 4). His investigations commenced in 1886 in Rome with studies such as "On the conversion of quinone into quinol by light" and "On the action of light on nitrobenzene in alcoholic solution."[35]

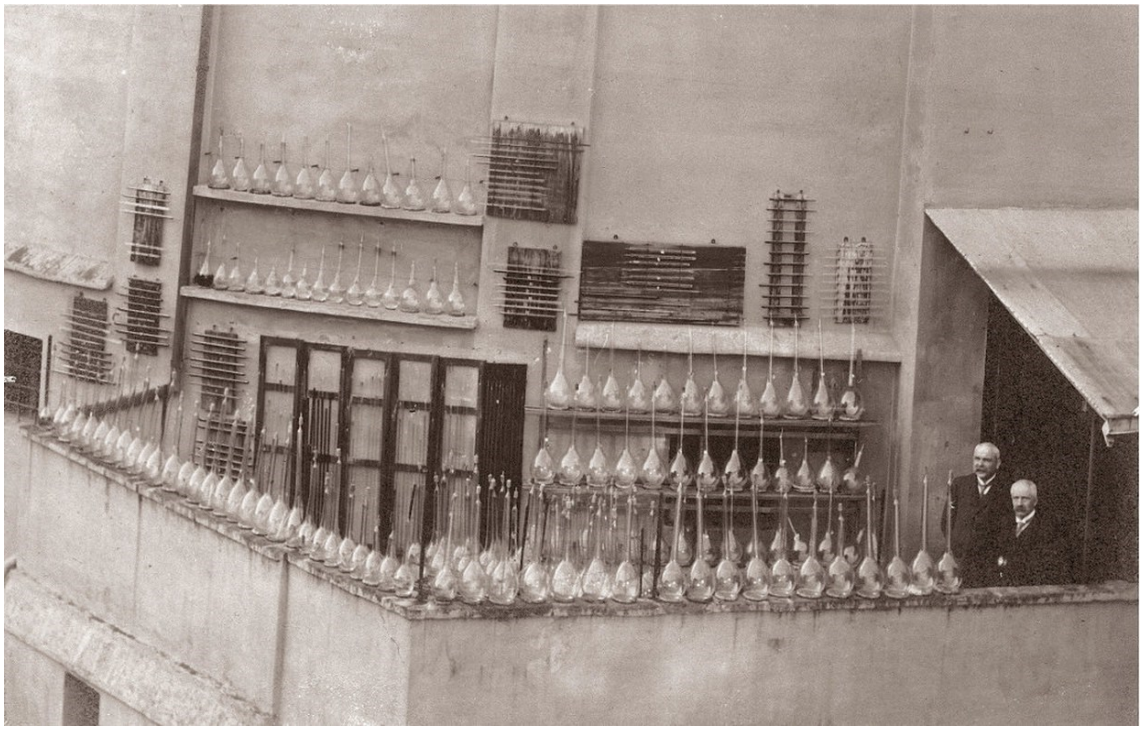

Figure 4: Ciamician and Silber, experiments on the roof laboratory in Bologna. From www.chemistry.unibo.it

Later, at the beginning of the 20th century, Emanuele Paternò conducted an experiment where a mixture of 2-methyl-2-butene and either benzaldehyde or benzophenone were exposed to sunlight in flasks arranged on the laboratory roof for around 100 days during the summer. Paternò was possibly looking for the oxidation of the alkene to form isoprene.

Instead, he observed the coupling of 2-methyl-2-butene with the partner carbonyl compounds resulting in the formation of a compound containing oxygen, but which was not an alcohol, aldehyde or ketone. He supposed that a four-membered cyclic ether had been formed. Only in 1954, George Buchi replicated the experiment, providing a rationalized mechanism and product characterization (Scheme 16)[36]. Consequently, the reaction originally attributed to Paternò was renamed the Buchi-Paternò reaction.

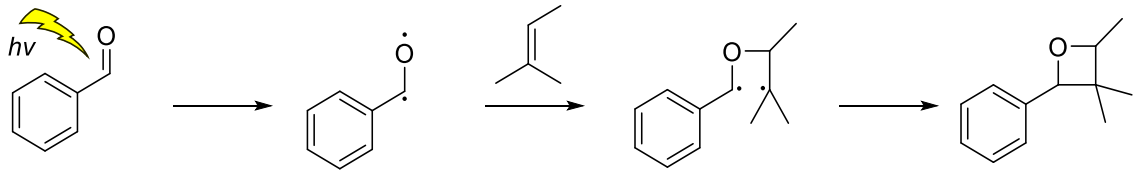

Scheme 16: Visible-light promoted Buchi-Paternò reaction with controlled regioselectivity.

Over the following decades, the use of light was mostly relegated to materials chemistry, particularly focusing on cost-effective transformations with titanium dioxide.[37,38]
However, within the past decade, there has been a renewed exponential interest in the application of photocatalysis to organic synthesis. This old, yet innovative approach has unlocked a series of transformations that were previously unimaginable.

2.2 Introduction: Energy transfer vs Electron transfer

Two competing and sometimes complementary mechanisms are involved in visible-light promoted reactions: energy transfer process (EnT, or sometimes eT) and single electron transfer process (SET, or sometimes ET) (Figure 5).

Energy transfer, the so-called photosensitization, involves the transmission of energy from an excited molecule, often called a sensitizer, to another molecule without an exchange of electrons. In other words, the energy from the excited state of the sensitizer molecule is transferred to the target molecule, boosting its energy level. This increased energy can enable the target molecule to undergo a chemical transformation that it might not have undergone otherwise. The formal definition describes Energy transfer as "the photophysical process in which an excited state of one molecular entity (the donor D) is deactivated to a lower-lying state by transferring energy to a second molecular entity (the acceptor A), which is thereby raised to a higher energy state."[39]

$$D^* + A \rightarrow D + A^*$$

On the other hand, electron transfer involves the transfer of electrons from one species to another. Often referred to as photoredox catalysis, this approach utilizes the high redox activity of an excited state molecule to induce a single electron transfer (SET) event, thus generating radical anions or cations (or neutral radicals when cationic or anionic starting materials are used). Subsequently, the expulsion of a leaving group commonly occurs, leading to the creation of a neutral radical, which serves as the reactive species to initiate a chemical transformation.

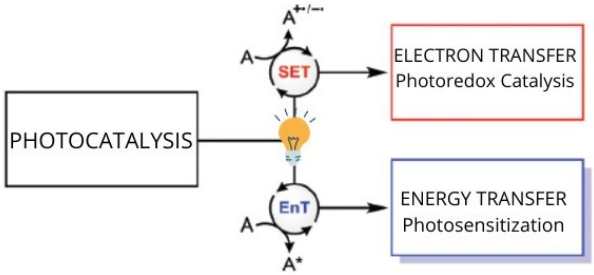

Figure 5: Simplified terminology of photocatalysis, as described by Glorius.[40]

These complementary strategies led to countless applications and are at the core of intense efforts around the globe.[40–42]

2.3 Introduction: Multi-photon strategies

Nowadays, intrinsic thermodynamic limitations of traditional approaches involving visible light are becoming more apparent. Although SET (Single Electron Transfer) represents a big step towards sustainable chemistry, its efficacy is limited by the energy of visible light photons (which max out at approximately 300 kJ mol^{-1}). Therefore, the range of redox potentials in which robust visible light-absorbing photocatalysts can successfully operate is relatively narrow. Increasing the photon energy, moving towards UV light, would lead to photodamage and undesired side reactions, since many organic substrates immediately absorb UV irradiation. For this reason, in order to drive thermodynamically demanding reactions using visible light and known photocatalysts, multi-photon excitation, which combine the energy of two (or more) photons for each catalytic turnover, has recently emerged.[43,44]

Multi-photon strategies are significantly underdeveloped, despite their huge potential. Within this class of reactions, consecutive photo-excitation is the simplest case. More sophisticated alternatives exist, such as the Reductive Excited-State Quenching followed by Excitation of One-Electron-Reduced Species or the Exploitation of Sensitized Triplet–Triplet Annihilation Upconversion (TTA-UC), which is a process involving two photon absorptions that generate an excited singlet from two activated triplets. This multi-photon strategy is a formal up-conversion of visible light, holding for ample potential, but suffers from statistical challenges that still limits its widespread application in synthesis.[43,45]

Another interesting strategy involves a two-photon-promoted sequential Energy transfer/Electron transfer process, such as the Photoreduction of Triplet-Excited Substrates. One example of this method comes from the group of Prof. Konig, which reported in 2019 the "Birch-Type Photoreduction of Arenes and Heteroarenes by Sensitized Electron Transfer".[46] In this paper, they highlight the impact of a two photons approach, compared to single-photon, since the energy accumulation of two visible-light photons allows the dearomatization of arenes and heteroarenes, which otherwise remains very challenging (Scheme 17).

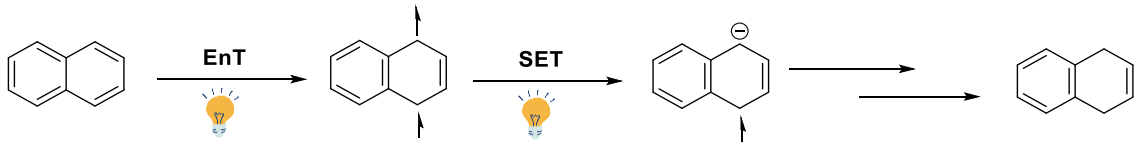

Scheme 17: Reduction of arenes through sequential Energy transfer (EnT), photoinduced single-electron transfer (SET) and hydrogen-atom transfer (HAT). By Konig et al.[46]

Moving away from the Photoreduction field, a second example of sequential EnT/SET approach, which instead involves the Photooxidation of Triplet-Excited Substrates, has been reported by our research team in 2019.[34] In that case, Lanzi and Maestri presented the activation of dienynes, which appeared to be redox-inactive. Instead of manipulating the redox potentials, the substrates were activated through a sequential two photon-promoted process using photocatalysts capable to induce both Energy transfer and Electron transfer (Iridium photocatalysts). This method, led to a cascade reactivity yielding a combination of tri- and tetracyclic frameworks, starting from a variety of linear dienynes. Product formation involves the generation of four new C-C bonds and six contiguous stereocenters (Scheme 18) with great diastereoselectivity (2 out of 32 possible diastereoisomers, d.r. 1:1).

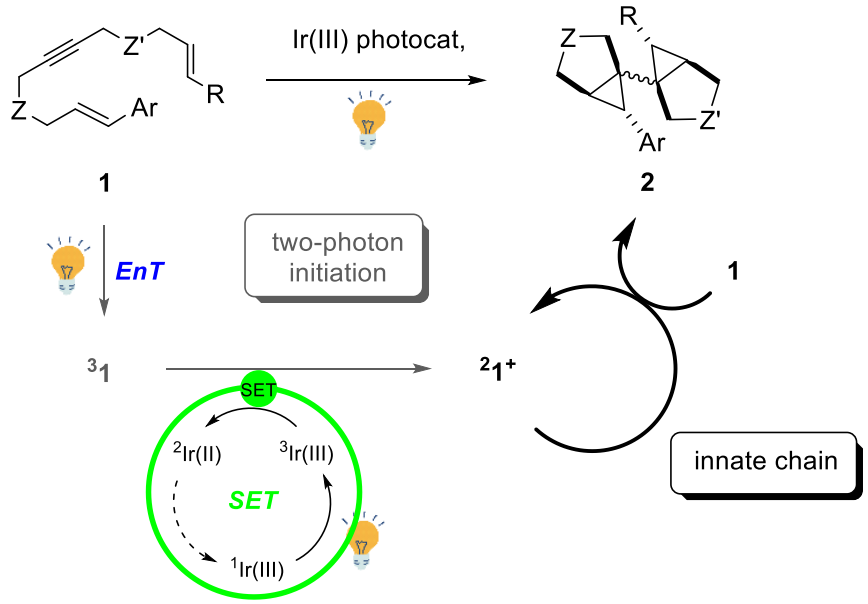

Scheme 18: Polycyclizations of linear Dienynes through sequential Energy transfer and electron transfer. By Maestri e al.[34]

2.4 From the PhD thesis of Dr. Andrea Serafino: Intermolecular cascades of 1,6-enynes and alkenes via visible-light two-photon promoted oxidation of unbiased vinylarenes[47]

Inspired by the two-photon promoted polycyclizations of linear dienynes[34] developed by Lanzi and Maestri and mentioned a moment ago, Serafino and Maestri concentrated their efforts on the extension of that work from intra- to intermolecular pathway.[47] They successfully expanded the reactivity, even though the generality of this novel intermolecular reaction remained limited by the uncontrolled decomposition of many potential substrates.

This novel reaction was thoroughly optimized using enyne **5a** and norbornene as the alkene partner (Scheme 19). Various parameters were investigated including temperature, reaction time, nature of the solvent, concentration of the substrate, equivalents of the alkene partner and photocatalyst.

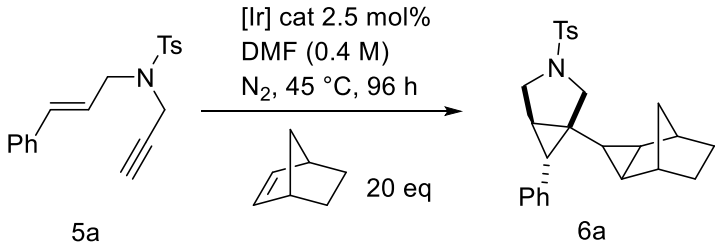

Scheme 19: Model reaction after optimization by Serafino.[47]

Ultimately, the optimum conditions were established: 45°C, 96 h, N_2 atmosphere, DMF, 0.4M, 20 equivalents of norbornene and 2.5 mol% of Iridium photocatalyst $Ir(dF(CF_3)ppy)_2(dtbbpy)(PF_6)$ (Figure 6). The maximum yield observed for the conversion of **5a** into **6a**, with the optimized conditions in hand, was 51%.

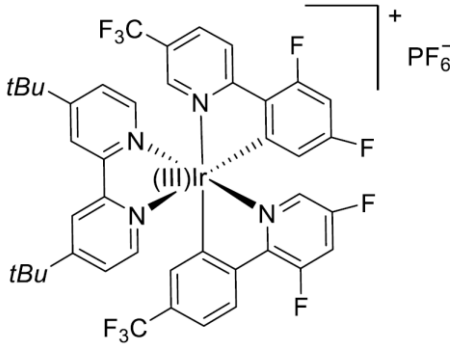

Figure 6: Structure of the best performing Iridium phtocatalyst $Ir(dF(CF_3)ppy)_2(dtbbpy)(PF_6)$.

Then, Maestri's research team proceeded with testing the generality of the method. Focusing the attention on the enynes (Figure 7), it was noted that styrenes decorated with electron withdrawing groups (EWGs) worked unexpectedly well (EWGs usually make oxidation process more challenging). These products were obtained in moderate to good yield (**6b-g** 30-52%). Ortho-methyl substituted styrene **5h** afforded product **6h** in 21% yield. Methyl substituted enyne delivered the corresponding product in 48% yield as a 2:1 mixture of diastereomers. The comparable enyne decorated with a bulky phenyl group (instead of the methyl group) led to the formation of one single diastereoisomer **6j** in 39% yield. Trisubstituted styrene **5k** instead led to an intriguing [3.1.0] unit with two contiguous tetrasubstituted headbridging carbons in 42% yield.

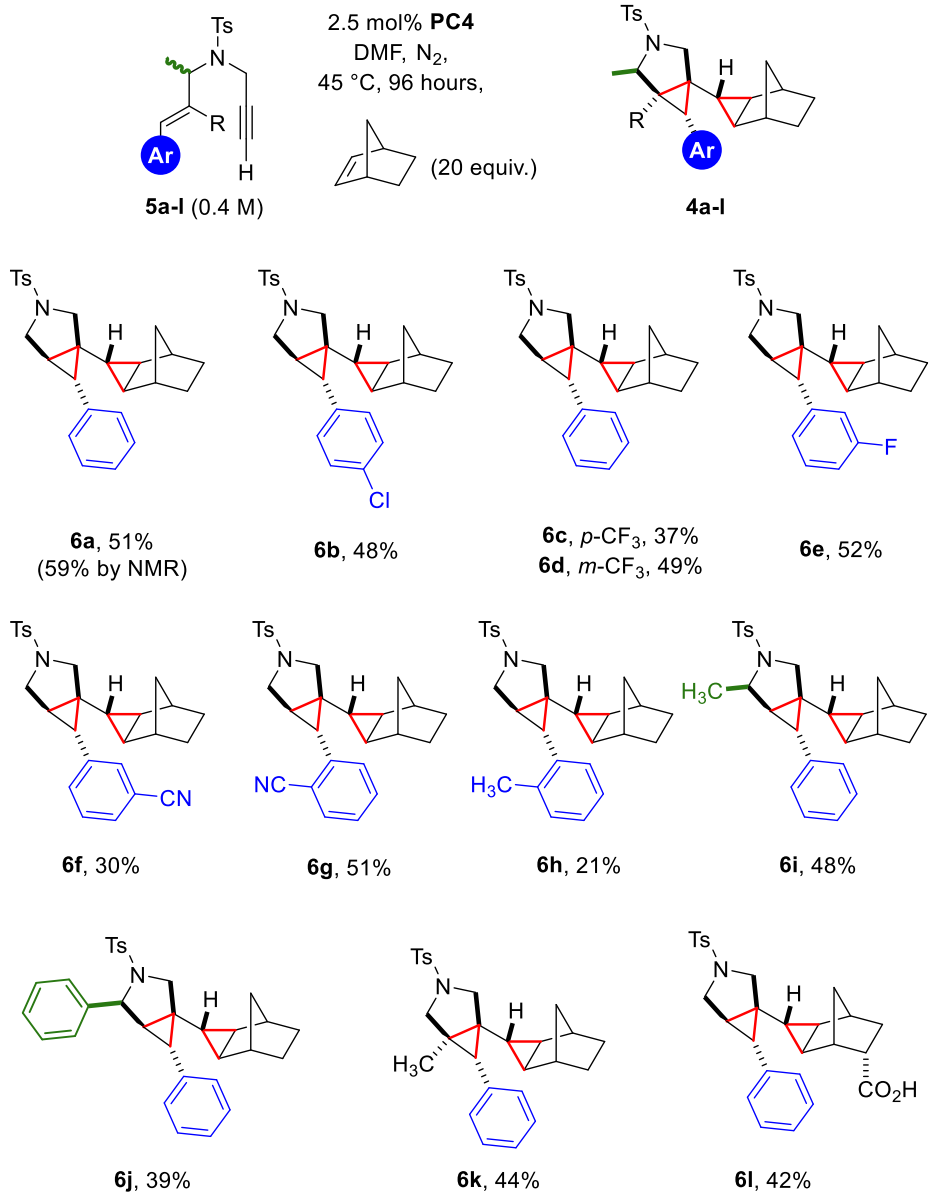

Figure 7: Scope of the reaction of different enynes with norbornene, by Serafino.[47]

Some limitations on the enyne side were reported in this work.[47] Bromine in *para* position of the styryl fragment was not tolerated. Substituting the Tosyl group with a less common Nosyl group, again, inhibited the reactivity. Moreover, propargylic substitutions were not endured. Finally, the presence of the tosylamide tether resulted to be crucial: replacement with an oxygen or a methylene tether completely blocked the reaction.

Then, the study proceeded with the investigation on the alkene partner: norbornene was replaced with various terminal alkenes (Figure 8). A variety of functional groups are tolerated by the method, including esters, different alcohols, monosubstituted tosylamides, nitriles and silyl groups. Highly apolar alkenes gave the corresponding product in low yield, most likely because miscibility issues in DMF (**6m-n**, 24-40%).

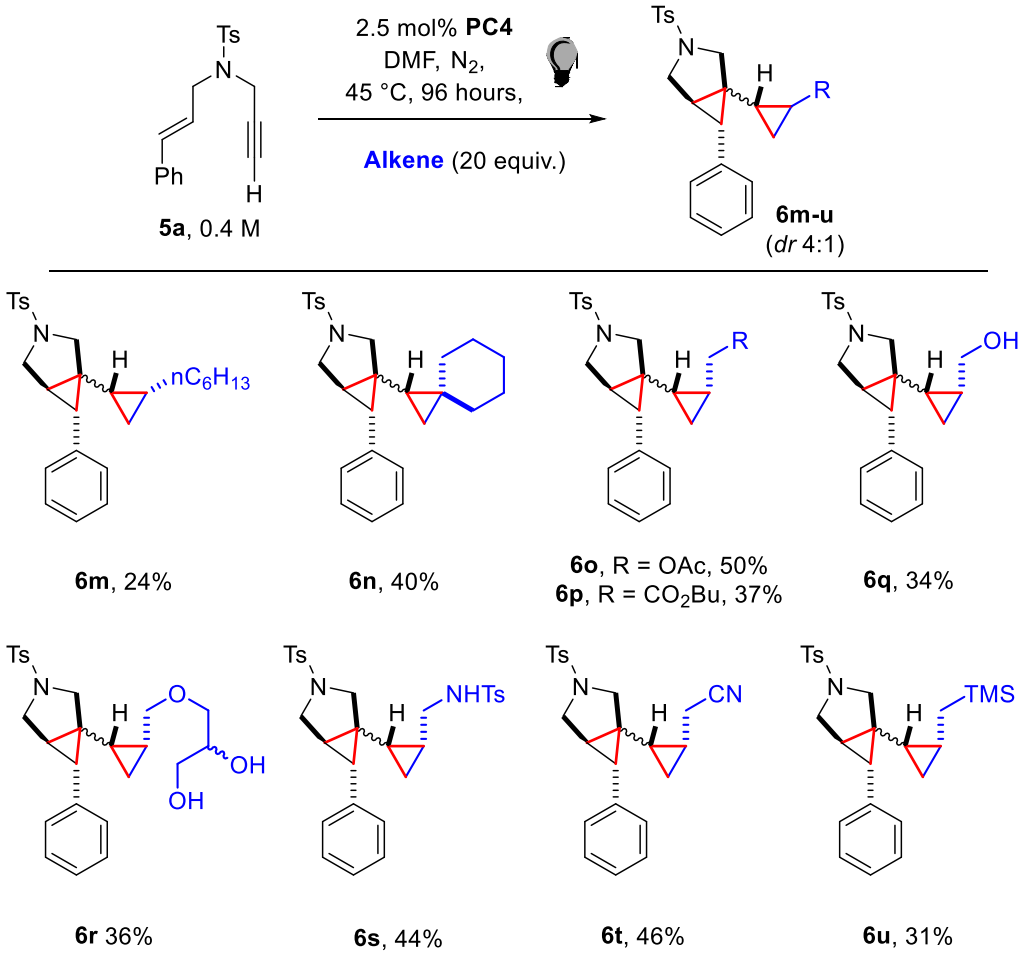

Figure 8 : Scope of the reaction of different alkenes with enyne 5a, by Serafino.[47]

Other limitations of the method emerged after this scope expansion. Total loss of regio and stereochemical control was observed using trisubstituted olefins. Alkenes that could easily undergo radical/ionic polymerization at high concentrations, such as acrylates and

terminal styrenes, resulted unsuccessful. Moreover, the use of a terminal allene failed to afford the expectable vinylidene cyclopropane ring.

DFT calculation showed that any Electron transfer process between ^{3}Ir(III) and substrates were thermodynamically disfavored. On the contrary, the triplet state energies of the catalyst and the enyne resulted to be compatible (+48.3 and +48.8 kcal/mol respectively) for an energy transfer. However, even after energy transfer occurred, it was not possible to predict any energetically possible pathway to afford product **6**. A possible solution, which would confirm the two photon promoted sequential Energy transfer/Electron transfer which was first hypothesized by our group in 2019,[34] involves the oxidation of the previously excited substrate ^{3}**5** by means of a second photoexcited Iridium catalyst. This step, after a series of cationic intermediates, leads to product **6**.

Our team concluded this work investigating the effect of the intensity of the light on this two photon promoted reactivity (and on its intramolecular counterpart).[47] The results, reported in Figure 9, show the marked influence of the intensity of the light source on the rate and the selectivity of the reaction.

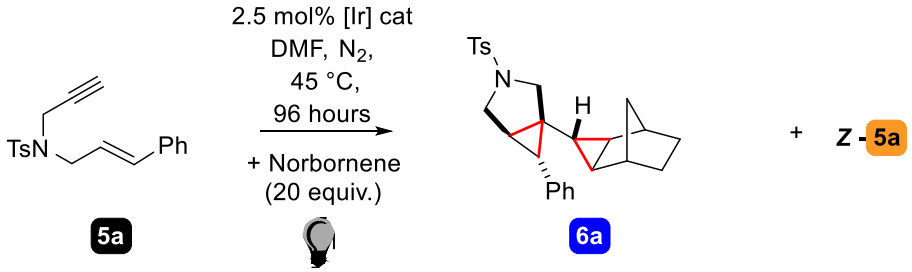

entry	Lux (appr.)	5a	6a	Z - 5a
1	1800	34%	27%	30%
2	2300	23%	32%	29%
3	4300	3%	36%	4%
4	5000	<1%	51%	<1%

Figure 9: Influence of the light intensity on the reactivity (single vs multi photon pathway). From Serafino.[47]

2.5 Results and Discussion

Inspired by the remarkable influence of the light source on the studied polycyclization we decided to dug deeper on that direction. First, we elaborated a more reliable method to measure the light intensity: we substituted the Illuminance measurement in lux with the measure of Irradiance or Spectral Irradiance, performed with a portable Spectroradiometer *Specbos 1211*. Irradiance is the radiant flux received by a surface per unit area, which is measured in Watts per square meter ($W \cdot m^{-2}$). Spectral irradiance is the irradiance of a surface per wavelength, measured in Watts per square metre per nanometre ($W \cdot m^{-2} \cdot nm^{-1}$).

For each Illuminance measure (lux) previously obtained, we re-measured the Irradiance in the visible spectrum (380-780 nm) and the spectral irradiance at their wavelength of maximum irradiance within the blue range (Table 2). Other peaks, outside of the blue range, were ignored, since lower energy irradiation is not suitable for the excitation of common iridium complexes.

Table 2: Adaptation of the previously used approximate illuminance measurement to irradiance/spectral irradiance measurement. Reactor A (power mode from 1 to 5).

Power Mode	**Lux**	Wm^{-2} **(380-780 nm)**	$Wm^{-2}nm^{-1}$ **(460 nm)**
1	600	2.2	0.02
2	1800	3.1	0.03
3	2300	4.0	0.04
4	4300	5.9	0.06
5 (max)	5000	7.6	0.08

The irradiance was measured keeping the sensor of Spectroradiometer *Specbos 1211* at the center of the reactor and precisely 15 cm above the last row of the led stripes, as illustrated in Figure 10. Each irradiance value was measured three times in a row, in order to check the robustness of the measure. The median values are reported.

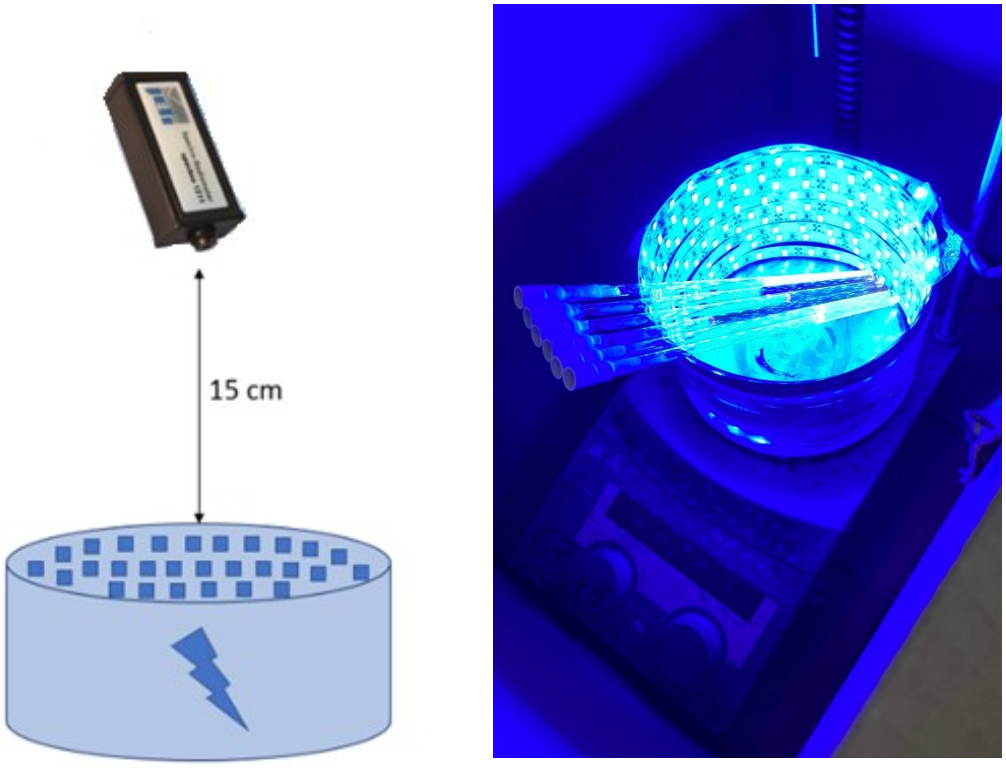

Figure 10:

[sx] Schematic representation of the measurements with Spectroradiometer Specbos 1211.

[dx] Picture of the newly prepared reactor C, blue led stripe

Once the measurement system proved to be optimized and robust, we concentrated our effort in assembling reactors with new led stripes, more powerful transformers and other little precautions in order to maximize the Irradiance (e.g. disposition of the led stripes, aluminium foil to reflect light). These newly prepared Reactors B and C were compared to Reactor A at its maximum power, as used by Serafino[47] (Figure 11).

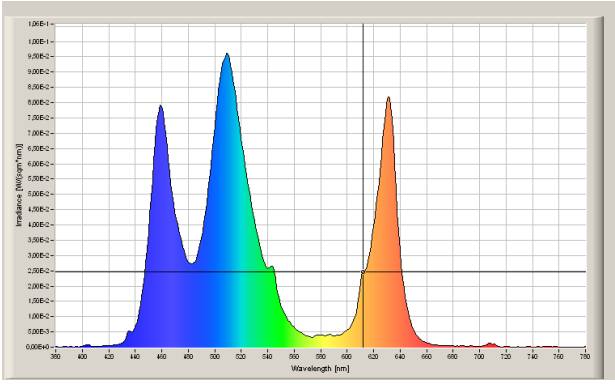

Reactor A (power mode 5)
Spectral irradiance @**460 nm** (max):
0.08 $W \cdot m^{-2} \cdot nm^{-1}$

Irradiance (380-780 nm):
7,6 $W \cdot m^{-2}$

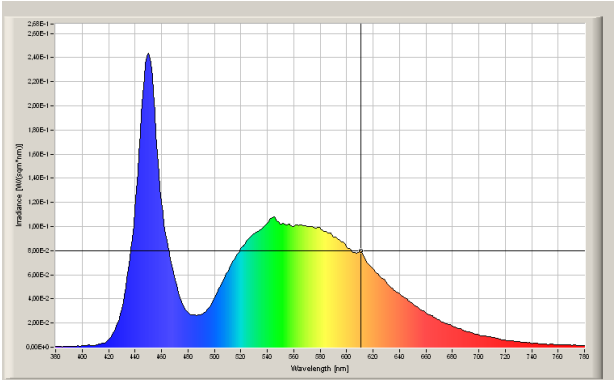

Reactor B
Spectral irradiance @**450 nm** (max):
0.24 $W \cdot m^{-2} \cdot nm^{-1}$

Irradiance (380-780 nm):
18,6 $W \cdot m^{-2}$

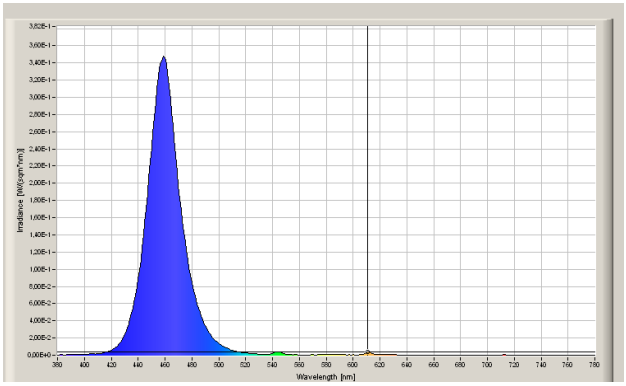

Reactor C
Spectral irradiance @**459** nm (max):
0.35 $W \cdot m^{-2} \cdot nm^{-1}$

Irradiance (380-780 nm):
10,7 $W \cdot m^{-2}$

Figure 11: Irradiance spectra of Reactors A-B-C measured with Specbos 1211.

Reactor B, in the same way of Reactor A, was assembled using white LED stripes, as can be seen by the widespread irradiance over almost the entire visible light range. However, both the irradiance and the spectral irradiance of Reactor B are way higher compared to those of Reactor A. The measurements on Reactor C, on the contrary, showed a sharp peak around 459 nm, which is in accordance with the blue LED we used to assemble the reactor. Due to the sharpness of the peak of Reactor C, the irradiance resulted to be lower (10.7 $W \cdot m^{-2}$) compared to that of Reactor B (18.6 $W \cdot m^{-2}$). Considering spectral irradiance though, Reactor C (0.35 $W \cdot m^{-2} \cdot nm^{-1}$ at 459 nm) possess absolutely the highest value at its wavelength of maximum irradiance (Reactor B stops at 0.24 $W \cdot m^{-2} \cdot nm^{-1}$ at 450 nm).

With these new setups available, we tried to perform the model reaction of Serafino's Intermolecular cascades of 1,6-enynes and alkenes[47] (Scheme 20) using new Reactors B-C and drastically reducing the reaction time from 4 days (as previously reported with Reactor A) to 15 hours. Surprisingly, crude NMR showed total conversion of the substrate after 15 h, maintaining an equivalent yield, around 50%. Apparently, 96 hours are no more necessary to consume the starting material, using these improved setups.

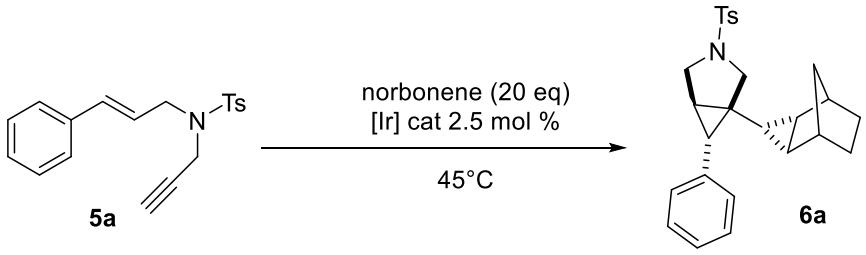

Reactor	*Time to complete conversion*
A	96 h
B	15 h
C	15 h

Scheme 20: Intermolecular cascades of 1,6-enynes and alkenes: model reaction. Investigation on the reaction time.

Subsequent attempts to further reduce the reaction time led to partial conversion of the starting material. For this reason, we chose 15 h as new parameter for the standard conditions, with new reactors B and C.

Then, exploiting the improved light setup, we attempted to overcome one of the reported limitations for the Intermolecular cascades of 1,6-enynes and alkenes:[47] the enyne with the oxygen tether. We repeated the reaction keeping the exact same conditions as reported before, except for the light intensity.

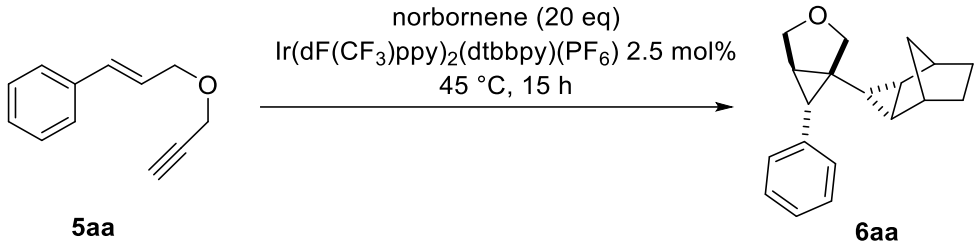

5aa **6aa**

Reactor	*Isolated yield*
A	0%
B	39%
C	39%

Scheme 21: Investigation on the effect of the light intensity on the selected reactivity.

As shown in Scheme 21, the effect of the light intensity is drastic. The reaction moved from 0% to 39% yield, when using the newly installed reactors B and C. No differences were observed between the two new setups. This result suggests that the selectivity of the reaction can be influenced by the amount of incident photons. The similar values obtained with B and C indicates that beyond a certain value, a ceiling is hit and no significant differences were observed with a further increment in the Irradiance.

Inspired by the straightforward overcoming of this first reactivity's limitation, we decided to move forward. Using Reactor B, we tested the same oxygen tethered enyne **5aa** with a different alkene (allyl acetate) and, again, we easily obtained the corresponding product **6ab** with 37% yield (d.r. 5.5/1) (Scheme 22).

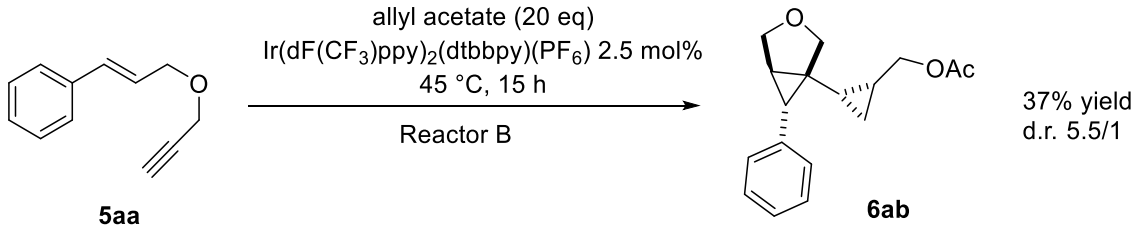

5aa **6ab**

Scheme 22: Reactivity of the oxygen tethered enyne with a different alkene partner.

Then, keeping the same experimental conditions, we moved on to re-attempt two other former limitations: the bromine group in para position of the styryl fragment of **5ac** and the methylene tethered enyne **5ad**. Although with moderate yield (27% and 26% respectively), we demonstrated that, varying only the light intensity, we were able to overcome these previously unsurmountable limitations (Scheme 23). Allyl acetate was used as the alkene partner.

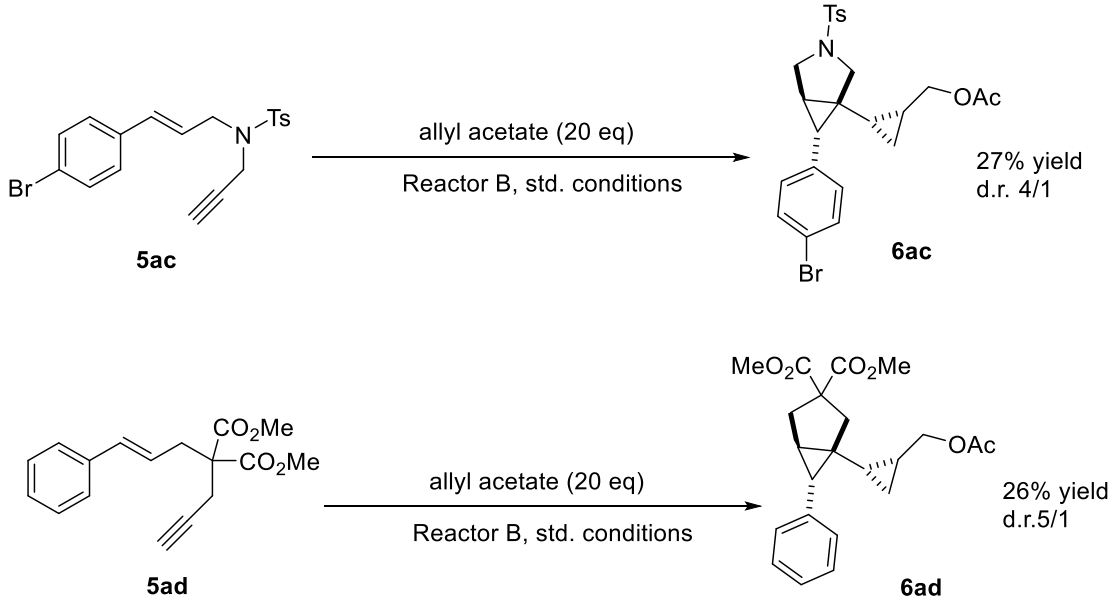

Scheme 23: Two additional overcome limitations.

At that point, having noticed little variations on the d.r. of the products obtained, we decided to investigate more on that direction. The C-C forming step may be sensitive to different substituents on the enyne.

Having already three examples with allyl acetate and different enynes, we decided to stick with that idea and we added two more experiments keeping constant the alkene and varying the enyne partner, adding a para-CF_3 substituent (**5c**) or an ortho-methyl substituent (**5h**) on the arene (Scheme 24). Results show that the d.r. in the intermolecular C–C forming step is slightly sensitive to the arene of the enyne. Looking at Schemes 23-24, it is possible to notice that when an ortho-methyl substituent is present, an increase in diastereoselectivity is observed (d.r. from 4/1[47] to 5/1). On the contrary, when para-CF_3 and para-Br arenes are used, the same d.r. of the simple enyne with the unsubstituted phenyl is observed (4/1). Moreover, variations outside of the enyne's arene can influence the d.r. too: when the NTs tether is substituted with an oxygen or a malonate tether, the d.r. increases to 5.5/1 and 5/1 respectively.

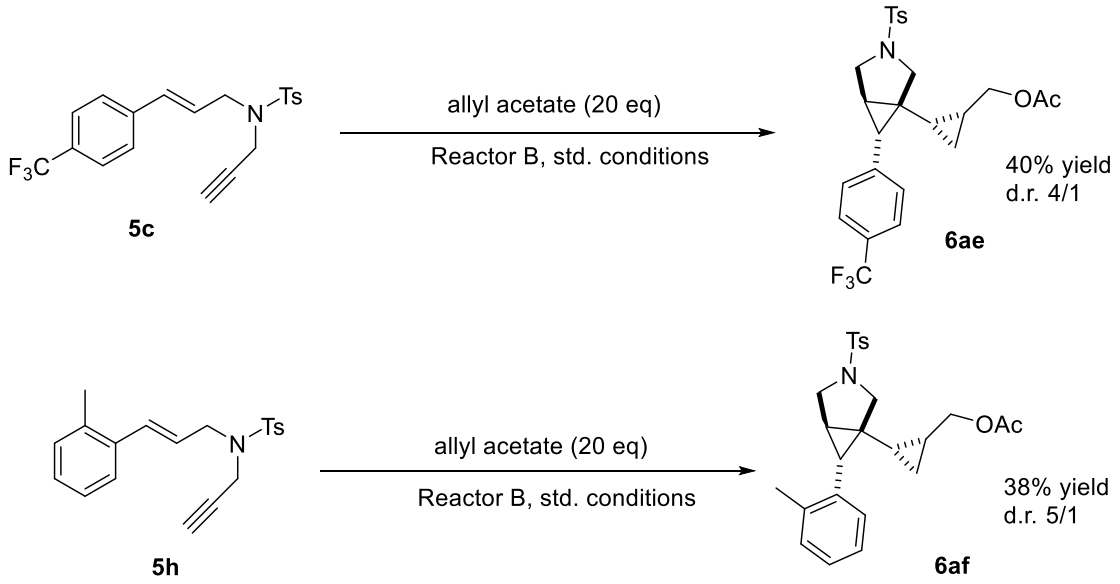

Scheme 24: Additional experiments with allyl acetate and different enyne partners.

Then, maintaining the same experimental conditions, we further extended the scope of the reaction using three new enynes, all bearing a Mesyl group on the nitrogen, instead of the previously used Tosyl group (Scheme 25).

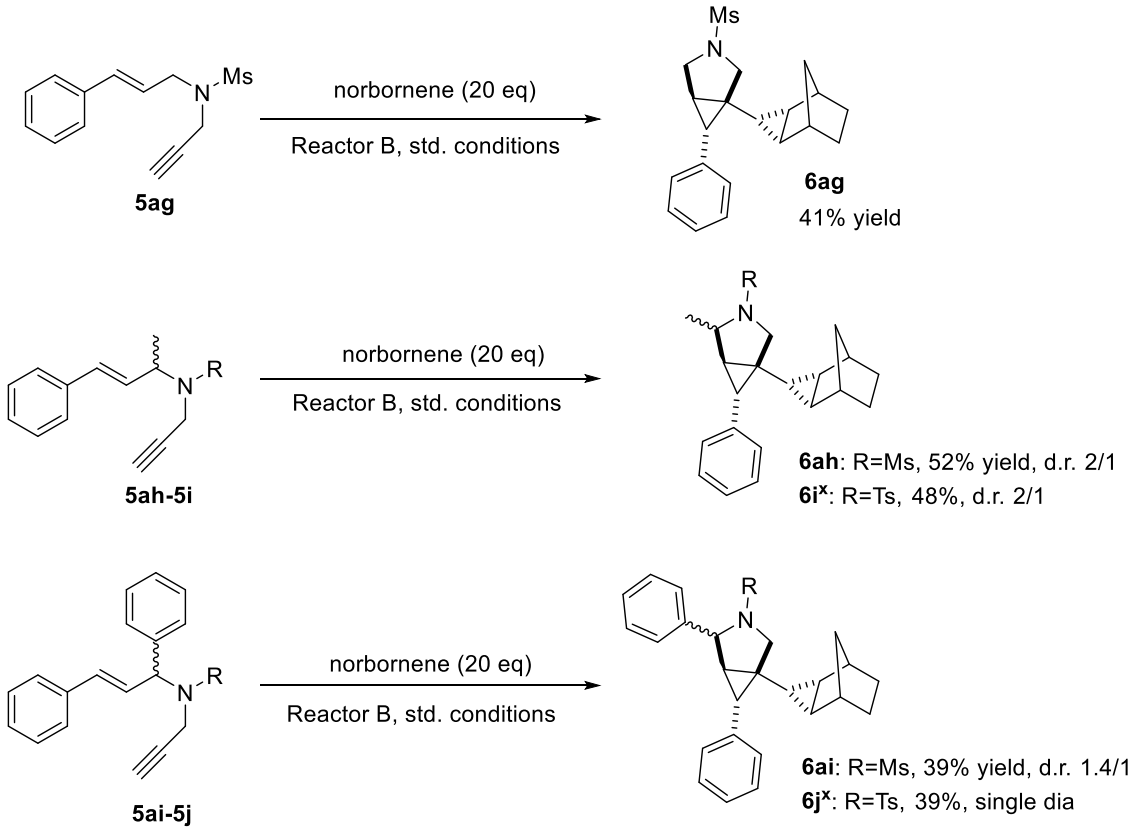

Scheme 25: Enynes with NMs amide tether. [x] entry from Serafino[47]

The standard mesylated product **6ag** was obtained with 41% yield. The mesylated methyl substituted product **6ah** was isolated in 52% yield and d.r. 2/1 (the same d.r. that was reported by Serafino with the corresponding tosylated enyne). On the other hand, regarding the mesylated phenyl substituted product **6ai**, two diastereoisomers were singularly isolated with a total yield of 39%. This outcome is opposite to the results reported by Serafino working on the corresponding tosylated enyne, which yielded instead a single diastereoisomer. The formation of two diastereoisomers in this new-found case is probably due to the lower steric hindrance granted by the Mesyl group in comparison to the Tosyl group. The hindrance of the phenyl substituent is not enough to grant a single product when the relatively small Mesyl group is used to protect the nitrogen tether.

Then, in order to better comprehend the reaction, we decided to investigate if the formation of the *Z*-enyne could be a dead end or if, on the contrary, the cis-substrate could still be capable of undergoing the present reactivity. To do so, we isolated the 100% *Z*-enyne and then we irradiated it in standard conditions (Scheme 26). Surprisingly, the same product isolated from the corresponding *E*-isomer was isolated in this experiment. However, the isolated yield is lower when the *Z*-isomer is used as starting material. This experiment proves that, using Reactor B in standard conditions, the *Z*-isomer is able to form the desired product (directly or through re-isomerization to the *E* counterpart), instead of accumulating as a side product during the reaction, as we previously believed.

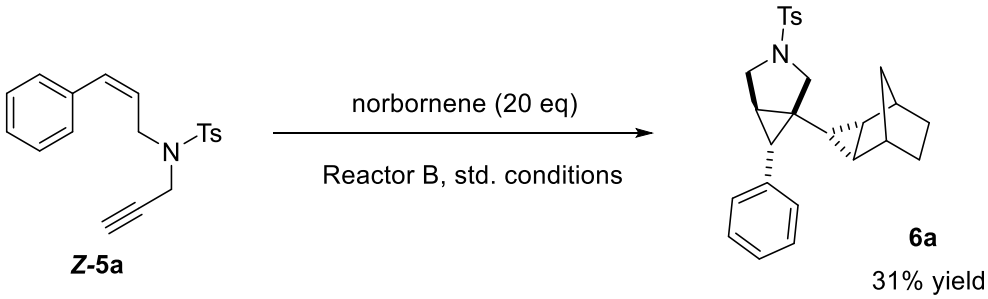

Scheme 26: Reactivity of the Z-enyne.

Computational and experimental mechanistic investigations allowed us to propose a mechanism for this polycyclization reaction (Scheme 27).The excited oxidation potential of the iridium catalyst in question is too low (-0.89 V) to promote a direct electron transfer from the substrate, which has an oxidation halfwave potential of +1.69 V. This result rules out the possibility that the direct oxidation of the substrate could take place under these conditions.

On the contrary, the substrate is prone to sensitization by interaction with the iridium catalyst. The triplet energy of the photocatalyst (+55.1 kcal/mol for $Ir(ppy)_3$) and of the substrate (+48.8 kcal/mol) are comparable: an EnT process is reasonable. However, after that, we were unable to picture any direct pathway to account for the formation of the product from the excited substrate (^{3}**Sub**). Instead, the oxidation of ^{3}**Sub** by means of second photoexcited ^{3}Ir(III) species is favorable according to DFT and leads to the formation of radical cation ^{2}**Sub**$^+$. This intermediate can undergo *5-exo-dig* cyclization through a low barrier transition state (+8.7 kcal/mol in ΔG) forming **I**. This species has a carbenoid character that allows its concerted cycloaddition with an alkene, delivering **II**. The huge olefin excess (20 eq) is likely required to avoid that carbenoid **I** can revert back to ^{2}**Sub**$^+$ and be eventually reduced by ^{2}**Ir(II)**, reforming the substrate.

The ΔG of a propagation step involving **II** and a molecule of **Sub** is slightly positive (+2.4 kcal/mol) indicating a low probability for this stage. The reduction of intermediate **II** that delivers the product can take place by means of a reduced ^{2}**Ir(II)** species. The electron transfer is highly advantageous from an energetic perspective (-67.8 kcal/mol in ΔG). However, the statistically challenging nature of this SET, due to the very low concentration of ^{2}**Ir(II)** in solution, could allow **II** to evolve into radical cation **III**, in which the ring opening of the cyclopropane easily occurs. Radical cation **III** would then reform the cyclopropyl ring via the reverse process (**II'**). The formation of intermediate **III** and the subsequent regeneration of **II'**, account for the formation of the product with the deuterium nucleus both in a *syn*- as well as in an *anti*-arrangement with respect to the *exo*- carbinol group.

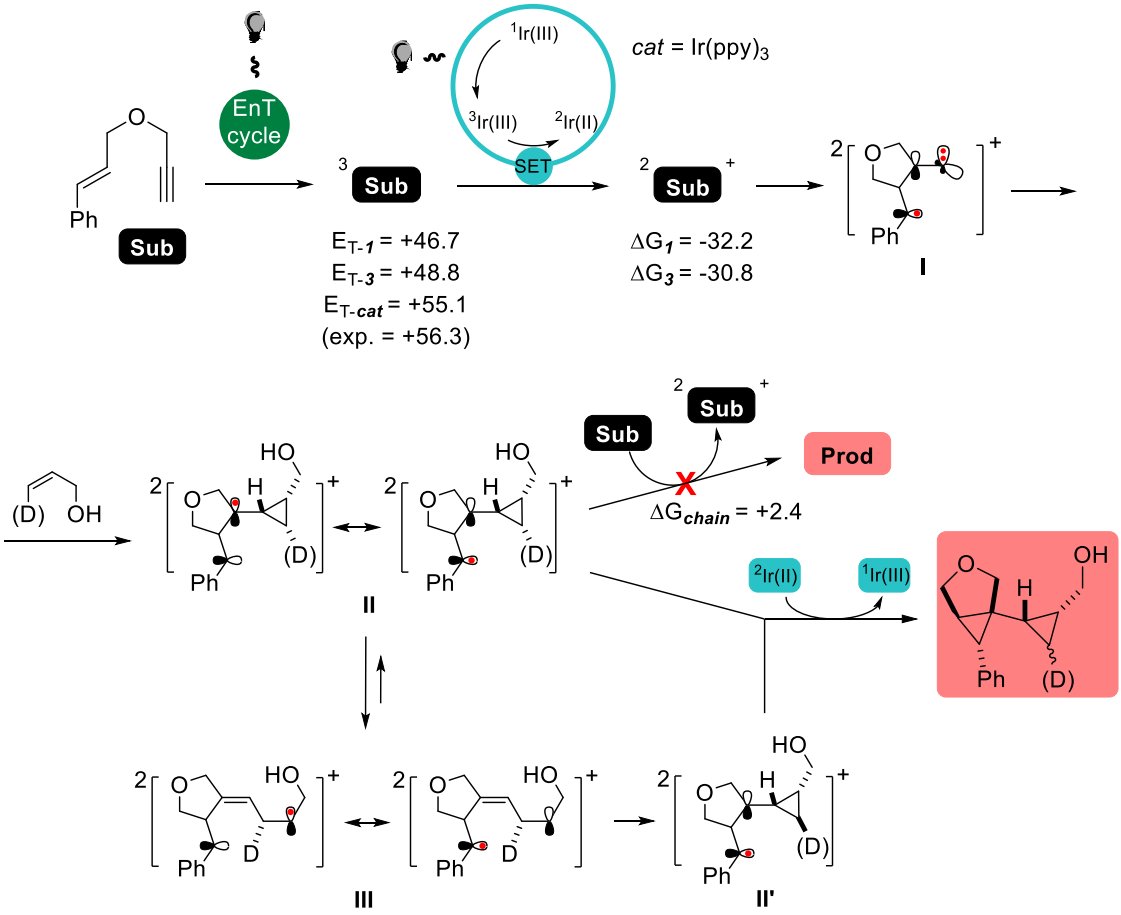

Scheme 27: Proposed mechanistic rationale; values in kcal/mol calculated at the M06/Def2-TZVP level using DMF as implicit solvent.

Considering this mechanism, it is possible to look at the present reactivity as a competition between substrate isomerization (one photon, energy transfer) and polycyclization reaction (two photon, energy transfer and electron tranfer) (Scheme 28).

Scheme 28: Competition between substrate isomerization vs polycyclization

The idea of the two-photon promoted polycyclization was backed up already by Serafino in his PhD thesis, where it is demonstrated that the quantity of incident photons and the photocatalyst concentration influence a process that involves two photon absorptions

(polycyclization) more than a single-photon process, such as the *Z*/*E* isomerization (See Section 2.4).

The scenario illustrated in this chapter, where previously unsurmountable limitations where overcome increasing the quantity of incident photons (i.e. the irradiance) is compatible with the proposed rationale. In fact, the concentration of the excited photocatalyst [PC*] grow linearly with the rise of the available photons. Being the decomposition path a one-photon promoted process (with rate equation $v=K[PC^*][Sub]$), and the polycyclization path a two-photon promoted process (with rate equation $v=K[PC^*]^2[Sub]$), an improved irradiance leads to a higher concentration of PC* and so it helps to discriminate between the two possible pathways, favoring the latter.

2.6 Conclusions

In conclusion, we established a new reliable method for measuring the light intensity in photocatalyzed processes and we assembled new reactors with drastically improved irradiance on the reacting sample. Furthermore, we overcame many limitations previously reported as unsurmountable and we expanded the scope of the intermolecular cascades of 1,6-enynes and alkenes.[47] Moreover, we investigated the effect of substituents on the diastereomeric ratio of the products. Finally, we optimized the conditions of this reactivity, drastically reducing the required reaction time.

2.7 Experimental Section

General Remarks

All chemicals those syntheses are not reported hereafter were purchased from commercial sources and used as received. Solvents were dried passing through alumina columns using an Inert® system and were stored under nitrogen. Present visible-light promoted reactions did not required the use of dry solvents but presence of molecular oxygen exerts a negative effect on their rate. Chromatographic purifications were performed under gradient using a Combiflash® system and prepacked disposable silica cartridges or through isocratic flash chromatography using commercial 60 Å silica gel or via preparative TLCs. All reactions that required heating were performed with the use of high-vacuum grade silicon oil. Reactions promoted by visible light were performed into standard 5 mm NMR tubes, surrounded by a commercial strip of 300 RGB household LEDs. The tubes were inside an oil bath fitted with a thermometer to monitor the temperature. ^{1}H and ^{13}C NMR spectra were recorded at 300 K on a Bruker 400 MHz using residual non-deuterated solvents as internal standards (7.26 ppm for ^{1}H NMR and 77.00 ppm for ^{13}C NMR for $CDCl_3$. The terms m, s, d, t, q and quint represent multiplet, singlet, doublet, triplet, quadruplet and quintuplet respectively, and the term br means a broad signal. Reported assignments were based on decoupling, COSY, NOESY, HSQC and HMBC correlation experiments. Mass analyses were recorded on an Infusion Water Acquity Ultra Performance LC HO6UPS-823M instrument equipped with a SQ detector (Electrospray source); high-resolution mass analyses were recorded on a LTQ ORBITRAP XL Thermo Mass Spectrometer (Electrospray source).

Synthesis of substrates

General procedure 1a (GP-1a)[47]

N-allyl-4-methylbenzenesulfonamide (1 equiv.), (*o*-Tol)3P (0.1 equiv.) and $Pd(OAc)_2$ (0.05 equiv.) were sequentially added to a Schlenk tube equipped with magnetic stirring bar. CH_3CN (0.41 M), TEA (2 equiv.) and the desired aryl halide (1 equiv.) were added under N_2 atmosphere and the mixture was stirred at 80 °C for 3 hours. A second batch of the desired aryl halide (0.42 equiv.), $Pd(OAc)_2$ (0.026 equiv.) and (*o*-Tol)3P (0.05equiv.) were then added. The mixture was stirred at 80 °C for further 6 hours, allowed to cool to room temperature, diluted with water and extracted with EtOAc (3 x 30 mL). The combined organic layers were dried over Na_2SO_4, filtered and concentred under reduced pressure. The resulting crude was purified by chromatography on silica gel (n-hexane/EtOAc 9:1).

The substituted cinnamyl tosylamide (1 equiv.) was dissolved in acetone (0.2 M). K_2CO_3 (3 equiv.) and propargyl bromide (85% in toluene, 1.5 equiv.) were then added. The mixture was subsequently placed in a preheated oil bath at 60 °C and stirred overnight. After consumption of the starting material, the reaction mixture was cooled down to room temperature and water was added. The mixture was extracted with EtOAc (3 x 30 mL). The combined organic fractions were dried over Na_2SO_4 and concentrated under reduced pressure. The resulting crude was purified by chromatography on silica gel (*n*-hexane/EtOAc 8:2).

General procedure 1e (GP-1e)

To a solution of 4-methyl-*N*-(prop-2-yn-1-yl)benzenesulfonamide (1 equiv.), (*Z*)-3-phenylprop-2-en-1-ol (1 equiv) and triphenyl phosphine (1equiv.) in dry THF (0.13 M), DIAD (1 equiv.) was added at 0 °C. The mixture was allowed to warm to room temperature and stirred 24 hours. After completion as monitored by TLC, the solvent was evaporated under reduced pressure. The resulting crude was purified by chromatography on silica gel (*n*-hexane/EtOAc 85:15).

General procedure 1f (GP-1f)

Cinnamaldehyde (1 mL, 7.9 mmol), methanesulfonamide (751 mg, 7.9 mmol) and NEt_3 (3.3 mL, 23.7 mmol) were dissolved in dry CH_2Cl_2 (21 mL). The resulting solution was cooled to 0°C and a 1M solution of $TiCl_4$ (4 mL, 4 mmol) was added under stirring. The resulting mixture was stirred at r.t for 1h, until completion. After evaporating the solvents, toluene was added and the resulting precipitate was filtered off. Toluene was then evaporated under

reduced pressure and the crude product was purified by crystallization in CH_2Cl_2/Hexane to give pure *N*-((*1E*,*2E*)-3-phenylallylidene)methanesulfonamide.

To a solution of *N*-((*1E*,*2E*)-3-phenylallylidene)methanesulfonamide (1 equiv.) in THF (0.17 M) under a N2 atmosphere at -30 °C, a solution of the desired Grignard reagent (1.1 equiv.) was added under vigorous magnetic stirring and the solution was allowed to warm to room temperature. After 3 hours the mixture was quenched with a saturated solution of NH4Cl and extracted with EtOAc (3 x 15mL). The combined organic layers were dried with Na_2SO_4 and the solvent was evaporated under vacuum. The resulting crude was purified by chromatography on silica gel (*n*-hexane/EtOAc 7:3).

The substituted cinnamyl mesylamide (1 equiv.) was dissolved in acetone (0.2 M on substrate). K_2CO_3 (3 equiv.) and propargyl bromide (85% in toluene, 1.5 equiv.) were then added. The mixture was subsequently placed in a preheated oil bath at 60 °C and stirred overnight. After consumption of the starting material, the reaction mixture was cooled down to room temperature and water was added. The mixture was extracted with EtOAc (3 x 30 mL). The combined organic fractions were dried over Na_2SO_4 and concentrated under reduced pressure. The resulting crude was purified by chromatography on silica gel (*n*-hexane/EtOAc 8:2).

Characterization of substrates

N-cinnamyl-*N*-(prop-2-yn-1-yl)methanesulfonamide

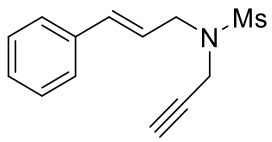

Following the literature procedure,[25] **5ag** was isolated as a white solid. (650 mg, 88%). The spectral data for this compound corresponds to the literature.[25] **^{1}H NMR** (400 MHz, $CDCl_3$) δ = δ 7.48 – 7.21 (m, 5H), 6.67 (d, J = 15.8 Hz, 1H), 6.17 (dt, J = 15.8, 6.8 Hz, 1H), 4.11 (d, J = 2.5 Hz, 2H), 4.06 (d, J = 6.5 Hz, 2H), 2.99 (s, 3H), 2.41 (t, J = 2.4 Hz, 1H).

(*E*)-(3-(prop-2-yn-1-yloxy)prop-1-en-1-yl)benzene

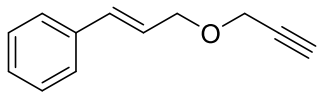

Following the literature procedure,[48] **5aa** was isolated as a transparent oil. (723 mg, 95%). The spectral data for this compound corresponds to the literature.[48] **^{1}H NMR** (400 MHz, $CDCl_3$) δ = 7.42 – 7.38 (m, 2H), 7.35 – 7.30 (m, 2H), 7.28 – 7.24 (m, 1H), 6.65 (dd, *J* = 16.0, 1.5 Hz, 1H), 6.28 (dt, *J* = 15.9, 6.2 Hz, 1H), 4.25 (dd, *J* = 6.2, 1.5 Hz, 2H), 4.21 (d, *J* = 2.4 Hz, 2H), 2.46 (t, *J* = 2.4 Hz, 1H).

Dimethyl 2-cinnamyl-2-(prop-2-yn-1-yl)malonate

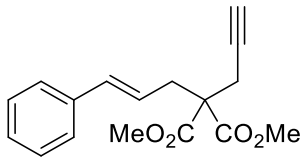

Following the literature procedure,[49] **5ad** was isolated as a yellowish oil. (355 mg, 85%). The spectral data for this compound corresponds to the literature.[49] **^{1}H NMR** (400 MHz, $CDCl_3$) δ = 7.35 – 7.27 (m, 4H), 7.25 – 7.19 (m, 1H), 6.52 (d, J = 15.7 Hz, 1H), 6.00 (dt, J = 15.5, 7.7 Hz, 1H), 3.76 (s, 6H), 2.97 (dd, J = 7.7, 1.3 Hz, 2H), 2.85 (d, J = 2.7 Hz, 2H), 2.06 (t, J = 2.7 Hz, 1H).

(*E*)-*N*-(3-(4-bromophenyl)allyl)-4-methyl-*N*-(prop-2-yn-1-yl)benzenesulfonamide

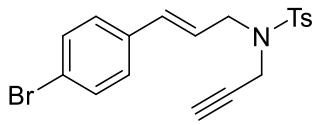

Following the **GP-1a** product **5ac** was isolated as white solid. (274 mg, 82%) The spectral data for this compound corresponds to the literature.[26] **^{1}H NMR** (400 MHz, $CDCl_3$) δ = 7.76 (d, J = 8.4 Hz, 2H), 7.43 (d, J = 8.5 Hz, 2H), 7.31 (d, J = 7.8 Hz, 2H), 7.19 (d, J = 8.5 Hz, 2H), 6.51 (d, J = 15.9 Hz, 1H), 6.08 (dt, J = 15.8, 6.8 Hz, 1H), 4.12 (d, J = 2.4 Hz, 2H), 3.98 (dd, J = 6.8, 1.4 Hz, 2H), 2.43 (s, 3H), 2.05 (t, J = 2.4 Hz, 1H).

(*Z*)-4-methyl-*N*-(3-phenylallyl)-*N*-(prop-2-yn-1-yl)benzenesulfonamide

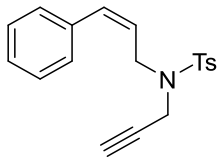

Following the **GP-1e** product **Z-5a** was isolate as transparent oil (210.0 mg, 90%). **^{1}H NMR** (400 MHz, $CDCl_3$) δ = 7.73 (d, J = 8.3 Hz, 2H), 7.37 – 7.21 (m, 7H), 6.69 (dd, J = 11.6, 1.9 Hz, 1H), 5.65 (dt, J = 11.7, 6.7 Hz, 1H), 4.14 (dd, J = 6.7, 1.8 Hz, 2H), 4.12 (d, J = 2.4 Hz, 2H), 2.44 (s, 3H), 1.87 (t, J = 2.5 Hz, 1H). **^{13}C NMR** (101 MHz, $CDCl_3$) δ = 143.7, 136.1, 136.1, 133.9, 129.6, 128.9, 128.4, 127.9, 127.4, 126.3, 73.7, 44.5, 36.5, 21.7. **ESI-MS** calcd for $C_{19}H_{19}NO_2S$ [M+Na]+ 348.11 found 348.13.

(*E*)-*N*-(4-phenylbut-3-en-2-yl)-*N*-(prop-2-yn-1-yl)methanesulfonamide

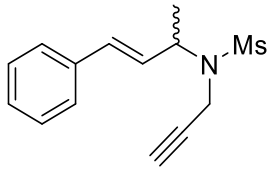

Following the **GP-1f** product **5ah** was isolated as transparent oil. (274.0 mg, 58%) **^{1}H NMR** (400 MHz, $CDCl_3$) δ = 7.42 – 7.26 (m, 5H), 6.58 (d, J = 16.0 Hz, 1H), 6.35 (dd, J = 16.0, 6.5 Hz, 1H), 4.76 (p, J = 6.9 Hz, 1H), 4.08 (d, J = 2.5 Hz, 2H), 3.05 (s, 3H), 2.37 (t, J = 2.5 Hz, 1H), 1.52 (d, J = 7.0 Hz, 3H). **^{13}C NMR** (101 MHz, $CDCl_3$) δ = 136.3, 132.3, 128.8, 128.8,

128.2, 126.7, 80.5, 73.4, 55.4, 41.2, 32.4, 18.9. **ESI-MS** calcd for $C_{14}H_{17}NO_2S$ [M+Na]+ 296.10 found 296.04.

(*E*)-*N*-(1,3-diphenylallyl)-*N*-(prop-2-yn-1-yl)methanesulfonamide

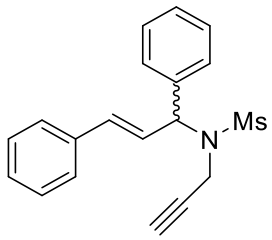

Following the **GP-1f** product **5ai** was isolated as white solid. (244.0 mg, 52%) **^{1}H NMR** (400 MHz, $CDCl_3$) δ = 7.49 – 7.43 (m, 4H), 7.42 – 7.29 (m, 6H), 6.86 (dd, J = 15.8, 9.0 Hz, 1H), 6.73 (d, J = 15.8 Hz, 1H), 5.77 (d, J = 9.0 Hz, 1H), 4.22 (dd, J = 18.8, 2.5 Hz, 1H), 3.74 (dd, J = 18.8, 2.5 Hz, 1H), 3.07 (s, 3H), 2.40 (t, J = 2.5 Hz, 1H). **^{13}C NMR** (101 MHz, $CDCl_3$) δ = 138.1, 136.1, 134.6, 128.98, 128.96, 128.5, 128.4, 128.0, 126.8, 125.4, 80.3, 73.9, 63.8, 41.4, 33.6. **ESI-MS** calcd for $C_{19}H_{19}NO_2S$ [M+Na]+ 348.11 found 348.27.

Synthesis of products

General Procedure 2 (GP-2) [47]

To a vial charged with substrate (1 equiv.) and $Ir(dF(CF_3)ppy)_2(dtbbpy)(PF_6)$ (0.025 equiv.), dry and degassed DMF (0.4 M) was added. The solution was transferred in a 5 mm-wide (external diameter) NMR tube and degassed via freeze-pump cycles (2x 10 minutes). The homogeneous solution was placed in an oil bath preheated at 45° C and irradiated with LED stripes for 96 hours. The mixture was then concentrated and the residue was purified by chromatography on silica gel.

Characterization of products

(1S,5R,6S)-3-(methylsulfonyl)-6-phenyl-1-((1R,2S,3r,4R,5S)-tricyclo[3.2.1.02,4]octan-3-yl)-3-azabicyclo[3.1.0]hexane

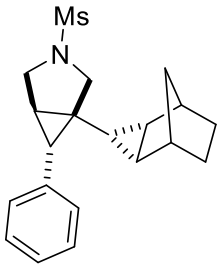

6ag was isolated following the **GP-2** using (49.9 mg, 0.2 mmol) and norbornene (376.6 mg, 4 mmol) as reagents. Yield **41**% (28.1 mg, 0.082 mmol). **^{1}H NMR** (400 MHz, $CDCl_3$) δ = 7.31 – 7.26 (m, 2H), 7.22 – 7.16 (m, 3H), 3.62 (dd, J = 13.3, 9.2 Hz, 2H), 3.37 (dd, J = 9.2, 3.8 Hz, 1H), 3.26 (d, J = 9.2 Hz, 1H), 2.85 (s, 3H), 2.21 (d, J = 4.1 Hz, 1H), 2.15 (bs, 1H), 1.80 (bs, 1H), 1.72 (t, J = 4.0 Hz, 1H), 1.40 – 1.26 (m, 2H), 1.19 – 1.03 (m, 2H), 0.72 – 0.66 (m, 1H), 0.66 – 0.62 (m, 1H), 0.57 – 0.51 (m, 1H), 0.47 (d, J = 10.6 Hz, 1H), 0.32 – 0.25 (m, 1H).**^{13}C NMR** (101 MHz, $CDCl_3$) δ = 137.3 (Cq), 129.2 (2 CH), 128.1 (2CH), 126.2 (CH), 54.3 (CH_2), 50.6 (CH_2), 35.9 (CH_3), 35.64 (CH), 35.62 (CH), 34.3 (Cq), 30.1 (CH), 29.5 (CH_2), 29.4 (CH_2), 28.4 (CH_2), 25.8 (CH), 23.6 (CH), 22.0 (CH), 11.5 (CH). **ESI-MS** calcd for $C_{20}H_{25}NO_2S$ [M+Na]+ 366.16 found 366.02.

((1R,2S)-2-((1S,5R,6S)-3-tosyl-6-(4-(trifluoromethyl)phenyl)-3-azabicyclo[3.1.0]hexan-1-yl)cyclopropyl)methyl acetate (dr 4:1)

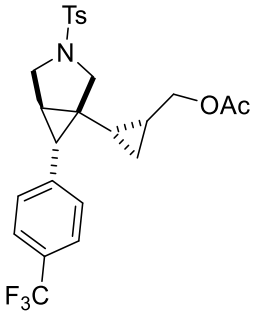

6ae was isolated following the **GP-2** using **5c** (78.7 mg, 0.2 mmol, **dr 4:1**) and allyl acetate (432 μL, 4.0 mmol) as reagents. Yield **40**% (40.0 mg, 0.081 mmol). **^{1}H NMR** (400 MHz, $CDCl_3$) δ = 7.71 (d, J = 8.3 Hz, 2H), 7.49 (d, J = 8.2 Hz, 2H), 7.34 (d, J = 8.0 Hz, 2H), 7.23

(d, J = 8.0 Hz, 2H), 3.85 – 3.78 (m, 1H), 3.76 – 3.68 (m, 2H), 3.59 – 3.50 (m, 1H), 3.25 (dd, J = 9.5, 3.7 Hz, 1H), 3.11 (d, J = 9.4 Hz, 1H), 2.42 (s, 3H), 2.20 – 2.16 (m, 1H), 1.92 (s, 3H), 1.85 – 1.79 (m, 1H), 1.08 – 0.97 (m, 2H), 0.29 (td, J = 8.7, 5.6 Hz, 1H), -0.26 (q, J = 5.7 Hz, 1H). **^{13}C NMR** (101 MHz, $CDCl_3$) δ = 170.9 (Cq), 143.9 (Cq), 141.4 (Cq), 134.0 (Cq), 129.9 (2 CH), 129.5 (2 CH), 127.5 (2 CH), 125.1 (2 CH), 64.1 (CH_2), 54.8 (CH_2), 49.8 (CH_2), 33.5 (Cq), 29.0 (CH), 26.2 (CH), 21.6 (CH_3), 20.9 (CH_3), 14.9 (CH), 14.2 (CH), 10.1 (CH_2). **ESI-MS** calcd for $C_{25}H_{26}F_3NO_4S$ [M+Na]+ 516.15 found 515.92.

((1R,2S)-2-((1S,5R,6S)-6-(4-bromophenyl)-3-tosyl-3-azabicyclo[3.1.0]hexan-1-yl)cyclopropyl)methyl acetate (dr 4:1)

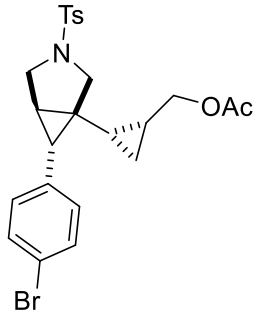

6ac was isolated following the **GP-2** using **5ac** (61.3 mg, 0.15 mmol) and allyl acetate (324 µL, 3.0 mmol) as reagents. Yield **27**% (20.1 mg, 0.040 mmol, **dr 4:1**). **^{1}H NMR** (400 MHz, $CDCl_3$) δ = 7.74 – 7.68 (m, 2H), 7.39 – 7.31 (m, 4H), 7.01 – 6.97 (m, 2H), 3.85 – 3.77 (m, 1H), 3.73 – 3.64 (m, 2H), 3.58 – 3.51 (m, 1H), 3.23 (dd, J = 9.5, 3.8 Hz, 1H), 3.10 (d, J = 9.4 Hz, 1H), 2.42 (s, 3H), 2.10 – 2.06 (m, 1H), 1.92 (s, 3H), 1.73 (t, J = 4.0 Hz, 1H), 1.05 – 0.98 (m, 2H), 0.32 (td, J = 8.7, 5.6 Hz, 1H), -0.27 (q, J = 5.7 Hz, 1H). **^{13}C NMR** (101 MHz, $CDCl_3$) δ = 170.9 (Cq), 143.8 (Cq), 136.1 (Cq), 134.0 (Cq), 131.3 (2 CH), 130.9 (2CH), 129.9 (2CH), 127.5 (2CH), 120.2 (Cq), 64.2 (CH2), 54.8 (CH2), 49.8 (CH2), 33.1 (Cq), 28.7 (CH), 26.1 (CH), 21.6 (CH_3), 21.0 (CH_3), 15.0 (CH), 14.2 (CH), 10.1 (CH_2). **ESI-MS** calcd for $C_{24}H_{26}BrNO_4S$ [M+Na]+ 526.08 found 526.10.

((1R,2S)-2-((1S,5R,6S)-6-(o-tolyl)-3-tosyl-3-azabicyclo[3.1.0]hexan-1-yl)cyclopropyl)methyl acetate (dr 5:1)

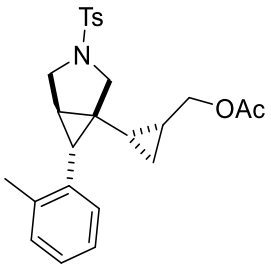

6af was isolated following the **GP-2** using **5h** (67.9 mg, 0.2 mmol) and allyl acetate (432 μL, 4.0 mmol) as reagents. Yield **38**% (33.5 mg, 0.076 mmol, **dr 5:1**). **^{1}H NMR** (400 MHz, $CDCl_3$) δ = 7.72 (d, J = 8.3 Hz, 2H), 7.33 (d, J = 7.9 Hz, 2H), 7.14 – 7.03 (m, 3H), 6.97 – 6.93 (m, 1H), 3.90 – 3.83 (m, 1H), 3.75 (d, J = 9.5 Hz, 1H), 3.69 (d, J = 9.6 Hz, 1H), 3.64 – 3.55 (m, 1H), 3.34 (dd, J = 9.7, 3.8 Hz, 1H), 3.25 (d, J = 9.5 Hz, 1H), 2.41 (s, 3H), 2.24 (s, 3H), 1.94 (s, 3H), 1.89 – 1.86 (m, 1H), 1.86 – 1.82 (m, 1H), 1.03 – 0.91 (m, 1H), 0.15 (td, J = 8.6, 5.7 Hz, 1H), -0.34 (q, J = 5.8 Hz, 1H). **^{13}C NMR** (101 MHz, $CDCl_3$) δ = 171.0 (Cq), 143.7 (Cq), 138.1 (Cq), 135.1 (Cq), 134.2 (Cq), 129.84 (2 CH), 129.79 (CH), 127.9 (CH), 127.5 (2 CH), 126.4 (CH), 125.5 (CH), 64.1 (CH_2), 55.0 (CH_2), 50.0 (CH_2), 33.1 (Cq), 28.3, 24.9, 21.6 (CH_3), 21.0 (CH_3), 19.9 (CH_3), 14.1 (CH), 13.6 (CH), 9.9 (CH_2). **ESI-MS** calcd for $C_{25}H_{29}NO_4S$ [M+Na]+ 462.18 found 461.85.

(1S,5R,6S)-4-methyl-3-(methylsulfonyl)-6-phenyl-1-((1R,2S,3r,4R,5S)-tricyclo[3.2.1.02,4]octan-3-yl)-3-azabicyclo[3.1.0]hexane

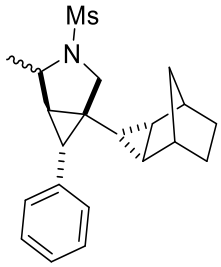

6ah was isolated following the **GP-2** using **5ah** (79.0 mg, 0.3 mmol) and norbornene (565.0 mg, 6 mmol) as reagents. Yield **52**% (55.3 mg, 0.155 mmol, ratio 1:0.5). **^{1}H NMR** (400 MHz, CDCl3) δ = δ 7.33 – 7.14 (m, 5HA, 5HB), 4.08 (q, J = 6.4 Hz, 1HB), 3.89 – 3.81 (m, 1HA), 3.63 – 3.58 (m, 1HA, 1HB), 3.43 – 3.35 (m, 1HA, 1HB), 2.87 (s, 3HA), 2.86 (s, 3HB), 2.24 (d, J = 4.1 Hz, 1HA), 2.20 – 2.14 (m, 1HA, 1HB), 2.01 (d, J = 4.2 Hz, 1HB), 1.82 – 1.75 (m, 2HA, 1HB), 1.45 (d, J = 6.0 Hz, 3HA), 1.44 – 1.41 (m, 1HB), 1.38 – 1.30 (m, 2HA, 2HB), 1.28 (d, J = 6.4 Hz, 3HB), 1.19 – 1.02 (m, 2HA, 2HB), 0.74 – 0.68 (m, 1HA, 1HB), 0.66 (t, J = 3.0 Hz, 1HA, 1HB), 0.57 – 0.45 (m, 2HA, 2HB), 0.27 – 0.21 (m, 1HA, 1HB). **(Major)**

^{13}C NMR (101 MHz, CDCl3) δ = 137.7 (Cq),129.27 (2CH), 128.09 (2CH), 126.19 (CH), 57.73 (CH), 57.40 (CH2), 36.49 (CH_3), 35.86 (CH), 35.61 (CH), 33.62 (CH), 31.47 (Cq), 29.52 (CH2), 29.43 (CH2), 28.38 (CH2), 28.10 (CH), 23.50 (CH), 21.87 (CH), 18.89 (CH3), 11.62 (CH). **(Minor) ^{13}C NMR** (101 MHz, CDCl3) δ =137.3 (Cq), 129.21 (2CH), 128.09 (2CH), 126.19 (CH), 58.52 (CH), 52.69 (CH2), 39.68 (CH_3), 35.89 (CH), 35.62 (CH), 34.31 (Cq), 32.47 (CH), 30.53 (CH), 29.52 (CH2), 29.41 (CH2), 28.48 (CH2), 23.68 (CH), 21.76 CH), 21.35 (CH3), 11.04 (CH). **ESI-MS** calcd for $C_{21}H_{27}NO_2S$ [M+Na]+ 380.18 found 380.03.

(1S,5R,6S)-3-(methylsulfonyl)-4,6-diphenyl-1-((1R,2S,3r,4R,5S)-tricyclo[3.2.1.02,4]octan-3-yl)-3-azabicyclo[3.1.0]hexane

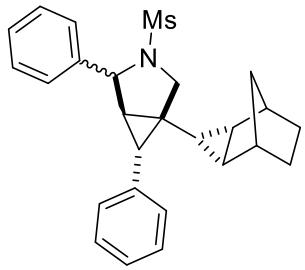

6ai was isolated following the **GP-2** using **5ai** (97.6 mg, 0.3 mmol) and norbornene (565.0 mg, 6 mmol) as reagents. Yield **Dia1 23**% (29.1 mg, 0.069 mmol). Yield **Dia2 16**% (20.0 mg, 0.048 mmol).

Dia1: **^{1}H NMR** (400 MHz, CDCl3) δ = 7.49 – 7.28 (m, 7H), 7.27 – 7.17 (m, 3H), 5.02 (s, 1H), 3.85 (d, J = 9.5 Hz, 1H), 3.55 (d, J = 9.5 Hz, 1H), 2.40 (s, 3H), 2.36 – 2.32 (m, 1H), 2.20 – 2.17 (m, 1H), 1.92 – 1.88 (m, 1H), 1.83 (d, J = 4.1 Hz, 1H), 1.40 – 1.30 (m, 2H), 1.21 – 1.09 (m, 2H), 0.75 – 0.66 (m, 3H), 0.51 (d, J = 10.2 Hz, 1H), 0.47 – 0.44 (m, 1H). **^{13}C NMR** (101 MHz, $CDCl_3$) δ = 141.2 (Cq), 137.1 (Cq), 129.15 (2 CH), 129.09 (2 CH), 128.3 (CH), 128.1 (2 CH), 127.1 (2 CH), 126.2 (CH), 66.0 (CH), 53.7 (CH_2), 39.2 (CH_3), 36.0 (CH), 35.7 (CH), 34.9 (Cq), 33.6 (CH), 31.5 (CH), 29.5 (CH_2), 29.4 (CH_2), 28.3 (CH_2), 23.1 (CH), 21.6 (CH), 11.6 (CH). **ESI-MS** calcd for $C_{26}H_{29}NO_2S$ [M+Na]+ 442.19 found 441.81.

Dia2: **^{1}H NMR** (400 MHz, CDCl3) δ = 7.51 – 7.44 (m, 2H), 7.38 – 7.27 (m, 3H), 7.27 – 7.15 (m, 3H), 7.12 – 7.05 (m, 2H), 4.80 (d, J = 4.1 Hz, 1H), 3.76 – 3.69 (m, 2H), 2.70 (d, J = 4.2 Hz, 1H), 2.54 (s, 3H), 2.23 – 2.18 (m, 1H), 1.99 (t, J = 4.2 Hz, 1H), 1.82 – 1.77 (m, 1H), 1.38 – 1.29 (m, 2H), 1.17 – 1.06 (m, 2H), 0.76 – 0.70 (m, 2H), 0.68 – 0.63 (m, 1H), 0.53 – 0.47

(m, 1H), 0.28 – 0.23 (m, 1H). **^{13}C NMR** (101 MHz, $CDCl_3$) δ = 139.2 (Cq), 137.4 (Cq), 129.4 (2 CH), 128.7 (2 CH), 128.4 (CH), 128.1 (2 CH), 127.7 (2CH), 126.3 (CH), 65.2 (CH), 56.5 (CH_2), 39.6 (CH_3), 35.9 (CH), 35.6 (CH), 35.2 (CH), 31.7 (Cq), 29.5 (CH2), 29.4 (CH2), 28.9 (CH), 28.4 (CH2), 23.4 (CH), 21.9 (CH), 11.8 (CH). **ESI-MS** calcd for $C_{26}H_{29}NO_2S$ [M+Na]+ 442.19 found 441.94.

(1S,5R,6S)-6-phenyl-1-((1R,2S,3r,4R,5S)-tricyclo[3.2.1.02,4]octan-3-yl)-3-oxabicyclo[3.1.0]hexane

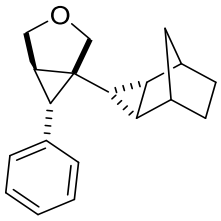

6aa was isolated following the **GP-2** using **5aa** (34.5 mg, 0.2 mmol) and norbornene (376.6 mg, 4 mmol) as reagents. Yield **39**% (28.1 mg, 0.077 mmol). **^{1}H NMR** (400 MHz, $CDCl_3$) δ = 7.31 – 7.25 (m, 2H), 7.22 – 7.15 (m, 3H), 3.92 (d, *J* = 8.1 Hz, 1H), 3.85 (d, *J* = 8.2 Hz, 1H), 3.75 (dd, *J* = 8.1, 2.9 Hz, 1H), 3.64 (d, *J* = 8.2 Hz, 1H), 2.16 – 2.13 (m, 1H), 2.07 (d, *J* = 4.3 Hz, 1H), 1.86 (dd, *J* = 3.4, 1.7 Hz, 1H), 1.72 – 1.68 (m, 1H), 1.37 – 1.28 (m, 2H), 1.20 – 1.06 (m, 2H), 0.76 – 0.69 (m, 1H), 0.68 – 0.63 (m, 1H), 0.60 – 0.53 (m, 1H), 0.47 (d, *J* = 10.5 Hz, 1H), 0.37 – 0.32 (m, 1H). **^{13}C NMR** (101 MHz, $CDCl_3$) δ = 138.4 (Cq), 129.1 (2CH), 128.0 (2CH), 125.8 (CH), 73.8 (CH_2), 70.5 (CH_2), 36.0 (CH), 35.7 (CH), 35.4 (Cq), 29.6 (CH_2), 29.5 (CH_2), 29.4 (CH), 28.4 (CH_2), 27.4 (CH), 23.6 (CH), 21.8 (CH), 10.1 (CH). **ESI-MS** calcd for $C_{19}H_{22}O$ [M+Na]+ 289.17 found 289.41.

((1R,2S)-2-((1S,5R,6S)-6-phenyl-3-oxabicyclo[3.1.0]hexan-1-yl)cyclopropyl)methyl acetate (dr 5.5:1)

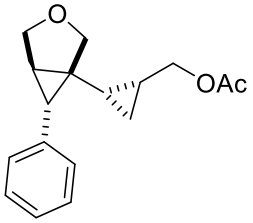

6ab was isolated following the **GP-2** using **5aa** (104.5 mg, 0.6 mmol) and allyl acetate (1.3 mL, 12 mmol) as reagents. Yield **37**% (60.1 mg, 0.22 mmol, **dr 5.5:1**). **^{1}H NMR** (400 MHz,

$CDCl_3$) δ = 7.29 – 7.23 (m, 2H), 7.22 – 7.16 (m, 3H), 4.10 – 4.04 (m, 1H), 4.00 – 3.87 (m, 3H), 3.85 – 3.81 (m, 1H), 3.72 (d, J = 8.2 Hz, 1H), 2.15 (d, J = 4.3 Hz, 1H), 2.05 (s, 3H), 1.90 – 1.87 (m, 1H), 1.13 – 1.03 (m, 2H), 0.40 (td, J = 8.6, 5.4 Hz, 1H), -0.11 (q, J = 5.7 Hz, 1H). **^{13}C NMR** (101 MHz, $CDCl_3$) δ = 171.2 (Cq), 137.8 (Cq), 129.2 (2CH), 128.1 (2CH), 126.0 (CH), 74.3 (CH_2), 69.7 (CH_2), 65.0 (CH_2), 34.3 (Cq), 28.6 (CH), 27.7 (CH), 21.2 (CH_3), 14.0 (CH), 13.8 (CH), 10.2(CH_2). **ESI-MS** calcd for $C_{17}H_{20}O_3$ [M+Na]+ 295.14 found 295.95.

Dimethyl (1R,5R,6S)-1-((1S,2R)-2-(acetoxymethyl)cyclopropyl)-6-phenylbicyclo[3.1.0]hexane-3,3-dicarboxylate (dr 5:1)

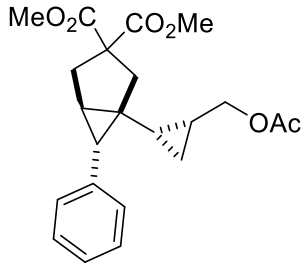

6ad was isolated following the **GP-2** using **5ad** (57.3 mg, 0.2 mmol) and allyl acetate (432 μL, 4 mmol) as reagents. Yield **26**% (20.4 mg, 0.053 mmol, **dr 5:1**). **^{1}H NMR** (400 MHz, $CDCl_3$) δ = 7.25 – 7.19 (m, 2H), 7.18 – 7.11 (m, 3H), 4.11 (dd, J = 11.6, 6.7 Hz, 1H), 3.88 (dd, J = 11.6, 8.1 Hz, 1H), 3.72 (d, J = 17.6 Hz, 6H), 2.87 (d, J = 14.1 Hz, 1H), 2.77 (d, J = 13.8 Hz, 1H), 2.63 – 2.54 (m, 2H), 2.07 (s, 3H), 1.78 (d, J = 4.2 Hz, 1H), 1.71 (t, J = 4.5 Hz, 1H), 1.16 – 1.00 (m, 2H), 0.22 (td, J = 8.7, 5.5 Hz, 1H), -0.26 (q, J = 5.7 Hz, 1H). **^{13}C NMR** (101 MHz, $CDCl_3$) δ = 173.4 (Cq), 172.3 (Cq), 171.4 (Cq), 138.3 (Cq), 129.4 (2CH), 128.0 (2CH), 125.9 (CH), 64.9 (CH_2), 60.1 (Cq), 53.14 (CH_3), 53.12 (CH_3), 42.6 (CH_2), 36.2 (CH_2), 34.6 (Cq), 30.3 (CH), 27.7 (CH), 21.3 (CH_3), 17.5 (CH), 14.2 (CH), 10.3 (CH_2). **ESI-MS** calcd for $C_{22}H_{26}O_6$ [M+Na]+ 409.17 found 409.24.

A new family of efficient Ir(III) photosensitizers featuring pendant radical-stabilizing naphthyl functions

3.1 Introduction: Iridium Photosensitizers

As clarified in the previous chapter, the activation of a substrate either involves an energy transfer (EnT) or an electron transfer process (SET). Sometimes the two mechanisms may overlap or, less often, they may work in synergy. In the following section we will always refer to the simple Energy transfer mediated photocatalysis. Photocatalysts which undergo energy transfer are frequently referred to as photosensitizers.

When photosensitizers absorb photons from incident light, they undergo a transformation into an excited singlet state, which then goes through Intersystem crossing, causing the lone electron to switch its intrinsic spin state, resulting in the creation of an excited triplet state (Figure 12). The prolonged lifespan of the triplet states, compared to the singlet state, enhances the likelihood of energy transfer by interaction with neighboring molecules.

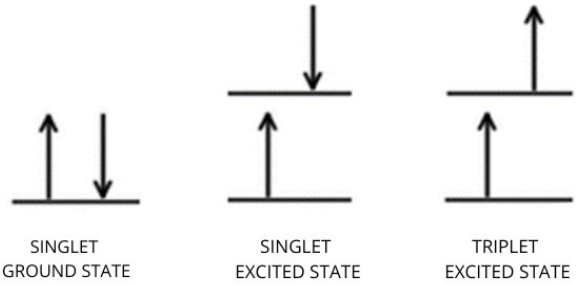

Figure 12: Excitation via absorption of radiation and Intersystem crossing

Photosensitizers can be distinguished into three broad categories, based on their molecular structure: organometallic photosensitizers, organic photosensitizers, and nanomaterial photosensitizers. In this chapter we are going to focus our attention solely on the first group.

Organometallic photosensitizers consist of a metal atom coordinated with at least one organic ligand. Popular metals for this application are Iridium, Rhodium and Ruthenium, thanks to their electron rich centers (highly filled d-orbitals). The interaction between the metal center and the ligand, in the form of a MLCT, leads to a large continuum of orbitals which allows for excited electrons to switch multiplicities via intersystem crossing. In these organometallic complexes, the MLCT absorption energy correspond to the visible part of the spectrum, since the metal d-orbitals are relatively close in energy to the ligand π^* orbitals.

Among organometallic photosensitizers, Iridium is the most common metallic center, due to the high triplet-state energy and lifetime of the corresponding cyclometalated complexes. Indeed, fac-Ir(ppy)$_3$, which is the most accessible Ir photosensitizer, has a triplet energy of 59.5 kcal mol^{-1} and a triplet lifetime of 4.7 μs measured in degassed CH_3CN (see

Experimental Section). Modifications of the coordination environment around the metallic center lead to complexes with a broad variety of photophysical parameters. Exploiting this property, a large pool of different Iridium photocatalysts have been proposed in the last decade.[50–53]

Two major subclasses can be detected among Iridium photocatalysts: homoleptic and heteroleptic Iridium cyclometalated complexes (Figure 13). The first class comprehend fac-Ir(ppy)$_3$ and its direct derivatives with general formula Ir(C^N)$_3$, such as fac-[Ir(dF-ppy)$_3$]. On the other hand, heteroleptic Iridium complexes are cationic molecules bearing an ancillary bipyridine ligand resulting in the general formula [Ir(C^N)$_2$(N^N)]$^+$. Among this class, the most common catalysts are Ir(dF(CF$_3$)ppy)$_2$(dtbbpy)(PF$_6$), Ir(dF(CF$_3$)ppy)$_2$(bpy)(PF$_6$) and Ir(ppy)$_2$(dtbbpy)(PF$_6$).

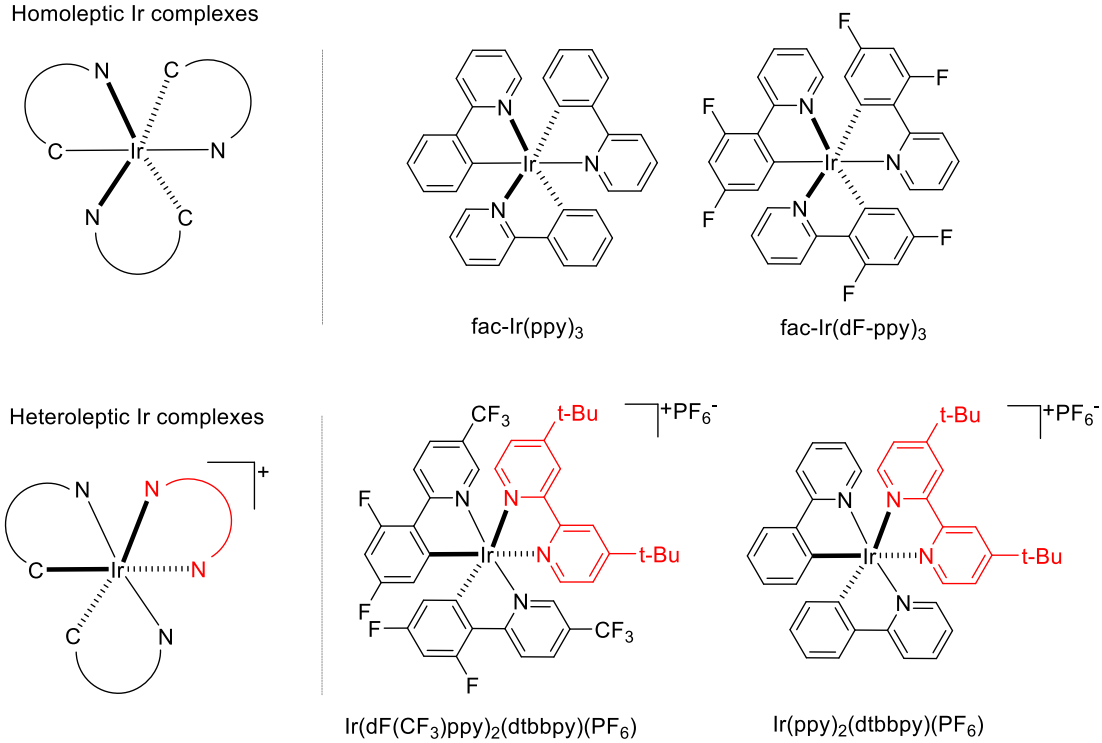

Figure 13:General formula and examples of Homoleptic and Heteroleptic Iridium complexes.

Di Luzio, Bernhard and co-workers reported in 2021 the High-Throughput Screening of the Triplet Photophysical Properties of Structurally Diverse Heteroleptic Iridium(III) Complexes.[54] Their huge effort (1440 distinct heteroleptic[Ir(C^N)$_2$(N^N)]$^+$ complexes were prepared via combinatorial parallelized synthesis) significantly increased the understanding on how the coordination environment of the metallic center can influence the properties of Iridium photocatalyst. The authors noticed that it was possible to intentionally adjust the photophysical characteristics of [Ir(C^N)$_2$(N^N)]$^+$ complexes by modifying the energies of

the highest occupied molecular orbital (HOMO) and lowest unoccupied molecular orbital (LUMO) (Figure 14). In most instances, these complexes exhibit a HOMO primarily concentrated on the Ir(III) d orbitals and, in addition, on the π orbitals of the cyclometalating ligand's phenyl ring. On the other hand, the LUMO is localized on π* orbitals of the ancillary ligands. As a result, the lowest energy absorption in $[Ir(C^N)_2(N^N)]^+$ can be attributed to a dπ→π* metal/ligand-to-ligand charge transfer (MLLCT) process.

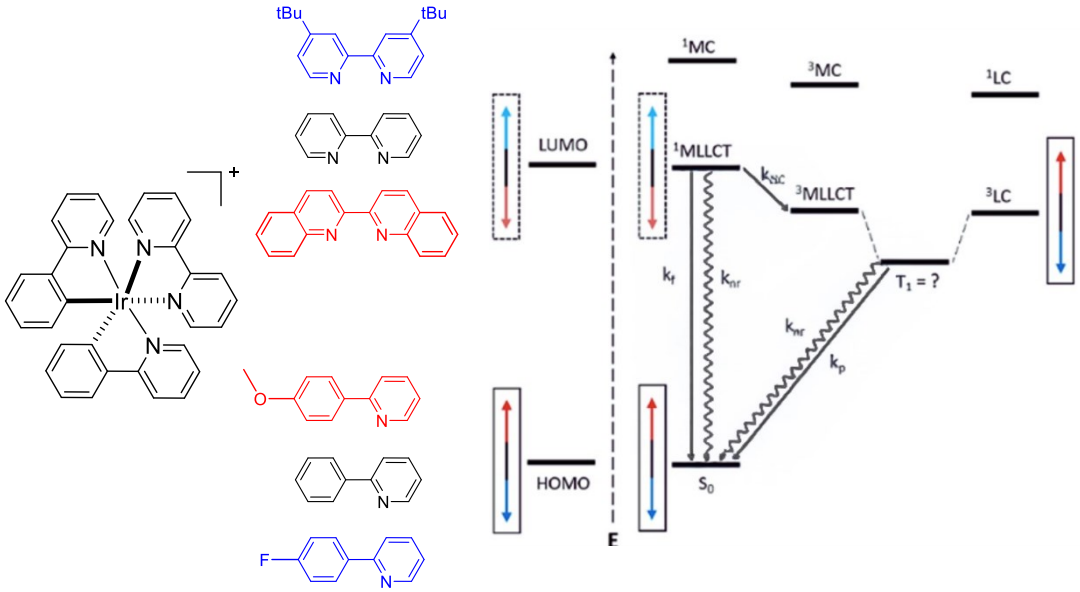

Figure 14: Archetypal $[Ir(C^N)_2(N^N)]^+$complex where cyclometalating and ancillary ligand are 2-phenylpyridine and 2,2'-bipyridine,respectively. Ligand manipulation affords Ir(III) complexes with variable HOMO-LUMO gap. From DiLuzio et al.[54]

This is not always the case, in fact the authors divided the enormous pool of synthetized Iridium (III) complexes into 4 categories according to their emission spectra, which is simply the result of the different charge-transfer bands. Type I excited states display broad and plain emission profiles, while Type IV states exhibit well-defined vibronic substructures. The characteristics of these two extreme excited states are classified as pure MLLCT for Type I and pure LC (ligand-centered) for Type IV. Both Type II/III are instead characterized as mixed MLLCT/LC character where MLLCT dominates the former and LC dominates the latter.

By increasing the energy gap, which can be achieved by incorporating electron-withdrawing substituents on the cyclometalating ligand (stabilization of the HOMO) or electron-donating substituents on the ancillary ligand (destabilization of LUMO), the difference in energy between the MLLCT and LC energy levels decreases. When these two states are sufficiently close in energy, the authors begin to classify these excited state Iridium complexes as Type II. Type II complexes are characterized by emission spectra with an

asymmetric shape and a single exponential decay in the excited state lifetime. Further pushing on the stabilization of the highest occupied molecular orbital (HOMO) and/or on the destabilization of the lowest unoccupied molecular orbital (LUMO) eventually leads to complexes with an increasing presence of LC characteristics (Type III and Type IV). Conceptually, the transition from Type I to Type III/IV excited states represents the intramolecular electron transfer from the ancillary ligand to the cyclometalating ligands.

The shift from Type I to Type III/IV complexes, roughly represented by the rise of the wavelength of maximum emission, comes with the gradual increase of the triplet state energy. Moreover, despite a difficult correlation, it is possible to see the lifetime of the excited state of these complexes as a proportional function of their triplet state energy or, in alternative, of their wavelength of maximum emission.

3.2 Introduction: Naphtalene as a radical stabilizing additive[55]

Our research group recently reported the "Visible-Light Promoted Intramolecular para-Cycloadditions on Simple Aromatics",[55] catalyzed by fac-Ir(ppy)$_3$, where an unprecedent stabilization effect of naphthalene, or its derivatives, towards transient (bi)-radicals was observed (Table 3).

Table 3: Selected optimization reactions showing the role of the additive in the model cycloaddition. [a]Reaction conditions: 0.15 mmol of S1-2 (0.1M in DMF), 1 mol% sensitizer, in 5 mm NMR tube under nitrogen atmosphere, isolated yields. [b]in toluene. [c] with 10 mol % of thioxanthone (TXT). [d] without light. From Maestri et al.[55]

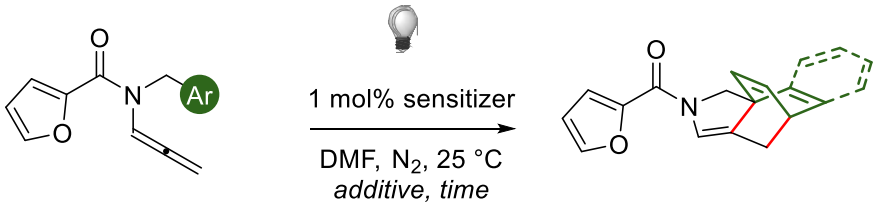

S1, Ar= Ph
S2, Ar= 1-naphtyl

P1-2

Entry	Reagent	Sensitizer	Additive (eq)	t (h)	Yield (%)
1	S1	Ir(ppy)$_3$	-	240	46
2[b]	S1	Ir(ppy)$_3$	-	240	44
3[c]	S1	TXT	-	240	-
4	S1	Ir(p-F-ppy)$_3$	-	96	45
5	S2	Ir(ppy)$_3$	-	3	99
6	S1	Ir(ppy)$_3$	$C_{10}H_8$ (10)	48	60
7	S1	Ir(ppy)$_3$	$C_{10}H_8$ (20)	38	64
8	S1	Ir(ppy)$_3$	$C_{10}H_8$ - OMe (10)	24	70
9	S2	-	-	96	-
10[d]	S2	Ir(ppy)$_3$	-	96	-

Naphthalene, which is used as an additive in super-stoichiometric ratio (20 equivalents in the optimized conditions), likely stabilize radicals through its π cloud, granting a drastic increase in the reaction rate and in the yield of the presented intramolecular cycloaddition.

In order to better comprehend this phenomenon, three different reactions were modelled in presence of a molecule of naphthalene (Figure 15). The first one has the naphthalene parallel to the allenyl arm of the substrate **S3**, the second one has it stacked to its benzyl ring, while the third one has two naphthalene units nearby each arm of the reagent (α, β and γ, respectively). These systems underwent a reoptimization process that considered dispersion

interactions. In all instances, the biradicals **I**, **TS**, and **II** exhibited greater stability compared to their respective entry channels. This stabilization effect was more pronounced for intermediates II, with an energy difference of 2.1–4.5 kcal/mol, while **I** and **TS** showed a relatively smaller stabilization ranging from 0.7 to 2.6 kcal/mol. Additionally, **TS2s** were found to be slightly favoured over **TS1s** by 0.1–2.4 kcal/mol, and the naphthalene-P3 adducts were less energetically demanding by 1.2–3.2 kcal/mol. These collective observations provide a plausible explanation for the increased reaction rate observed in the presence of naphthalene, as the additive reduces the likelihood of unproductive sensitization of the subtrate.[55]

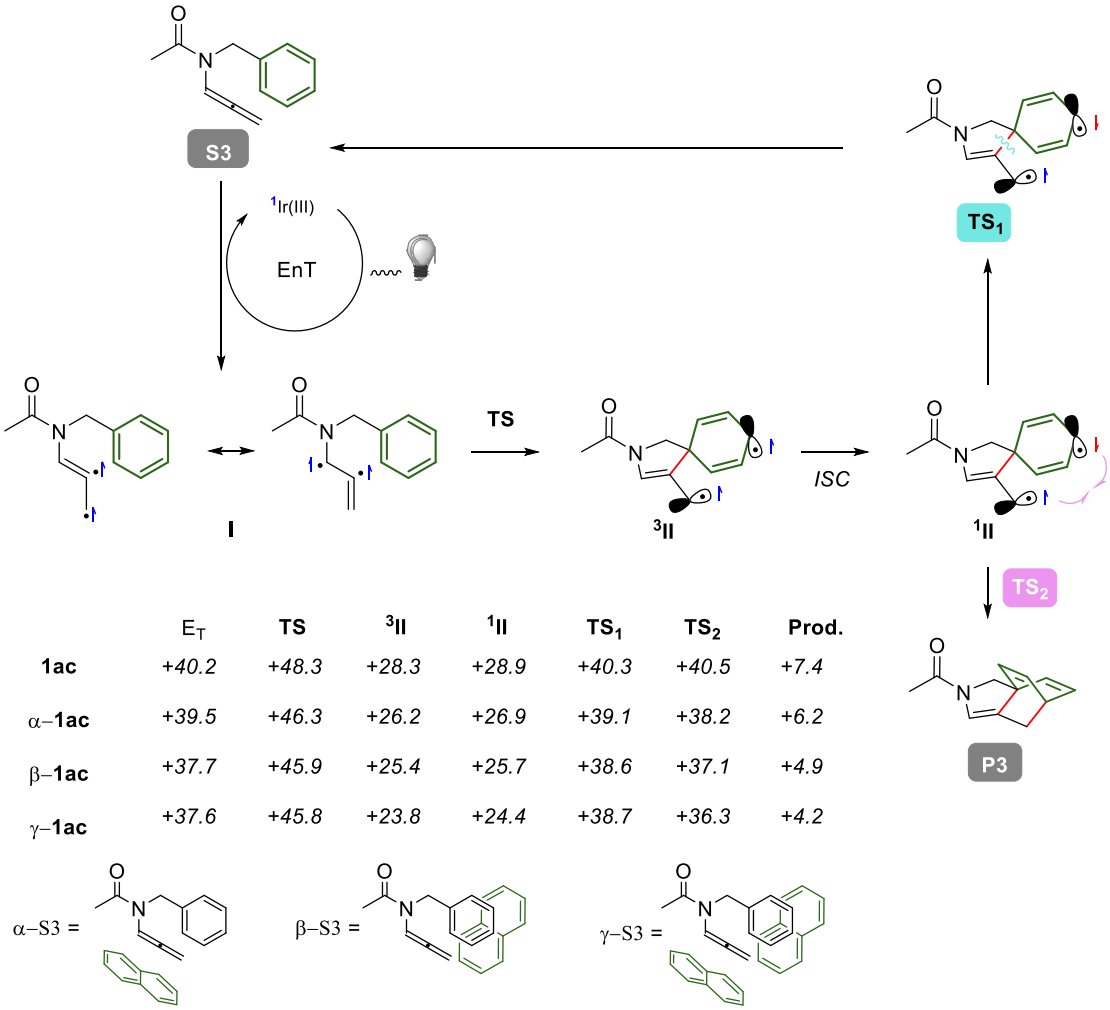

	E_T	TS	^{3}II	^{1}II	TS_1	TS_2	Prod.
1ac	*+40.2*	*+48.3*	*+28.3*	*+28.9*	*+40.3*	*+40.5*	*+7.4*
α–**1ac**	*+39.5*	*+46.3*	*+26.2*	*+26.9*	*+39.1*	*+38.2*	*+6.2*
β–**1ac**	*+37.7*	*+45.9*	*+25.4*	*+25.7*	*+38.6*	*+37.1*	*+4.9*
γ–**1ac**	*+37.6*	*+45.8*	*+23.8*	*+24.4*	*+38.7*	*+36.3*	*+4.2*

Figure 15: Mechanistic studies. M06/Def2-TVZP, D3 disp. Correction, CPCM=DMF, ΔG calues in kcal/mol @298.15 K. From Maestri et al.[55]

This concept has not been previously exploited in synthesis. Its unexplored potential suggests that there are numerous opportunities for further exploration and development in the coming years.

3.3 Results and discussion

Inspired by the key role of naphthalene as described in section 3.2, we conceived a novel approach to exploit its unique and unexplored attributes while combining it to an effective iridium photosensitizer. The idea was to achieve improved stability and reactivity, all while circumventing the necessity of the use of naphthalene in large excess. In other words, our ambition was to establish a clear departure from the reported approach that involves the excessive use of naphthalene as an additive. Instead, we aimed to seamlessly integrate this functionality into the Ir photosensitizers themselves, creating a more efficient and streamlined catalytic process.

To realize this concept, we started a synthetic effort to generate a series of novel iridium photosensitizers adorned with naphthyl functional groups, which we referred to as **PCSs**. In certain instances, the newly synthesized naphthyl-functionalized Ir photosensitizers (e.g. **PCS5**) demonstrated superior catalytic activity when compared to their simpler precursor $Ir(ppy)_2(bpy)$, as well as to the widely-used $Ir(ppy)_3$ and to the naphtyl-free counterpart **PCS7** (Figure 16). These promising findings showcased the potential of our approach and suggested that the introduction of naphthyl functionality had a significant impact on catalytic performance in various model cycloaddition reactions.

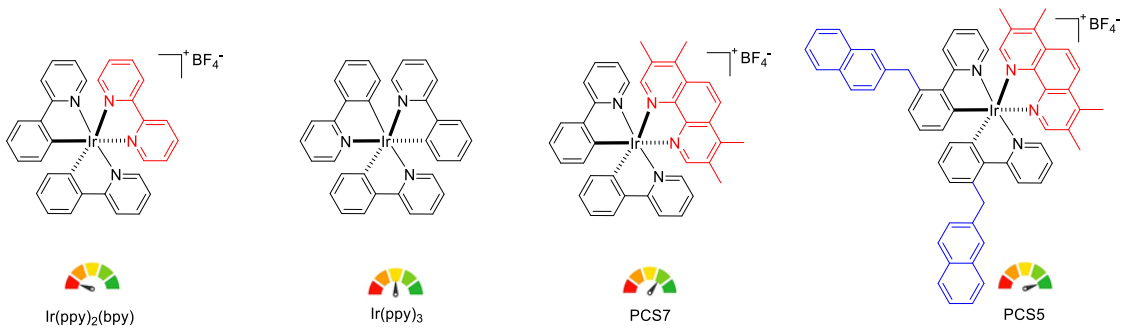

Figure 16: Qualitative indication on the catalytic activity of fac-$Ir(ppy)_3$, $Ir(ppy)_2(bpy)(BF_4)$ and selected PCSs in investigated cycloaddition reactions.

Our work not only expanded the scope of Ir-based photosensitizers but also underscored the importance of innovative molecular design in the realm of catalysis. By strategically incorporating naphthalene-derived motifs into these photosensitizers, we unlocked new avenues for enhancing reactivity and stability in selected model reactions.

The first step towards the synthesis of our naphthyl-functionalized Iridium photosensitizers (**PCSs**) demands the creation of the corresponding Iridium dimers, denoted as **8a-c**. This is achieved through a chemical process consisting in the reaction of $IrCl_3$ salt

with the corresponding C^N cyclometalated ligand. The reaction is conducted in a solvent mixture of ethoxy-ethanol and water, and it proceeds at 120 °C for 24 hours. The C^N cyclometalated ligand used as a starting point for this transformation can be the straightforward 2-Phenylpyridine **7a**, or its derivatives **7b-c**. These derivatives exhibit a structural modification where the phenyl ring is adorned with a pendant (2-Naphthyl)methylene unit. This pendant unit can be strategically positioned either in the ortho (**7b**) or para (**7c**) position relative to the pyridine ring. **7b** was obtained through C-H functionalization of **7a** upon treatment with 2-(Bromomethyl)naphthalene in the presence of a Ruthenium catalyst and blue light irradiation.[56] **7c** instead required a more complex synthetic route, which started from the preparation of 2-(4-Bromophenyl)pyridine from the simple 2-Bromopyridine. Then, the conversion to the corresponding boronic acid and the following Suzuki coupling with 2-(Bromomethyl)naphthalene finally gave the desired ligand **7c**.

Upon successfully generating the dimers **8a-c** by treatment of these ligands with $IrCl_3$, the subsequent step involves their reaction with various N^N bipyridine ligands labelled as **A** to **F**. This reaction takes place in a solvent mixture composed of CH_2Cl_2 and MeOH. Then, to finalize the synthesis of the desired Naphthyl-functionalized Iridium photosensitizers (**PCSs**), NH_4BF_4 is introduced into the reaction mixture. This entire synthetic process is illustrated in Scheme 29.

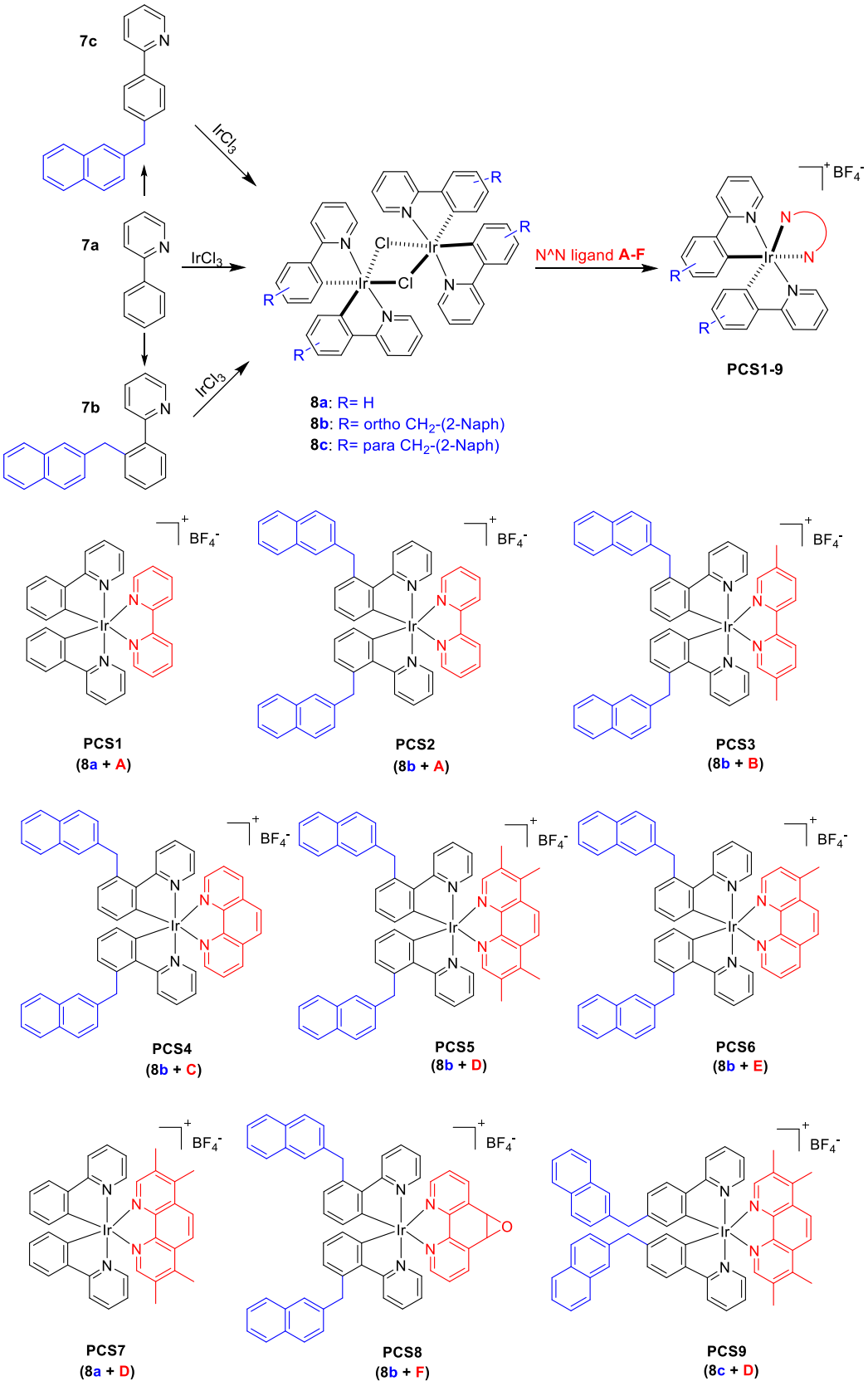

*Scheme 29: Synthesis of **PCS1-9**.*

PCS1 is the archetypical $[Ir(ppy)_2(bpy)]^+[BF_4]^-$. **PCS2** is the analogous of **PCS1**, which bears, in addition, a pendant naphthyl unit on ortho position on the phenyl ring of the two phenylpyridines. The crystal structure of **PCS2** has been obtained by XRD diffraction (Figure 17).

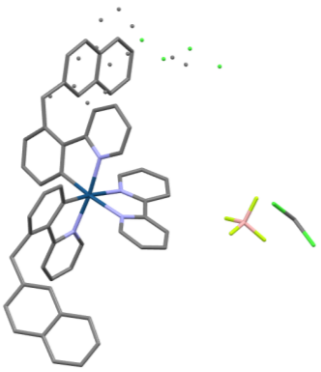

*Figure17: Crystal structure of **PCS2** obtained by XRD.*

Replacing the simple bipyridine of **PCS2** with di-methyl substituted bipyridine **B** or with differently functionalized phenanthrolines **C**-**D**-**E**-**F**, we obtained **PCS3, 4**, **5**, **6**, **8**. Instead, **PCS7** and **9** include the same ancillary ligand **D** contained in **PCS5**, but their cyclometalated ligands are simple unfunctionalized phenylpyridines (**PCS7**) or phenylpyridines para-functionalized with the pendant naphthyl unit (**PCS9**).

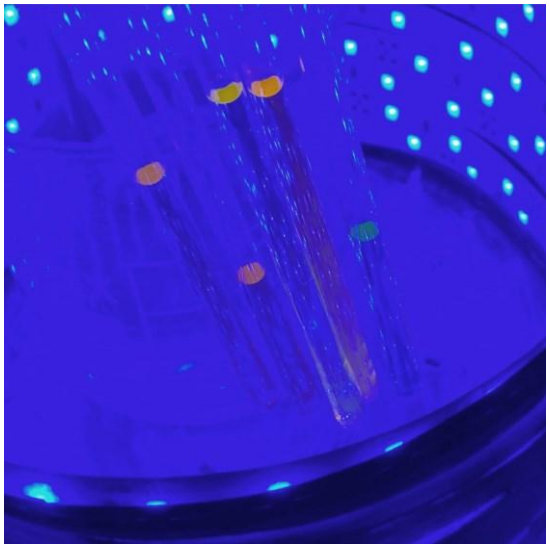

Figure 18: Different PCSs shows difference fluorescence under blue light irradiation.

In our quest to evaluate the catalytic ability of **PCS1-9**, we systematically investigated their performance in three model cycloaddition reactions. The first of these reactions, which is widely documented in the existing literature, is the isomerization of cinnamyl alcohol **9a**[57]. The choice of this specific reaction is deliberate, as it allows us to rigorously examine the

catalytic activity of **PCS1-9** under conditions that are well-documented and widely accepted within the scientific community (Scheme 29). Then, the 2+2 cycloaddition of styrene **9b** [58] was taken into consideration. This particularly challenging cycloaddition was chosen since commercially available photosensitizers such as fac-Ir(ppy)$_3$ and Ir(dF(CF$_3$)ppy)$_2$(dtbbpy)(PF$_6$) failed to give complete conversion and optimum yields in the mild conditions we adopted (Scheme 29). After that, we decided to investigate a third model reaction, which is the 4+2 dearomative cycloaddition of substrate **9c** (Scheme 30). Unlike the reactivity associated with **9a** and **9b**, the cycloaddition of **9c** was recently discovered, for the first time, by our group.

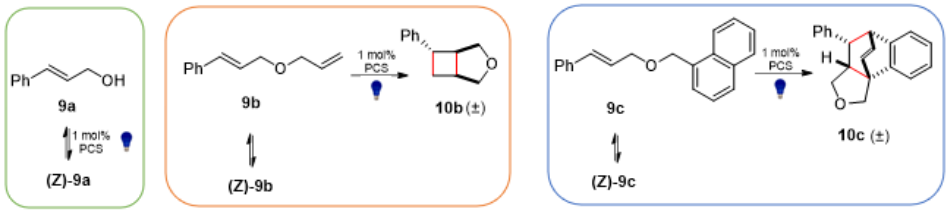

	9a	(Z)-9a	9b	(Z)-9b	10b[c]	9c	(Z)-9c	10c[d]
fac-Ir(ppy)$_3$	66	34	11	50	21	21	18	46
[Ir]-F[b]	69	31	2	4	65	14	9	64
PCS1	94	6	91	0	0	78	7	0
PCS2	93	7	92	traces	0	63	18	traces
PCS3	89	11	38	38	7	31	26	26
PCS4	97	3	70	11	traces	52	31	traces
PCS5	29	71	0	traces	86[a]	0	traces	89[a]
PCS6	91	9	28	42	5	30	32	13
PCS7	31	69	0	0	72[a]	0	0	81[a]
PCS8	97	3	80	traces	0	68	13	traces
PCS9	40	60	2	4	72[a]	0	0	85[a]

Scheme 30: Reaction conditions A: 0.1 mmol of 3a (0.1 M in MeCN/CHCl$_3$ 7/3), 1 mol % photosensitizer, 1h, blue led, r.t.; B: 0.1 mmol of 3b (0.05 M in MeCN), 1 mol % photosensitizer, 4h, blue led, r.t.; C: 0.1 mmol of 3c (0.1 M in CH$_2$Cl$_2$), 1 mol % photosensitizer, 16h, blue led, r.t.

[a] yield calculated on the isolated product (column chromatography) [b] Ir(dF(CF$_3$)ppy)$_2$(dtbbpy)(PF$_6$) [c] d.r. 86/14 [d]: d.r. 82/18

The conversion of **9a** towards its Z isomer, as well as the polycyclization of substrates **9b** and **9c**, worked only partly, in the selected conditions, using the commercially available sensitizers fac-Ir(ppy)$_3$ and the widely known cationic iridium complex Ir(dF(CF$_3$)ppy)$_2$(dtbbpy)(PF$_6$), sometimes abbreviated in [Ir]-F. Using instead the synthetized photosensitizers (**PCS1-9**) we observed a broad range of results. **PCS1**,**2**,**4**,**8** displayed almost total inertness in these conditions. **PCS3** and **PCS6** exhibited an improvement in terms of

catalytic activity, compared to the aforementioned PCSs, but only **PCS5**,**7**,**9** proved to be effective sensitizers, with conversions up to 71% in model reaction A, 86% in model reaction B and 89% in model reaction C.

These results evidently imply that the nature of the N^N ligand on the photosensitizer is crucial, indeed the best results were obtained with the three catalysts bearing N^N ligand **D** (**PCS5**,**7** and **9**). Surprisingly, these remarkably active PCSs outperformed the widely used Iridium photocatalysts fac-Ir(ppy)$_3$ and Ir(dF(CF$_3$)ppy)$_2$(dtbbpy)(PF$_6$).

The use of 3,4,7,8-Tetramethyl-1,10-phenanthroline (N^N ligand **D**) as ancillary ligand in ionic transition metal complexes (iTMCs) has been reported mainly for electroluminescent applications.[59,60] The marked electron donating properties of ligand **D**, together with the structural rigidity of the 1,10-phenanthroline scaffold, causes a relatively high destabilization of the LUMO, leading to a blue shift of the emission spectrum, due to the broadening of the Energy gap. In other words, the triplet state energy of the corresponding Iridium complexes increases significantly. For this reason, alongside Materials Chemistry's applications, these properties make ligand **D** an interesting ancillary ligand for a potential Iridium photosensitizer, rationalizing the results we observed in catalysis with our **PCS5**,**7** and **9**.

Moreover, the increase in the yield of the formation of **Z-9a**, **10b** and **10c** using **PCS5**, compared to the simple **PCS7**, suggests that the pendant naphthyl units effectively play a role in the process. We believe that the naphthyl's extended π cloud can support the stabilization of transient bi-radicals on the highly energetic intermediates involved, leading to a cleaner and faster reaction path, as exemplified for model reaction B in Scheme 31. Albeit limited, the yield's growth is noteworthy considering that, when used as a separate additive, 20 equivalents of naphthalene are required to significantly boost a reaction.[55]

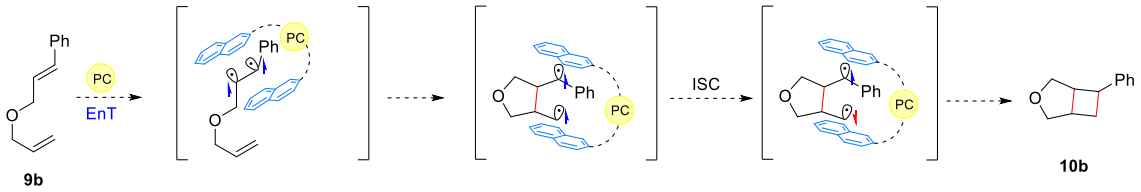

Scheme 31: Proposed rationalization of the positive effect of the pendant naphthyl unit on model cycloaddition B.

At that point, in order to better rationalize the catalytic behaviour of **PCS1-9**, we investigated their photophysical properties, namely the maximum wavelength of emission, the triplet state energy and triplet state lifetime (Table 4).

Table 4: [a] Triplet state energies were calculated measuring the intersection on the x axis of the tangent to the high energy side of the phosphorescence curve, $E_t=(h*c*Na)/\lambda$; [b] values reported by Glorius;[40] [c] τ were measured in degassed CH_3CN

Photosensitizer	$\lambda_{max\ emission}$	E_t (kcal mol^{-1}) [a]	τ (ns) [c]
$Ir(ppy)_3$	518	59.5 (58.1[b])	4679
$Ir(dF(CF_3)ppy)_2(dtbbpy))(PF_6)$	473	63.8	
PCS1	608	55.3	337[b]
PCS2	580	56.7	235
PCS3	551	57.9	873
PCS4	575	56.4	609
PCS5	**527**	**61.3**	**1825**
PCS6	565	57.2	821
PCS7	**525**	**61.6**	**1867**
PCS8	580	57.7	210
PCS9	551	59.5	

As expected, the photocatalysts bearing ancillary ligand **D** (**PCS5**,**7** and **9**) are the ones with the more blue-shifted emission spectrum (527, 525 and 551 nm respectively), resulting consequently in the highest triplet state energies (Table 4 and Figure 19). In particular, in the case of **PCS5** and **7**, the triplet state energy is comparable with that of powerful photosensitizer $Ir(dF(CF_3)ppy)_2(dtbbpy))(PF_6)$. Alongside the electronic influence of the methyl groups of ligand **D**, an additional contribution to the triplet state energy of these complexes comes from the structural rigidity of 1,10-phenanthroline which inhibit relaxation mechanisms involving torsional bond rotation that, on the contrary, normally occur with 2,2′-bipyridine type N^N ligands.[54]

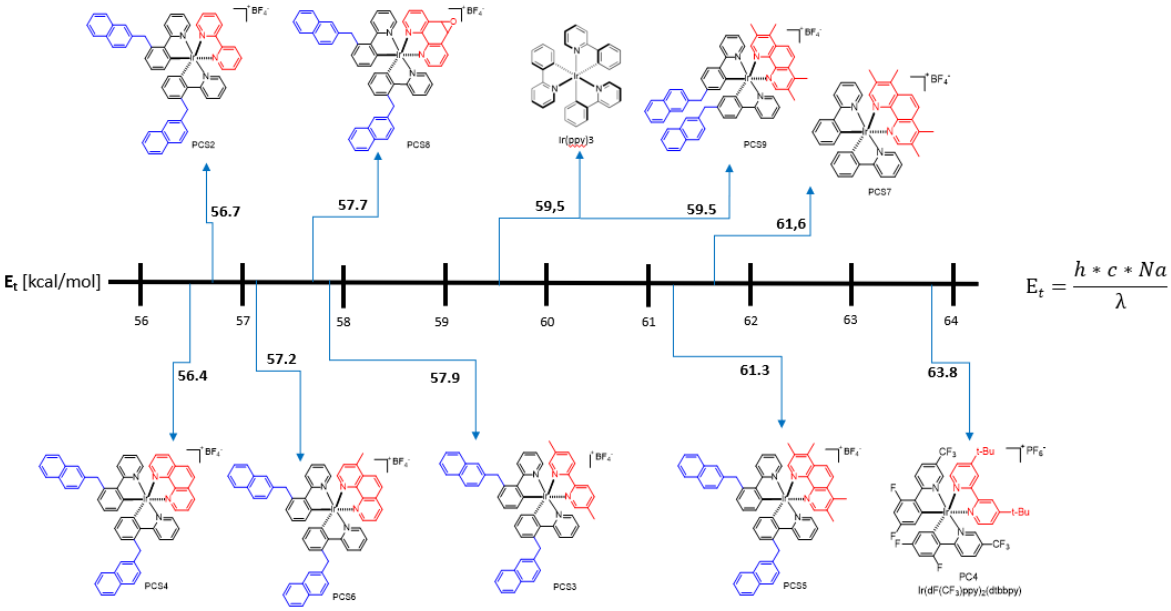

Figure 19: Visual representation of the measured values of triplet state energy.

Concerning triplet state lifetimes, the trend is not dissimilar (Figure 20). Aside from the neutral fac-Ir(ppy)$_3$, the photosensitizers with the highest energy (the most active in catalysis) are the ones with the longest triplet state lifetimes, in accordance with the Energy Gap Law. Moreover, regardless of the E_t, the inhibition of vibronic relaxation by torsional bond rotation granted by the structural rigidity of 1,10-phenanthroline, results in a further increase in the excited state lifetime.

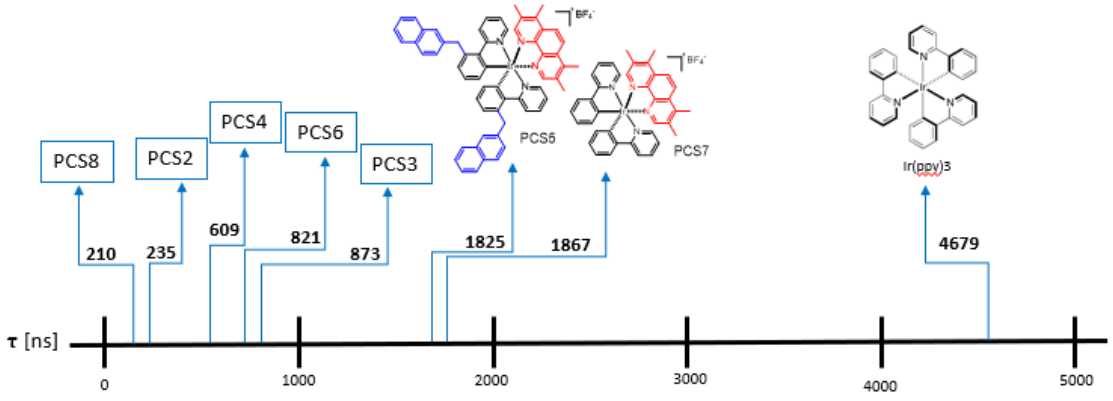

Figure 20: Visual representation of the measured values of triplet state lifetime.

Predictably, as testified by the Stern-Volmer plot, quenching experiments (Figure 21) with substrate **9b** showed a strong interaction (steep line) between the quencher and the catalytically active **PCS5** and **7**. The Stern-Volmer constant (K_{SV}) was calculated to be 578 and 1785 respectively. On the other hand, the inert **PCS4** does

not interact at all with **9b**, as testified by the unchanged intensity of the emission spectrum after each addition of quencher **9b** (see Experimental Section), which results in a planar straight line (K_{SV} of 13).

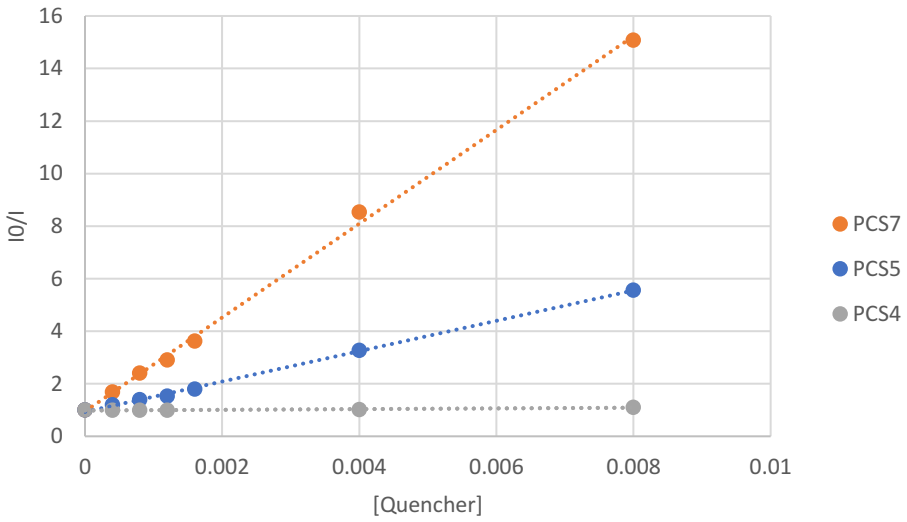

Figure 21: Stern-Volmer quenching experiments of PCS4,5 and 7 with substrate 9b

By way of example, I report here the photophysical characterization (absorption spectrum, emission spectrum and fluorescence lifetime decay spectrum) of one of the more significant cases: **PCS5**. The maximum absorption wavelength (Figure 22), in the visible region, stands around 390 nm. The intensity of the absorption in the UV range is way bigger compared to that in the visible range and it eventually hides the visible-light peak . Fluorescence emission instead (Figure 23) peaks at 527 nm. This information, together with the shape of the curve allow us to calculate the triplet state Energy, which is 61.3 Kcal mol^{-1}. The fluorescence lifetime decay (Figure 24) is mathematically extrapolated from the spectrum: the result is 1825 ns for **PCS5**.

The characterization of the other photocatalysts is reported, without spectra, in the Experimental Section (Photophysical Characterization Table).

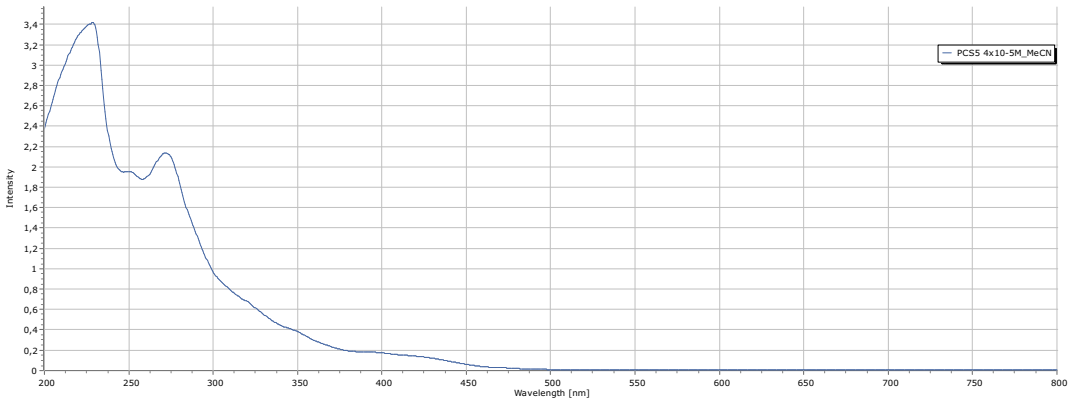

Figure 22: Absorption spectrum of PCS5.

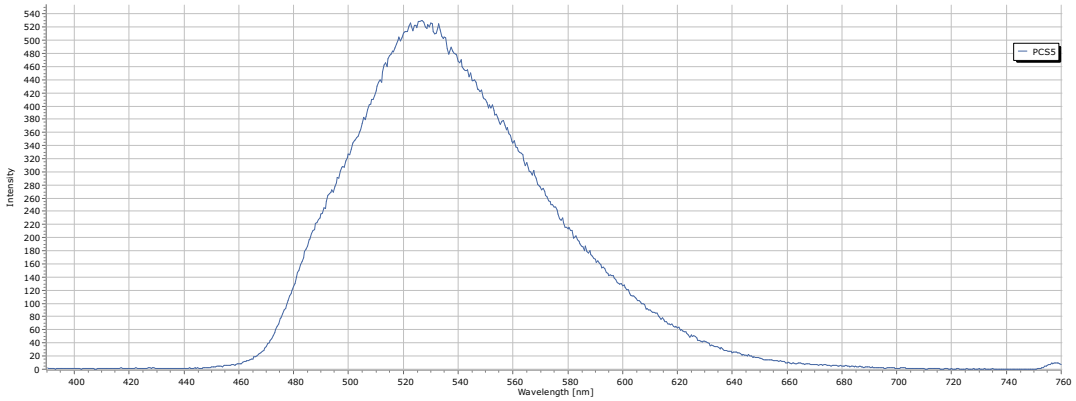

Figure 23: Fluorescence emission spectrum of PCS5.

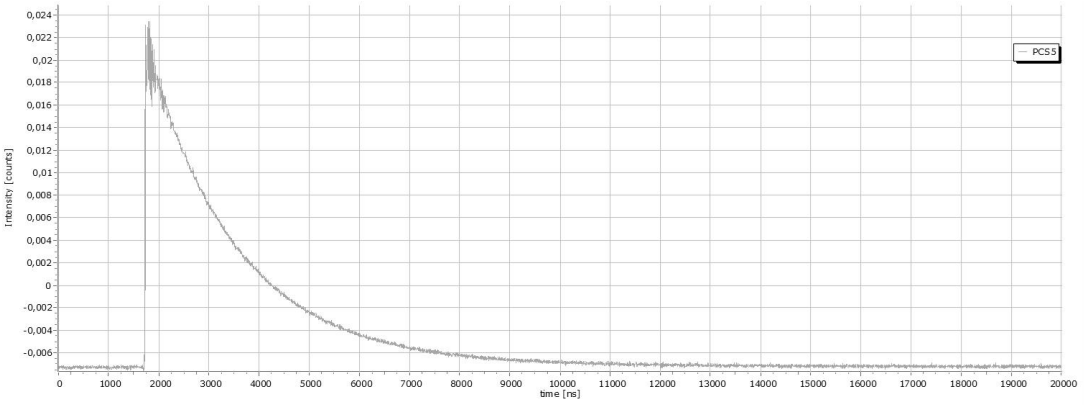

Figure 24: Fluorescence lifetime decay spectrum of PCS5.

3.4 Conclusions

In conclusion, our research introduces a novel family of napthyl-functionalized Iridium photosensitizers (PCSs) that exhibit significantly enhanced catalytic activity in various model cycloadditions when compared to commercially available photosensitizers. Through photophysical characterization, we have identified that the most catalytically active PCSs, all incorporating 3,4,7,8-tetramethyl-1,10-phenanthroline as ancillary ligand, possess the longest triplet-state lifetimes and the highest triplet energies.

Furthermore, the superior reactivity of PCSs featuring pendant naphthyl units, in contrast to their non-functionalized counterparts, underscores the capacity of this functional group to stabilize radical intermediates.

These findings not only advance our understanding of photosensitizer design but also hold promise for the development of more efficient and effective catalytic processes in various chemical applications.

3.5 Experimental Section

General Remarks

All chemicals those syntheses are not reported hereafter were purchased from commercial sources and used as received. Solvents were dried passing through alumina columns using an Inert® system and were stored under nitrogen. Chromatographic purifications were performed under gradient using a Combiflash® system and prepacked disposable silica cartridges or through isocratic flash chromatography using commercial 60 Å silica gel. When necessary, compounds were additionally purified by Preparative Thin-Layer Chromatography. All reactions that required heating were performed with the use of high-vacuum grade silicon oil. Reactions promoted by visible light were performed into standard 5 mm NMR tubes, surrounded by a commercial strip of 300 RGB household leds (12V, 14W). These were put at a distance of ca 10 cm and irradiated blue light (10.7 W·m−2 in the whole visible range; 0.35 W·m−2·nm−1 at their λmax: 459nm). The tubes were inside an oil bath fitted with a thermometer to monitor the temperature. Cooling was ensured by two fans recovered by outdated PCs to avoid reproducibility issues. During summertime, solutions are kept at 25 °C through the addition of a rubber spire inside the silicon oil bath. The spire is linked to a chiller that keeps pumping a cooled water/ethylene glycol solution to maintain the desired temperature. ^{1}H and ^{13}C NMR spectra were recorded at 300 K on a Bruker 400 MHz spectrometer using residual non-deuterated solvents as internal standards (7.26 ppm for 1H NMR and 77.00 ppm for 13C-NMR for CDCl3, 2.05 ppm for 1H NMR and 29.84 ppm for 13C NMR for acetone-d6). The terms m, s, d, t, q and quint represent multiplet, singlet, doublet, triplet, quadruplet and quintuplet respectively, and the term brs means a broad signal. Mass analyses were recorded on an Infusion Water Acquity Ultra Performance LC HO6UPS-823M instrument equipped with a SQ detector (Electrospray source); high-resolution mass analyses were recorded on a LTQ ORBITRAP XL Thermo Mass Spectrometer (Electrospray source).

Synthetic Procedures

Procedure for the preparation of ligand 7b

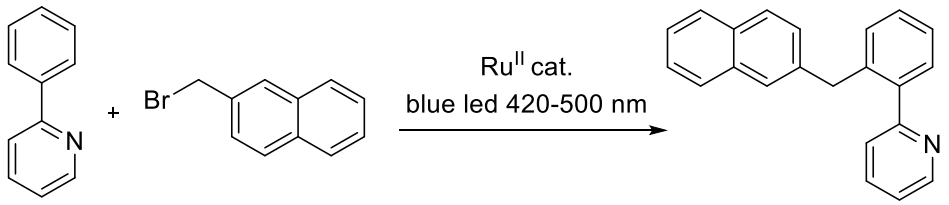

7a **7b**

Ortho-substituted 2-phenylpyridine **1b** was synthetized adapting a literature procedure by Ackermann.[56]

Dichloro(p-cymene)ruthenium(II) dimer (18 mg, 0.03 mmol, 5 mol%), sodium acetate (82 mg, 1 mmol, 2 eq) and 2-(Bromomethyl)naphthalene (110 mg, 0.5 mmol, 1 eq) were placed in a sealed vial, equipped with a stirring bar, under Nitrogen atmosphere. 1,4-Dioxane (2 mL) and 2-Phenylpyridine **7a** (216 µL, 1.5 mmol, 1.5 eq) were then added and the resulting mixture was stirred at r.t. for 18h under blue led irradiation (420-500 nm). The mixture was filtered through Celite and then the crude product was purified by chromatography on silica gel (Hexane:AcOEt 9:1) affording pure **7b** (89.6 mg, 61% yield).

Procedure for the preparation of ligand 7c

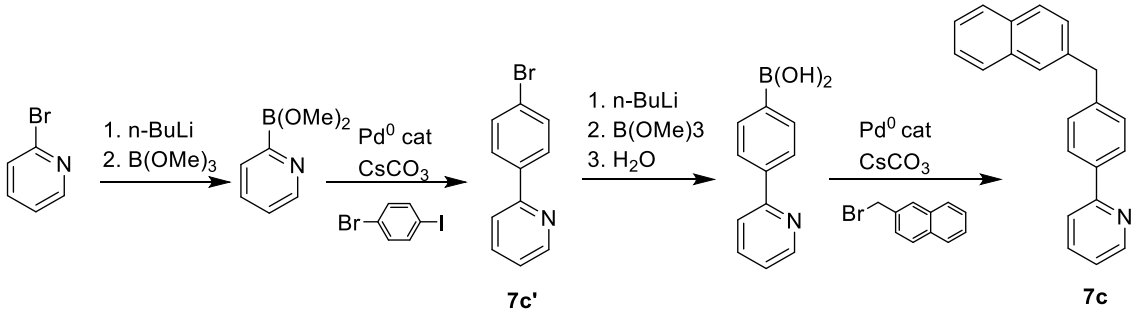

7c' **7c**

Commercialy available 2-bromopyridine (1.58 g, 10 mmol, 1 eq) was dissolved in Et_2O (0.4 M). The solution was cooled down to -78°C, then n-BuLi 2.5 M was added (4 mL, 10 mmol, 1 eq) and the mixture was stirred for 30 minutes. $B(OMe)_3$ (2.08 g, 20 mmol, 2 eq) was added over 30 minutes at -78°C, then the mixture was left stirring overnight, gradually reaching r.t.. The solvents were removed under reduced pressure, then MeOH was added and again removed, under reduced pressure.

The crude boronic ester was directly treated with 1-bromo-4-iodobenzene (2.55 g, 9 mmol, 0.9 eq), $CsCO_3$ (5.29 g, 15 mmol, 1.5 eq) and Tetrakis(PPh_3)Pd(0) (346 mg, 0.3 mmol, 0.03

eq) in Toluene (0.35 M) at 120°C for 18h. Then, the mixture was filtered over a pad of celite and purified by chromatography on silica gel (Hexane:AcOEt 9:1) affording **7c'** (489 mg, 2.1 mmol, 21% yield over 2 steps).

7c' (489 mg, 2.1 mmol, 1 eq) was dissolved in THF (0.65 M). The solution was cooled down to -78°C, then *n*-BuLi 2.5 M was added (1.08 mL, 2.7 mmol, 1.3 eq) and the mixture was stirred for 1 h. $B(OMe)_3$ (654 mg, 6.3 mmol, 3 eq) was added over 30 minutes at -78°C, then the mixture was left stirring overnight, gradually reaching r.t.. The reaction was quenched with water and the product was extracted with CH_2Cl_2. Solvents were partially removed under reduced pressure and petroleum ether was added forcing the precipitation of the boronic acid (210 mg, 1.05 mmol, 50% yield), which was filtered off.
The boronic acid was treated with 2-(bromomethyl)naphthalene (232 mg, 1.05 mmol, 1 eq), $CsCO_3$ (565 mg, 1.6 mmol, 1.5 eq) and Tetrakis(PPh_3)Pd(0) (60 mg, 0.052 mmol, 0.05 eq) in Toluene (0.35 M) at 100°C for 18h. Then, the mixture was filtered over a pad of celite and purified by chromatography on silica gel (Hexane:AcOEt 9:1) affording **7c** (69 mg, 0.233 mmol, 22% yield).

Procedures for the preparation of Iridium Dimers 8a-c

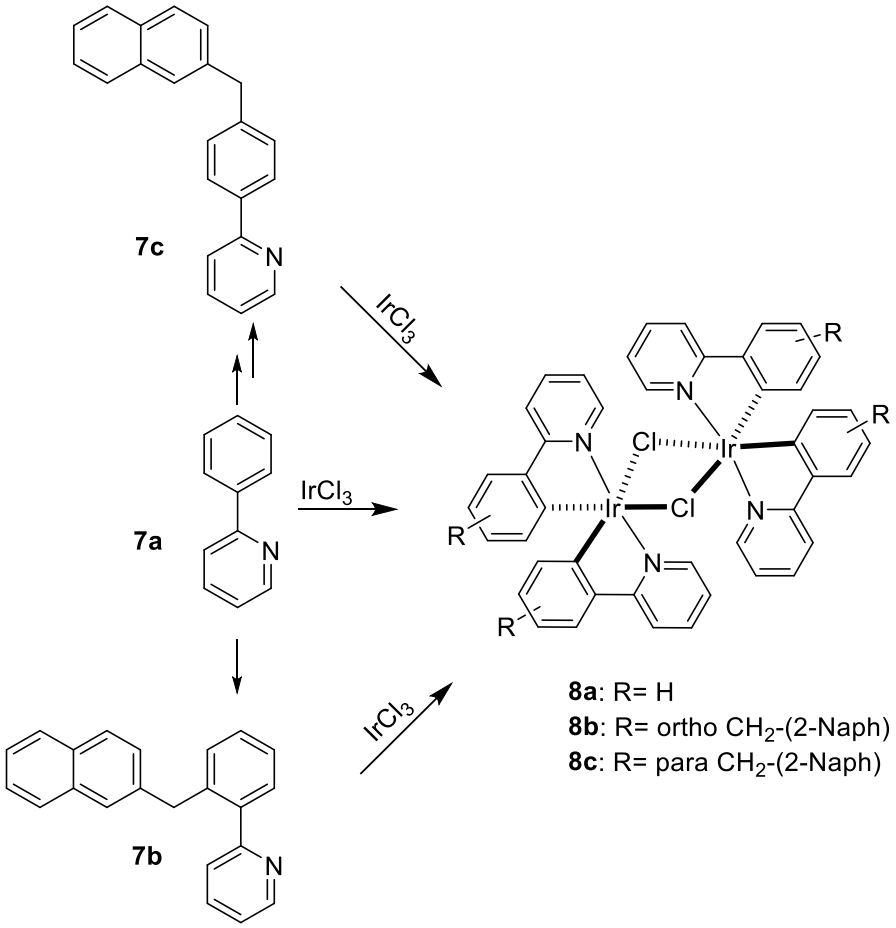

Dimers **8a-c** were synthetized adapting a literature procedure by Sun.[61]

8a:

$IrCl_3$ $3H_2O$ (178 mg ,0.5 mmol,1 eq) was placed in a sealed vial, equipped with a stirring bar, under Nitrogen atmosphere. A degassed 3/1 solution of 2-Ethoxyethanol and Water (12 mL) was added, followed by 2-phenylpyridine **7a** (332 µL, 1.35 mmol, 2.7 eq). The mixture was stirred at 120°C for 18h, then cooled to r.t. Water was added and the resulting yellow precipitate was filtered off, washed with more water and ethanol and finally dried under reduced pressure affording pure **8a** (212 mg, 79% yield).

8b:

$IrCl_3$ $3H_2O$ (44.8 mg, 0.13 mmol, 1 eq) was placed in a sealed vial, equipped with a stirring bar, under Nitrogen atmosphere. A degassed 3/1 solution of 2-Ethoxyethanol and Water (2 mL) was added, followed by substituted 2-phenylpyridine **7b** (108.8 mg, 0.37 mmol, 2.8 eq). The mixture was stirred at 120°C for 18h, then cooled to r.t. The yellow product is extracted

from the mixture using CH_2Cl_2, then washed with water and finally dried over sodium sulfate. The crude product **8b** (140 mg) is directly used for the following synthetic step, since it is easier to purify by chromatography the Heteroleptic Iridium Complexes than the Iridium Dimers.

8c:

$IrCl_3$ $3H_2O$ (17.6 mg, 0.05 mmol, 1 eq) was placed in a sealed vial, equipped with a stirring bar, under Nitrogen atmosphere. A degassed 3/1 solution of 2-Ethoxyethanol and Water (0.8 mL) was added, followed by substituted 2-phenylpyridine **7c** (31.0 mg, 0.105 mmol, 2.1 eq). The mixture was stirred at 120°C for 18h, then cooled to r.t. The yellow product is extracted from the mixture using CH_2Cl_2, then washed with water and finally dried over sodium sulfate. The crude product **8c** (48 mg) is directly used for the following synthetic step, since it is easier to purify by chromatography the Heteroleptic Iridium Complexes than the Iridium Dimers.

General procedure for the preparation of Heteroleptic Iridium Complexes PCS 1-9 (GP-3)

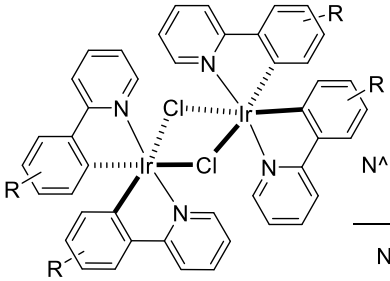

8a: R= H
8b: R= ortho CH_2-(2-Naph)
8c: R= para CH_2-(2-Naph)

N^N ligand
50°C
NH_4BF_4

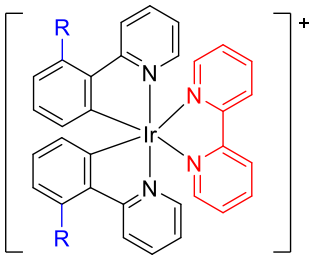

PCS1: R= H
PCS2: R= o-CH_2-2-Naphtyl

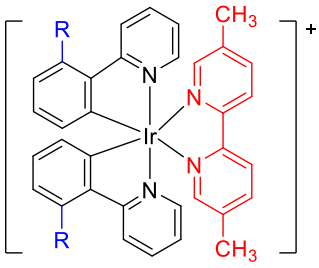

PCS3: R= o-CH_2-2-Naphtyl

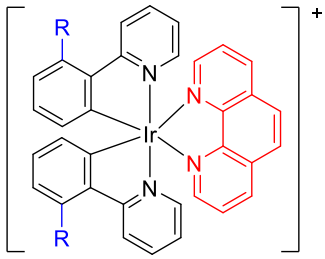

PCS4: R= o-CH_2-2-Naphtyl

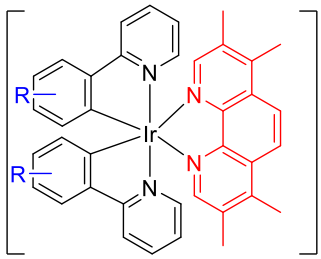

PCS5: R= o-CH_2-2-Naphtyl
PCS7: R= H
PCS9: R= p-CH_2-2-Naphtyl

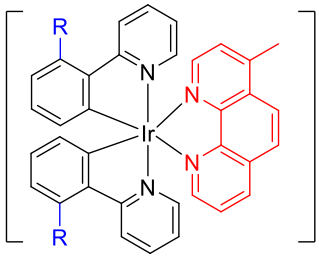

PCS6: R= o-CH_2-2-Naphtyl

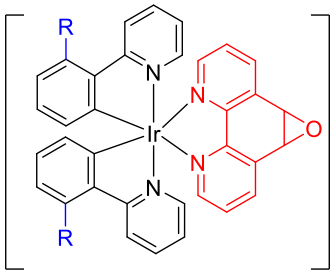

PCS8: R= o-CH_2-2-Naphtyl

Heteroleptic iridium complexes **PCS 1-9** were synthetized adapting a literature procedure by Daniellou.[62]

Iridium dimer **8a-c** (1 eq) and the desired bidentate *N-N'* ligand (2.2 eq) were placed in a sealed vial, equipped with a stirring bar, under Nitrogen atmosphere. A degassed 2/1 solution of CH_2Cl_2 and MeOH (0.005M) was added and the solution was stirred at 50°C for 4h. After cooling the solution to r.t., NH_4BF_4 (20 eq) was added and the mixture was stirred 20 more minutes. Solvents were removed under reduced pressure and the crude product was purified by chromatography on silica gel (CH_2Cl_2:MeOH 30:1) and, when necessary, by an additional preparative TLC (CH_2Cl_2:MeOH 20:1), affording pure **PCS1-9**.

General procedure for the preparation of substrates 9b-c (GP-4)

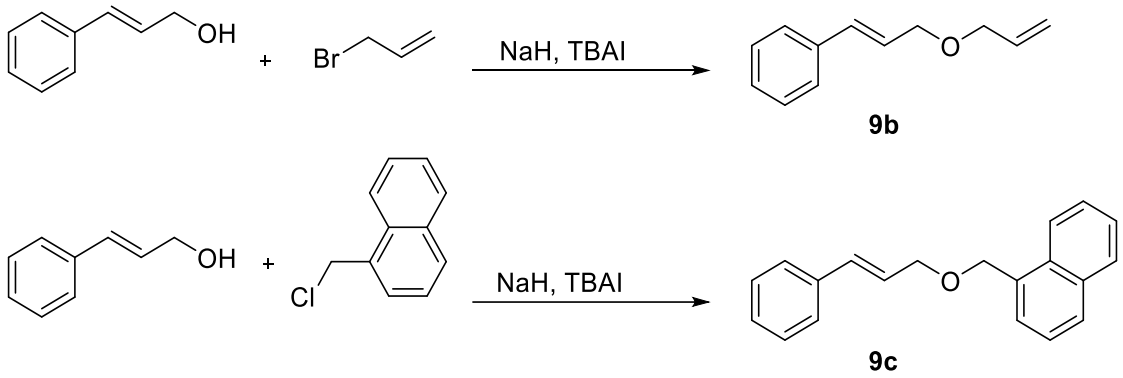

Sodium hydride (60% dispersion in mineral oil) (1.4 eq) and TBAI (1 mol%) were placed in a sealed vial, equipped with a stirring bar, and dissolved in THF (0.5 M), under Nitrogen atmosphere. Cinnamyl alcohol (1.1 eq) was added to the stirring solution at 0°C. After 30 minutes, the desired halide partner (1 eq) was added. The mixture was then allowed to gradually return to r.t.. After 24h, the reaction was quenched with water. The product was extracted with diethyl ether, washed with brine and then dried over sodium sulfate. The crude product was purified by chromatography on silica gel (Hexane:AcOEt 95:5) affording pure **9b-c**.

General procedure for the synthesis of product 10b (GP-5)

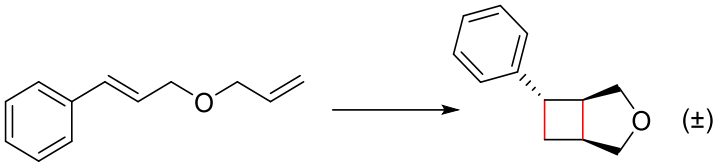

9b **10b**

To a vial charged with substrate **3b** (1 eq) and the desired Iridium photocatalyst (1 mol%), dry and degassed Acetonitrile (0.05 M) was added. The solution was transferred in a 5 mm-wide (external diameter) NMR tube and degassed via freeze-pump cycles (2x). The homogeneous solution was irradiated at r.t. with blue LED

Stripes (420-500 nm) for 4 hours. The mixture was then concentrated and purified by chromatography on silica gel affording product **4b** as a mixture of two diastereoisomers.

General procedure for the synthesis of product 10c (GP-6)

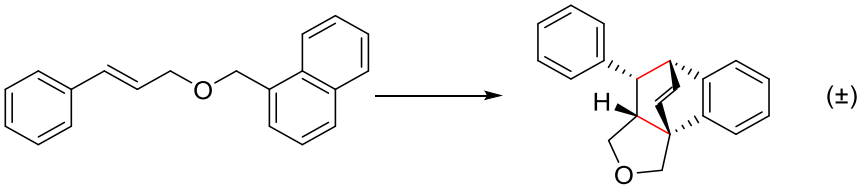

9c **10c**

To a vial charged with substrate **9c** (1 eq) and the desired Iridium photocatalyst (1 mol%), dry and degassed CH_2Cl_2 (0.1M) was added. The solution was transferred in a 5 mm-wide (external diameter) NMR tube and degassed via freeze-pump cycles (2x). The homogeneous solution was irradiated at r.t. with blue LED

Stripes (420-500 nm) for 18 hours. The mixture was then concentrated and purified by chromatography on silica gel affording product **10c** as a mixture of two diastereoisomers.

General procedure for the catalytic photoisomerization of 3a (GP-7)

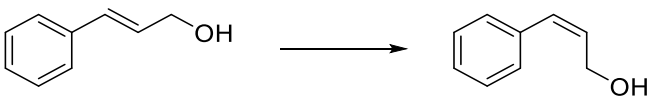

9a **(Z)-9a**

To a vial charged with substrate **9a** (0.1 mmol, 1 eq), an Iridium photosensitizer (1 mol%) and a dry and degassed mixture of MeCN/$CHCl_3$ (7:3, 0.1 M) were added through a syringe. Then, DIPEA (10 mol%) was added, and the solution was transferred into an NMR tube capped with a rubber septum and it was placed in an oil bath kept at 25 °C and irradiated with blue LED stripes (420-500 nm) for 1 hour. The mixture was then concentrated in vacuo. The *Z/E* ratio were determined by ^{1}H NMR spectra on the reaction crude.

Characterization of intermediates, substrates, products and synthesized photocatalysts

2-(2-(Naphthalen-2-ylmethyl)phenyl)pyridine, 7b

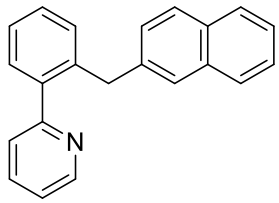

7b (89.6 mg, 0.303 mmol) was afforded with 61% yield.

^{1}H NMR (400 MHz, $CDCl_3$) δ 8.71 (ddd, J = 4.9, 1.8, 1.0 Hz, 1H), 7.78 – 7.73 (m, 1H), 7.69 – 7.60 (m, 3H), 7.44 – 7.38 (m, 3H), 7.38 – 7.31 (m, 3H), 7.29 – 7.25 (m, 2H), 7.23 (ddd, J = 7.6, 4.9, 1.2 Hz, 1H), 7.16 (dd, J = 8.5, 1.8 Hz, 1H), 4.29 (s, 2H). **^{13}C NMR** (101 MHz, $CDCl_3$) δ 160.1, 149.3, 140.8, 138.9, 138.8, 136.4, 133.6, 132.0, 130.9, 130.1, 128.6, 127.9, 127.8, 127.67, 127.65, 127.2, 126.6, 125.9, 125.3, 124.4, 121.9, 39.1. **ESI-MS** calcd for $C_{22}H_{17}N$ $[M+H]^+$ 296.14, found 296.25.

2-(4-Bromophenyl)pyridine, 7c'

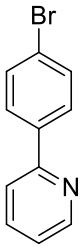

7c' (489 mg, 2.1 mmol) was afforded with 21% yield over 2 steps. Spectroscopic data are consistent with literature.[63]

^{1}H NMR (400 MHz, $CDCl_3$) δ 8.69 (ddd, J = 4.9, 1.8, 1.0 Hz, 1H), 7.90 – 7.85 (m, 2H), 7.76 (ddd, J = 7.9, 7.3, 1.8 Hz, 1H), 7.70 (dt, J = 8.0, 1.2 Hz, 1H), 7.62 – 7.58 (m, 2H), 7.29 – 7.21 (m, 1H).

2-(4-(Naphthalen-2-ylmethyl)phenyl)pyridine, 7c

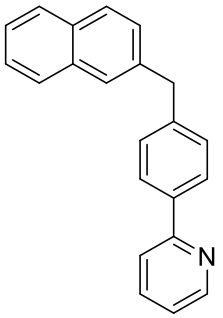

7c (69 mg, 0.233 mmol) was afforded with 22% yield over 2 steps.

^{1}H NMR (400 MHz, $CDCl_3$) δ 8.71 – 8.67 (m, 1H), 7.96 – 7.92 (m, 2H), 7.83 – 7.76 (m, 3H), 7.75 – 7.69 (m, 2H), 7.66 (bs, 1H), 7.51 – 7.41 (m, 2H), 7.38 – 7.32 (m, 3H), 7.21 (ddd, J = 6.7, 4.9, 1.7 Hz, 1H), 4.21 (s, 2H). **^{13}C NMR** (101 MHz, $CDCl_3$) δ 157.4, 149.7, 142.1, 138.5, 137.4, 137.0, 133.7, 132.2, 129.7, 128.3, 127.8, 127.7, 127.7, 127.3, 127.2, 126.1, 125.5, 122.1, 120.6, 42.0. **ESI-MS** calcd for $C_{22}H_{17}N$ $[M+H]^+$ 296.14, found 296.20.

[Ir(ppy)$_2$Cl]$_2$, 8a

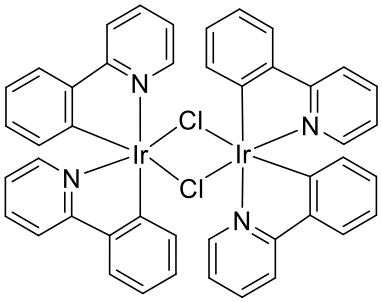

8a (212 mg, 0.198 mmol) was afforded with 79% yield. Spectroscopic data are consistent with literature.[64]

^{1}H NMR (400 MHz, $CDCl_3$) δ 9.24 (ddd, J = 5.8, 1.7, 0.8 Hz, 4H), 7.90 – 7.84 (m, 4H), 7.77 – 7.70 (m, 4H), 7.48 (dd, J = 7.8, 1.4 Hz, 4H), 6.80 – 6.71 (m, 8H), 6.56 (ddd, J = 7.8, 7.1, 1.4 Hz, 4H), 5.93 (dd, J = 7.8, 1.2 Hz, 4H).

[Ir(2-(2-(naphthalen-2-ylmethyl)phenyl)pyridine)$_2$Cl]$_2$, 8b, crude product

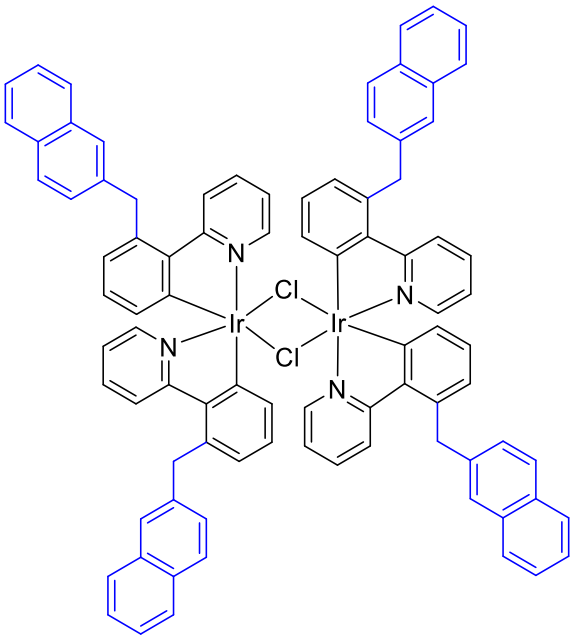

8b (450 mg, 1.64 mmol) was prepared and directly used for the synthesis of **PCS 2-6**.

^{1}H NMR (400 MHz, $CDCl_3$) δ 9.09 (dd, J = 5.8, 1.7 Hz, 4H), 7.82 – 7.73 (m, 8H), 7.61 (d, J = 8.1 Hz, 4H), 7.51 (s, 4H), 7.45 – 7.23 (m, 20H), 6.72 – 6.58 (m, 8H), 5.96 (ddd, J = 7.3, 5.8, 1.3 Hz, 4H), 5.80 (dd, J = 7.7, 1.3 Hz, 4H), 4.68 (d, J = 17.4 Hz, 4H), 4.57 (d, J = 17.4 Hz, 4H). **^{13}C NMR** (101 MHz, $CDCl_3$) δ 167.9, 152.1, 149.2, 143.7, 137.8, 136.6, 135.7, 133.8, 132.1, 129.7, 128.4, 128.14, 128.10, 127.6, 127.4, 126.9, 126.8, 126.1, 125.4, 122.5, 121.3, 42.1.

[Ir(ppy)$_2$(bpy)]BF$_4$, PCS1

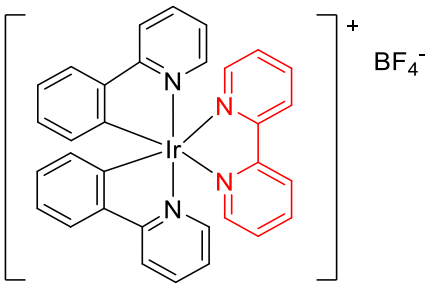

Following GP-3, **PCS1** (56.0 mg, 0.075 mmol) was afforded with 75% yield.

^{1}H NMR (400 MHz, Acetone) δ 8.86 (dt, J = 8.3, 1.1 Hz, 2H), 8.29 (td, J = 7.9, 1.6 Hz, 2H), 8.24 (dt, J = 8.2, 1.2 Hz, 2H), 8.10 (ddd, J = 5.4, 1.7, 0.8 Hz, 2H), 7.99 – 7.93 (m, 2H), 7.90 (dd, J = 7.7, 1.3 Hz, 2H), 7.85 – 7.82 (m, 2H), 7.70 (ddd, J = 7.6, 5.4, 1.2 Hz, 2H), 7.16 (ddd, J = 7.3, 5.8, 1.4 Hz, 2H), 7.03 (td, J = 7.6, 1.2 Hz, 2H), 6.91 (td, J = 7.4, 1.4 Hz, 2H),

6.35 (dd, J = 7.6, 1.2 Hz, 2H). **^{13}C NMR** (101 MHz, CDCl3) δ 168.6, 156.9, 151.5, 151.3, 150.1, 144.9, 140.5, 139.5, 132.5, 131.2, 129.4, 125.8, 125.8, 124.5, 123.4, 120.8. **ESI-MS** calcd for $C_{32}H_{24}IrN_4BF_4$ $[M\text{-}BF_4]^+$ 657.16, found 657.25.

[Ir(2-(2-(naphthalen-2-ylmethyl)phenyl)pyridine)$_2$(bpy)]BF$_4$, PCS2

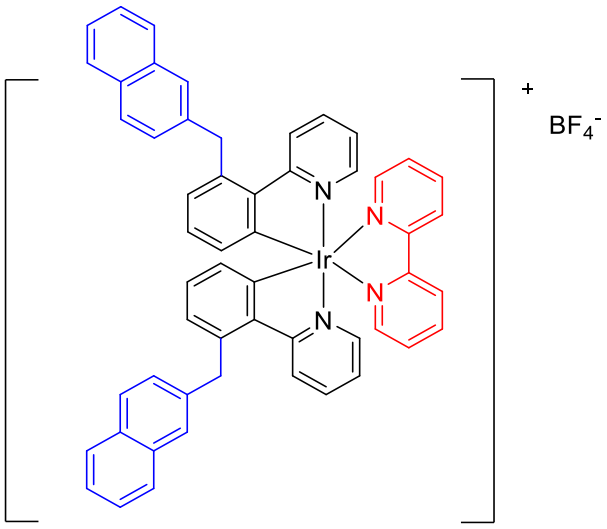

Following GP-3, **PCS2** (20.1 mg, 0.019 mmol) was afforded with 40% yield over two steps. **^{1}H NMR** (400 MHz, Acetone) δ 8.81 (dt, J = 8.3, 1.1 Hz, 2H), 8.27 (td, J = 8.0, 1.7 Hz, 2H), 8.22 (d, J = 8.4 Hz, 2H), 8.14 (dd, J = 5.6, 1.4 Hz, 2H), 7.91 – 7.81 (m, 6H), 7.79 – 7.67 (m, 6H), 7.56 (bs, 2H), 7.48 – 7.42 (m, 6H), 7.03 – 6.98 (m, 4H), 6.92 (t, J = 7.5 Hz, 2H), 6.26 (dd, J = 7.6, 1.3 Hz, 2H), 4.82 (d, J = 17.2 Hz, 2H), 4.72 (d, J = 17.2 Hz, 2H). **^{13}C NMR** (101 MHz, Acetone) δ 167.8, 156.7, 154.6, 151.2, 150.5, 143.7, 140.6, 139.4, 138.9, 138.7, 134.6, 133.2, 131.4, 130.7, 129.4, 129.1, 128.9, 128.5, 128.4, 128.1, 127.4, 127.0, 126.4, 125.8, 125.1, 124.1, 42.4. **ESI-MS** calcd for $C_{54}H_{40}IrN_4BF_4$ $[M\text{-}BF_4]^+$ 937.29, found 937.42.

[Ir(2-(2-(naphthalen-2-ylmethyl)phenyl)pyridine)$_2$(5,5'-Dimethyl-bpy)]BF$_4$, PCS3

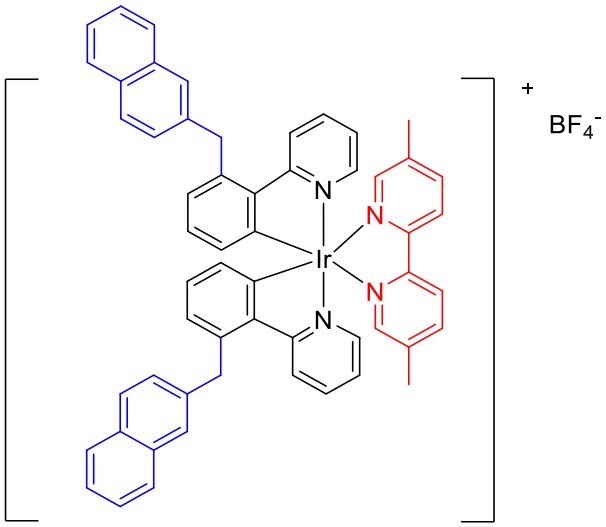

Following GP-3, **PCS3** (16.0 mg, 0.015 mmol) was afforded with 29% yield over two steps. **^{1}H NMR** (400 MHz, Acetone) δ 8.64 (d, J = 8.3 Hz, 2H), 8.23 (d, J = 8.3 Hz, 2H), 8.06 (ddd, J = 8.3, 2.1, 0.8 Hz, 2H), 7.93 – 7.83 (m, 8H), 7.76 – 7.69 (m, 4H), 7.63 (bs, 2H), 7.49 – 7.41 (m, 6H), 7.03 – 6.98 (m, 4H), 6.92 (t, J = 7.5 Hz, 2H), 6.26 (dd, J = 7.5, 1.4 Hz, 2H), 4.82 (d, J = 17.1 Hz, 2H), 4.72 (d, J = 17.1 Hz, 2H), 2.31 (s, 6H). **^{13}C NMR** (101 MHz, Acetone) δ 167.8, 154.7, 154.4, 151.0, 150.5, 143.7, 140.9, 139.7, 139.3, 138.9, 138.7, 134.6, 133.2, 131.3, 130.6, 129.1, 128.8, 128.5, 128.4, 127.9, 127.5, 127.0, 126.4, 125.0, 124.9, 124.0, 42.3, 18.7. **ESI-MS** calcd for $C_{56}H_{44}IrN_4BF_4$ $[M\text{-}BF_4]^+$ 965.32, found 965.44.

[Ir(2-(2-(naphthalen-2-ylmethyl)phenyl)pyridine)$_2$(phen)]BF$_4$, PCS4

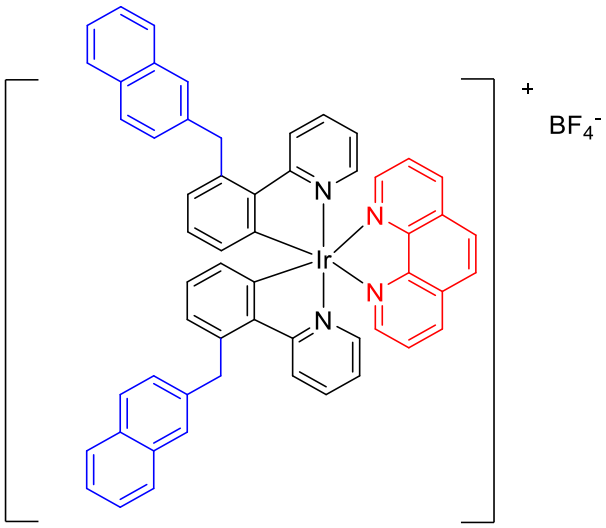

Following GP-3, **PCS4** (17.8 mg, 0.017 mmol) was afforded with 34% yield over two steps.

^{1}H NMR (400 MHz, Acetone) δ 8.88 (dd, J = 8.3, 1.5 Hz, 2H), 8.47 (dd, J = 5.0, 1.4 Hz, 2H), 8.36 (s, 2H), 8.21 (d, J = 8.4 Hz, 2H), 8.11 (dd, J = 8.3, 5.0 Hz, 2H), 7.89 (d, J = 8.5 Hz, 2H), 7.87 – 7.83 (m, 2H), 7.77 – 7.74 (m, 2H), 7.72 (dd, J = 5.8, 1.0 Hz, 2H), 7.65 (ddd, J = 8.6, 7.4, 1.7 Hz, 2H), 7.60 (bs, 2H), 7.50 – 7.41 (m, 6H), 7.04 (dd, J = 7.5, 1.4 Hz, 2H), 6.96 (t, J = 7.5 Hz, 2H), 6.82 (ddd, J = 7.3, 5.8, 1.3 Hz, 2H), 6.36 (dd, J = 7.5, 1.3 Hz, 2H), 4.84 (d, J = 17.2 Hz, 2H), 4.73 (d, J = 17.2 Hz, 2H). **^{13}C NMR** (101 MHz, Acetone) δ 167.8, 154.1, 151.8, 150.7, 147.6, 143.9, 139.7, 139.4, 138.8, 138.7, 134.6, 133.2, 132.6, 131.5, 130.6, 129.3, 129.1, 128.9, 128.5, 128.4, 128.1, 127.8, 127.4, 127.0, 126.4, 125.0, 123.9, 42.4. **ESI-MS** calcd for $C_{56}H_{40}IrN_4BF_4$ $[M\text{-}BF_4]^+$ 961.29, found 961.41.

[Ir(2-(2-(naphthalen-2-ylmethyl)phenyl)pyridine)$_2$(3,4,7,8-Tetramethyl-phen)]BF$_4$, PCS5

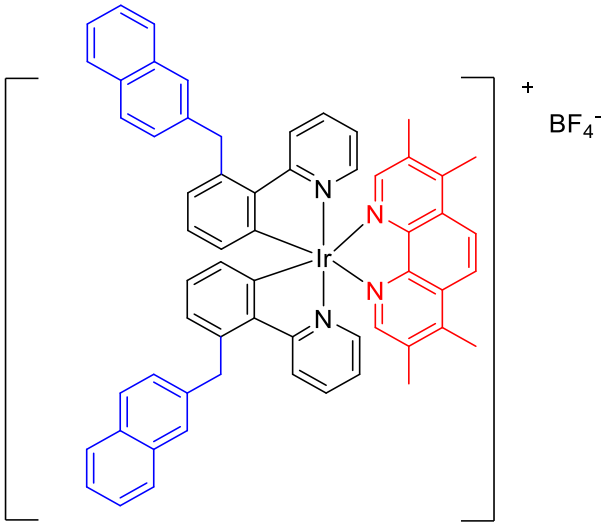

Following GP-3, **PCS5** (24.0 mg, 0.022 mmol) was afforded with 43% yield over two steps. **^{1}H NMR** (400 MHz, Acetone) δ 8.46 (s, 2H), 8.22 (d, J = 8.5 Hz, 2H), 8.13 (s, 2H), 7.90 – 7.84 (m, 4H), 7.76 – 7.70 (m, 4H), 7.68 – 7.63 (m, 4H), 7.48 – 7.40 (m, 6H), 7.02 (dd, J = 7.5, 1.4 Hz, 2H), 6.94 (t, J = 7.5 Hz, 2H), 6.82 (ddd, J = 7.3, 5.7, 1.3 Hz, 2H), 6.36 (dd, J = 7.5, 1.4 Hz, 2H), 4.84 (d, J = 17.0 Hz, 2H), 4.71 (d, J = 17.1 Hz, 2H), 2.84 (s, 6H), 2.45 (s, 6H). **^{13}C NMR** (101 MHz, Acetone) δ 167.9, 154.9, 151.9, 150.5, 147.4, 146.2, 143.8, 139.2, 138.7, 138.7, 136.1, 134.6, 133.2, 131.6, 130.9, 130.6, 129.1, 128.8, 128.5, 128.4, 127.9, 127.5, 127.0, 126.4, 125.3, 124.9, 123.9, 42.4, 18.2, 15.1. **ESI-MS** calcd for $C_{60}H_{48}IrN_4BF_4$ $[M\text{-}BF_4]^+$ 1017.35, found 1017.46.

[Ir(2-(2-(naphthalen-2-ylmethyl)phenyl)pyridine)$_2$(4-Methyl-phen)]BF$_4$, PCS6

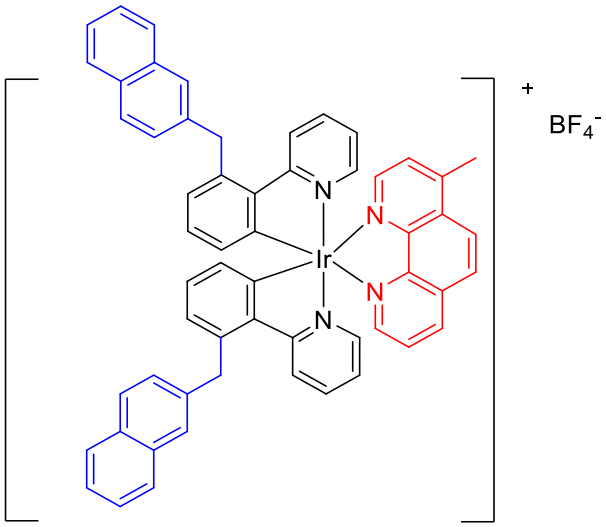

Following GP-3, **PCS6** (17.2 mg, 0.016 mmol) was afforded with 25% yield over two steps. **^{1}H NMR** (400 MHz, Acetone) δ 8.87 (dd, J = 8.3, 1.5 Hz, 1H), 8.50 – 8.44 (m, 2H), 8.38 (d, J = 9.2 Hz, 1H), 8.29 (d, J = 5.2 Hz, 1H), 8.22 (dd, J = 8.6, 3.9 Hz, 2H), 8.09 (dd, J = 8.3, 5.1 Hz, 1H), 7.93 (dd, J = 5.2, 1.0 Hz, 1H), 7.90 (s, 1H), 7.86 (dd, J = 11.2, 3.7 Hz, 3H), 7.76 (dd, J = 7.1, 2.9 Hz, 2H), 7.71 (tt, J = 5.8, 1.0 Hz, 2H), 7.65 (dddd, J = 8.7, 7.4, 3.5, 1.7 Hz, 2H), 7.59 (bs, 2H), 7.52 – 7.40 (m, 6H), 7.03 (dt, J = 7.6, 1.6 Hz, 2H), 6.95 (t, J = 7.5 Hz, 2H), 6.82 (dddd, J = 7.2, 6.0, 5.0, 1.3 Hz, 2H), 6.36 (td, J = 7.5, 1.3 Hz, 2H), 4.85 (dd, J = 17.2, 2.9 Hz, 2H), 4.73 (dd, J = 17.1, 3.3 Hz, 2H), 2.98 (s, 3H). **^{13}C NMR** (101 MHz, Acetone) δ 167.9, 167.8, 154.44, 154.41, 151.9, 151.1, 150.55, 150.54, 150.1, 147.7, 147.2, 143.94, 143.88, 139.6, 139.41, 139.38, 138.8, 138.74, 138.71, 134.63, 134.61, 133.2, 132.4, 132.2, 131.6, 131.5, 130.64, 130.62, 129.1, 129.0, 128.9, 128.5, 128.4, 128.44, 128.41, 128.17, 128.15, 127.7, 127.4, 127.0, 126.38, 126.37, 125.9, 125.8, 125.0, 123.94, 123.90, 42.5, 42.4, 19.1. **ESI-MS** calcd for $C_{57}H_{42}IrN_4BF_4$ $[M\text{-}BF_4]^+$ 975.30, found 975.46.

[Ir(ppy)$_2$(3,4,7,8-Tetramethyl-phen)]BF$_4$, PCS7

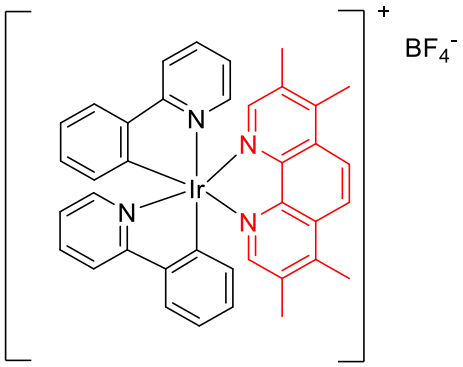

Following GP-3, **PCS7** (50.5 mg, 0.061 mmol) was afforded with 75% yield.

^{1}H NMR (400 MHz, Acetone) δ 8.52 (s, 1H), 8.22 (dt, J = 8.1, 1.1 Hz, 1H), 8.13 (s, 1H), 7.93 – 7.86 (m, 2H), 7.66 (ddd, J = 5.9, 1.6, 0.8 Hz, 1H), 7.06 (td, J = 7.5, 1.2 Hz, 1H), 6.98 – 6.92 (m, 2H), 6.44 (dd, J = 7.5, 1.2 Hz, 1H), 2.88 (s, 3H), 2.39 (s, 3H). **^{13}C NMR** (101 MHz, Acetone) δ 168.9, 152.2, 151.6, 150.1, 147.4, 146.4, 145.1, 139.3, 136.2, 132.7, 131.2, 130.9, 125.8, 125.4, 124.2, 123.2, 120.7, 18.0, 15.1. **ESI-MS** calcd for $C_{38}H_{32}IrN_4BF_4$ $[M\text{-}BF_4]^+$ 737.22, found 737.25.

[Ir(2-(4-(naphthalen-2-ylmethyl)phenyl)pyridine)$_2$(5,6-Epoxy-1,10-phenanthroline)]BF$_4$, PCS8

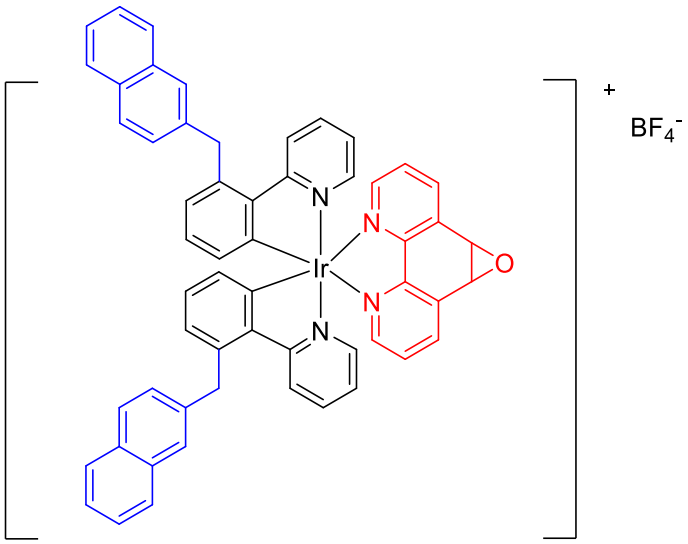

Following GP-3, **PCS8** (19.4 mg, 0.018 mmol) was afforded with 23% yield over two steps. A residue of ancillary ligand F remained unseparated from the desired product (25%).

^{1}H NMR (400 MHz, Acetone) δ 8.65 – 8.59 (m, 2H), 8.25 – 8.16 (m, 3H), 8.11 (dd, J = 5.4, 1.4 Hz, 1H), 7.92 – 7.81 (m, 7H), 7.76 – 7.67 (m, 5H), 7.58 (s, 1H), 7.54 (s, 1H), 7.48 – 7.40 (m, 6H), 7.03 – 6.97 (m, 3H), 6.95 – 6.88 (m, 3H), 6.27 (ddd, J = 8.5, 7.6, 1.3 Hz, 2H), 5.06 (d, J = 3.7 Hz, 1H), 5.03 (d, J = 3.7 Hz, 1H), 4.81 (dd, J = 17.2, 8.1 Hz, 2H), 4.70 (dd, J = 17.2, 10.7 Hz, 2H). **^{13}C NMR** (101 MHz, Acetone) δ 166.9, 166.8, 152.9, 151.3, 150.2, 150.1, 149.8, 149.7, 142.9, 142.8, 140.8, 140.6, 138.6, 138.2, 138.1, 137.8, 137.7, 134.8, 134.7, 133.7, 132.3, 130.5, 129.9, 129.8, 128.6, 128.4, 128.2, 128.1, 127.6 , 127.5, 127.3, 127.2, 126.6, 126.5, 126.13, 126.11, 125.5, 124.3, 124.2, 123.4, 123.1, 55.0, 54.7, 41.6, 41.5. **ESI-MS** calcd for $C_{56}H_{40}IrN_4OBF_4$ $[M\text{-}BF_4]^+$ 977.28, found 977.44.

[Ir(2-(4-(naphthalen-2-ylmethyl)phenyl)pyridine)$_2$(3,4,7,8-Tetramethyl-phen)]BF$_4$, PCS9

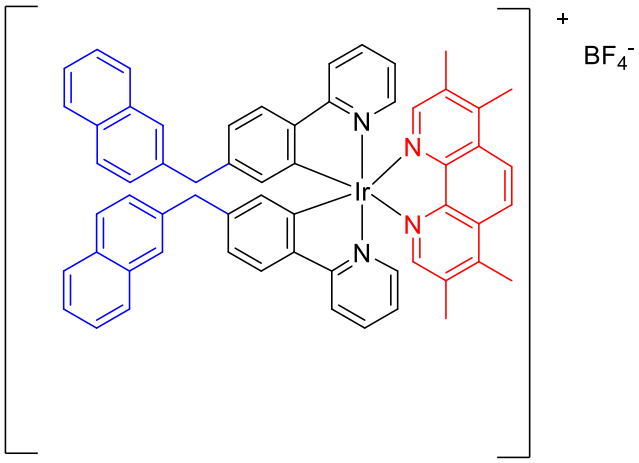

Following GP-3, **PCS9** (22.5 mg, 0.020 mmol) was afforded with 39% yield over two steps. **^{1}H NMR** (400 MHz, Acetone) δ 8.44 (s, 1H), 8.03 (s, 1H), 7.94 – 7.89 (m, 1H), 7.87 – 7.81 (m, 1H), 7.74 (d, J = 7.8 Hz, 3H), 7.53 – 7.44 (m, 4H), 7.40 – 7.37 (m, 1H), 7.20 (dd, J = 8.4, 1.8 Hz, 1H), 6.99 (dd, J = 8.0, 1.8 Hz, 1H), 6.56 (ddd, J = 7.4, 5.9, 1.4 Hz, 1H), 6.22 (d, J = 1.7 Hz, 1H), 4.00 (d, J = 15.1 Hz, 1H), 3.92 (d, J = 15.2 Hz, 1H), 2.82 (s, 3H), 2.31 (s, 3H). **^{13}C NMR** (101 MHz, Acetone) δ 168.6, 152.10, 152.06, 149.5, 147.3, 146.4, 144.5, 143.1, 139.8, 138.8, 136.1, 134.6, 133.09, 133.06, 130.8, 128.8, 128.5, 128.45, 128.43, 127.8, 126.8, 126.2, 125.7, 125.3, 124.1, 123.5, 120.2, 42.5, 18.0, 15.1. **ESI-MS** calcd for $C_{60}H_{48}IrN_4BF_4$ $[M\text{-}BF_4]^+$ 1017.35, found 1017.39.

(E)-(3-(Allyloxy)prop-1-en-1-yl)benzene, 9b

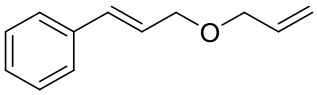

Following GP-4, **9b** (421 mg, 2.42 mmol) was afforded with 87% yield. Spectroscopic data are consistent with literature.[65]

^{1}H NMR (400 MHz, $CDCl_3$) δ 7.42 – 7.37 (m, 2H), 7.35 – 7.29 (m, 2H), 7.25 – 7.21 (m, 1H), 6.62 (dt, J = 15.9, 1.6 Hz, 1H), 6.31 (dt, J = 15.9, 6.0 Hz, 1H), 5.96 (ddt, J = 17.2, 10.4, 5.6 Hz, 1H), 5.32 (dd, J = 17.2, 1.7 Hz, 1H), 5.22 (dd, J = 10.4, 1.5 Hz, 1H), 4.17 (dd, J = 6.1, 1.5 Hz, 2H), 4.05 (dt, J = 5.6, 1.4 Hz, 2H).

1-((Cinnamyloxy)methyl)naphthalene, 9c

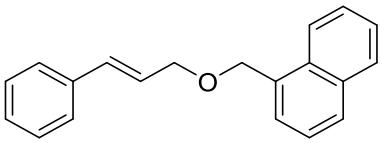

Following GP-4, **9c** (450 mg, 1.64 mmol) was afforded with 76% yield.

^{1}H NMR (400 MHz, $CDCl_3$) δ 8.18 (dd, *J* = 8.4, 1.2 Hz, 1H), 7.94 – 7.81 (m, 2H), 7.61 – 7.50 (m, 3H), 7.47 (dd, *J* = 8.2, 6.9 Hz, 1H), 7.44 – 7.40 (m, 2H), 7.34 (t, *J* = 7.4 Hz, 2H), 7.29 – 7.23 (m, 1H), 6.68 (d, *J* = 15.9 Hz, 1H), 6.39 (dt, *J* = 15.9, 6.0 Hz, 1H), 5.05 (s, 2H), 4.29 (dd, *J* = 6.1, 1.5 Hz, 2H). **^{13}C NMR** (101 MHz, $CDCl_3$) δ 137.0, 134.1, 134.0, 133.0, 132.1, 129.0, 128.9 (2C), 128.0, 126.8 (2C), 126.6, 126.4, 126.1, 125.6, 124.4, 71.2, 70.9. **ESI-MS** calcd for $C_{20}H_{18}NaO$ $[M+Na]^+$ 297.12, found 297.15.

(Z)-4-Phenylbut-3-en-1-ol, (Z)-9a

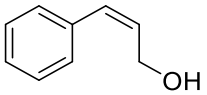

Following GP-7, **(*Z*)-9a** was prepared from the corresponding (*E*)-cinnamyl alcohol **9a**. Spectroscopic data are consistent with literature.

^{1}H NMR (400 MHz, $CDCl_3$) δ 7.36 – 7.17 (m, 5H), 6.58 (d, *J* = 11.8 Hz, 1H), 5.88 (dt, *J* = 11.7, 6.4 Hz, 1H), 4.45 (dd, *J* = 6.5, 1.7 Hz, 2H), 1.64 (s, 1H). **ESI-MS** calcd for $C_9H_{11}O$ $[M+H]^+$ 135.18, found 135.21.

6-Phenyl-3-oxabicyclo[3.2.0]heptane, 10b

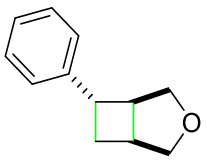

Following GP-5, **10b** was afforded with variable yields (see Results and Discussion)

^{1}H NMR (400 MHz, $CDCl_3$) δ 7.37 – 7.31 (m, Dia1, 2H; Dia2, 2H), 7.30 – 7.26 (m, Dia1, 2H), 7.24 – 7.19 (m, Dia1, 1H; Dia2, 3H), 4.01 (dd, J = 9.3, 7.3 Hz, Dia1, 2H), 3.86 (d, J = 9.0 Hz, Dia2, 1H), 3.72 (dd, J = 9.8, 1.6 Hz, Dia2, 2H), 3.63 (dd, J = 9.3, 5.7 Hz, Dia1, 1H), 3.53 (dd, J = 9.3, 4.6 Hz, Dia1, 1H), 3.45 (dd, J = 9.0, 4.4 Hz, Dia2, 1H), 3.38 (dd, J = 10.0, 6.7 Hz, Dia2, 1H), 3.30 – 3.17 (m, Dia1, 1H; Dia2, 1H), 3.07 – 2.93 (m, Dia1, 2H; Dia2, 1H), 2.45 (dddd, J = 12.4, 10.4, 8.2, 2.4 Hz, Dia2, 1H), 2.32 (dt, J = 12.4, 8.1 Hz, Dia1, 1H), 2.23 – 2.15 (m, Dia1, 1H; Dia2, 1H). **^{13}C NMR** (101 MHz, $CDCl_3$, Dia1) δ 146.2, 128.5 (2C),

126.5 (2C), 126.0, 74.5, 74.1, 47.3, 42.0, 35.4, 31.9. **ESI-HRMS** calcd for $C_{12}H_{14}O$ $[M+H]^+$ 175.1045, found 175.1050

4-Phenyl-3,3,4,5-tetrahydro-1H-5,9b-ethenonaphtho[1,2-c]furan, 10c

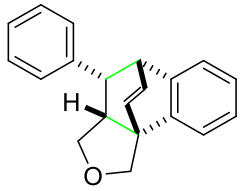

Following GP-6, **10c** was afforded with variable yields (see Results and Discussion). **^{1}H NMR** (400 MHz, $CDCl_3$) δ 7.43 (m, Dia2, 1H), 7.33 (m, Dia2, 2H), 7.28 – 7.06 (m, Dia1, 7H; Dia2, 6H), 6.91 (dd, *J* = 7.6, 6.2 Hz, Dia1, 1H), 6.79 (dd, *J* = 7.7, 1.2 Hz, Dia2, 1H), 6.64 (m, Dia1, 2H; Dia2, 1H), 6.38 (d, *J* = 7.6 Hz, Dia1, 1H), 4.96 (d, *J* = 8.7 Hz, Dia2, 1H), 4.52 (s, Dia1, 2H), 4.16 – 4.03 (m, Dia1, 1H; Dia2, 2H), 3.93 (d, *J* = 6.1 Hz, Dia1, 1H), 3.36 (dd, *J* = 11.0, 7.4 Hz, Dia1, 1H), 2.88 – 2.81 (m, Dia1 1H; Dia2, 2H), 2.56 (dd, *J* = 6.9, 1.6 Hz, Dia2, 1H), 2.41 (dt, *J* = 11.3, 7.1 Hz, Dia2, 1H), 2.21 (dddd, *J* = 11.0, 7.5, 6.3, 1.1 Hz, Dia1, 1H). **^{13}C NMR** (101 MHz, $CDCl_3$, Dia1) δ 144.2, 143.4, 140.3, 138.7, 136.0, 128.2 (2C), 127.6 (2C), 126.5, 126.3, 125.6, 125.1, 118.7, 72.7, 70.1, 55.5, 54.7, 50.0, 47.2. **ESI-HRMS** calcd for $C_{20}H_{18}O$ $[M+H]^+$ 275.3650, found 275.3663.

Photophysical Characterization's Table

	λ_{max} emission (nm)	Triplet Energy E_t (Kcal mol^{-1})	Triplet Lifetimes τ (ns)	**Quantum yield** in CH_3CN (%)	**Ksv** (Stern-Volmer constant, L mol^{-1})	**Kq** (Quenching rate constant, L mol^{-1} s^{-1})
$Ir(ppy)_3$	518	59.5	4679	40 [a]		
[Ir]-F [b]	473	63.8				
PCS1	617	55.3				
PCS2	580	56.7	235	0.5		
PCS3	550	57.9	873	4.9		
PCS4	575	56.4	609	1.9	13	2.1E+07
PCS5	527	61.3	1825	12.8	578	3.2E+08
PCS6	565	57.2	821	3.5		
PCS7	524	61.6	1867	15.2	1785	9.6E+08
PCS8	580	57.7	210	0.3		
PCS9	551	59.5				

[a]: Chem. Mater.2006, 18, 12, 2778–2780

[b]: $Ir(dF(CF_3)ppy)_2(dtbbpy)(PF_6)$

Emission spectra were recorded on a FLS 980 (Edinburg Instrument Ltd), in dry and degassed CH_3CN.

Triplet energy values were extrapolated from the intersection of the tangent to the high energy side of the curve on the x axis. The formula is $Et=(h*c*Na)/\lambda$.

Triplet state lifetimes were recorded on a Nanolog (Horiba Scientific) spectrofluorimeter composed of iH320 spectrograph equipped with a Synapse QExtra charge-coupled device, in dry and degassed CH_3CN.

The Stern-Volmer constant is the slope of the curve obtained by plotting I_0/I (intensity of the fluorescence emission before and after the addition of a quencher) vs the concentration of the quencher itself.

The quenching rate constant (Kq) is derived from the Stern-Volmer constant (Ksv) and the Triplet Lifetime measurement (τ).

Quenching Experiments

Fluorescence Quenching experiments were recorded on a FLS 980 (Edinburg Instrument Ltd) with a resolution of 1 nm. Samples were prepared in CH_3CN. The concentration of the photocatalyst was adjusted to reach an absorption around 0.2 at the excitation wavelength (measured with Perkin-Elmer Lambda 900 spectrophotometer). The exciting wavelength was set at 380 nm. A quartz cuvette (optical path = 1 cm) capped with a rubber septum was used. The solution was degassed bubbling nitrogen in it immediately prior to use and each time after the additions of the quencher.

*Quenching of **PCS4** with substrate **9b***

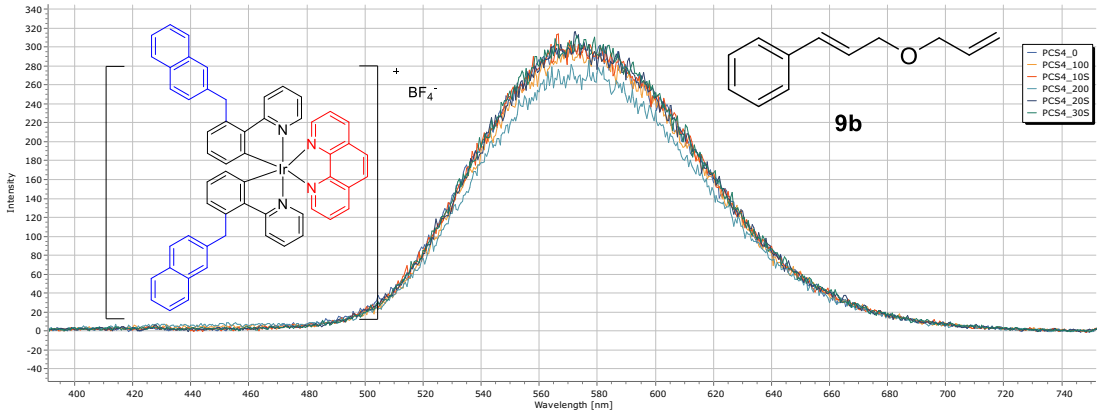

*Quenching of **PCS5** with substrate **9b***

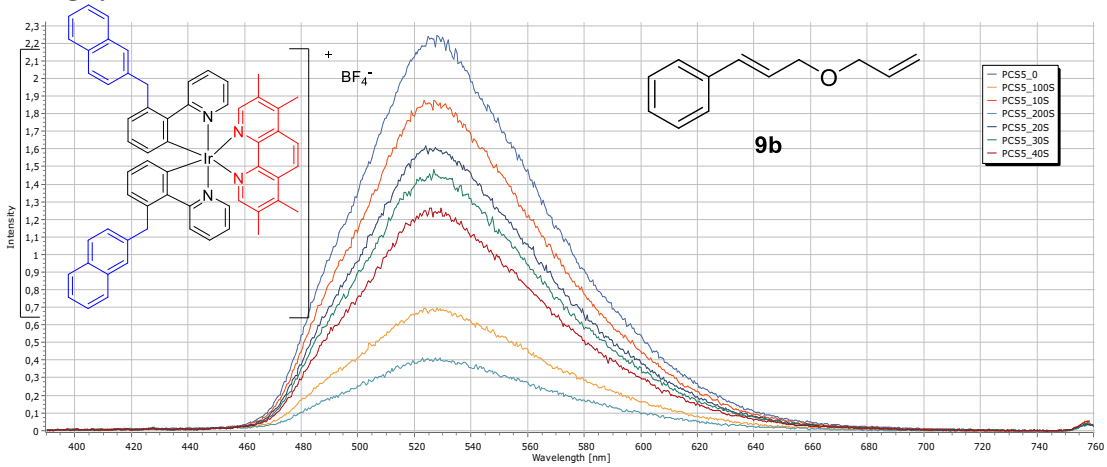

Quenching of **PCS7** with substrate **9b**

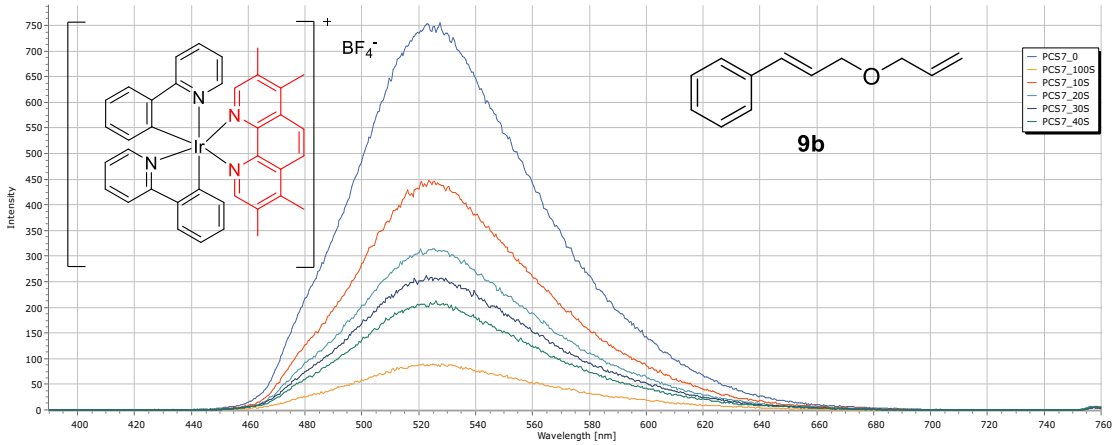

Cyclic Voltammetry Experiments

All the spectra were measure with IKA ElectraSyn 2.0 in dry and degassed CH_3CN using a glassy carbon disc working electrode, a platinum plate counter electrode and Ag/AgCl as reference electrode. The excited state redox potential were estimated from the measured ground state redox potential and the excited state Energy $E_{0,0}$ as described by Fox.[66]

CV of **PCS5** (2mM) in CH_3CN with $[(t\text{-}Bu)_4N][PF_6]$ 0.1M as electrolyte.

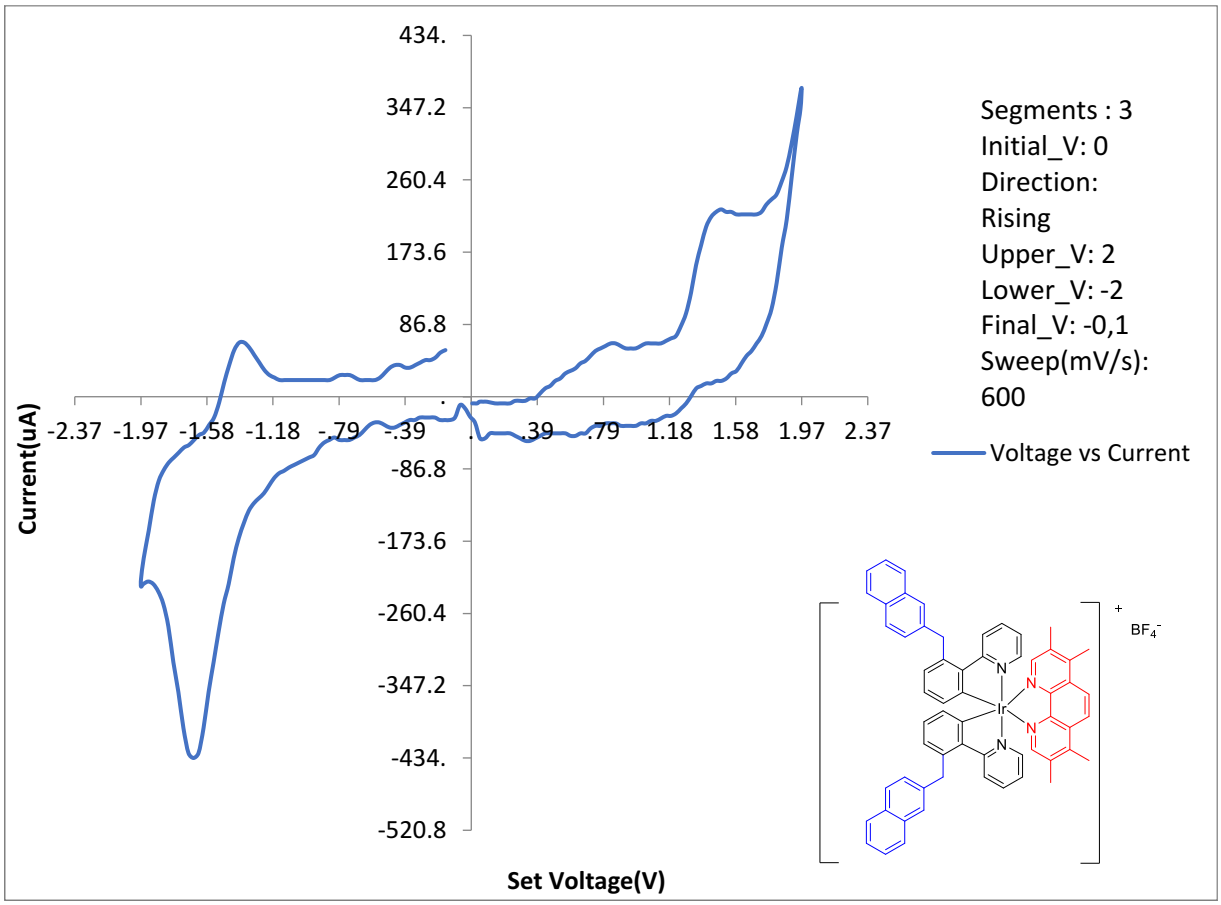

Ered (V vs Ag/AgCl)	-1.51
***Ered (V vs Ag/AgCl)**	1.14
Eox (V vs Ag/AgCl)	1.34
***Eox (V vs Ag/AgCl)**	-1.31

CV of **PCS7** (2mM) in CH_3CN with $[(t\text{-}Bu)_4N][PF_6]$ 0.1M as electrolyte.

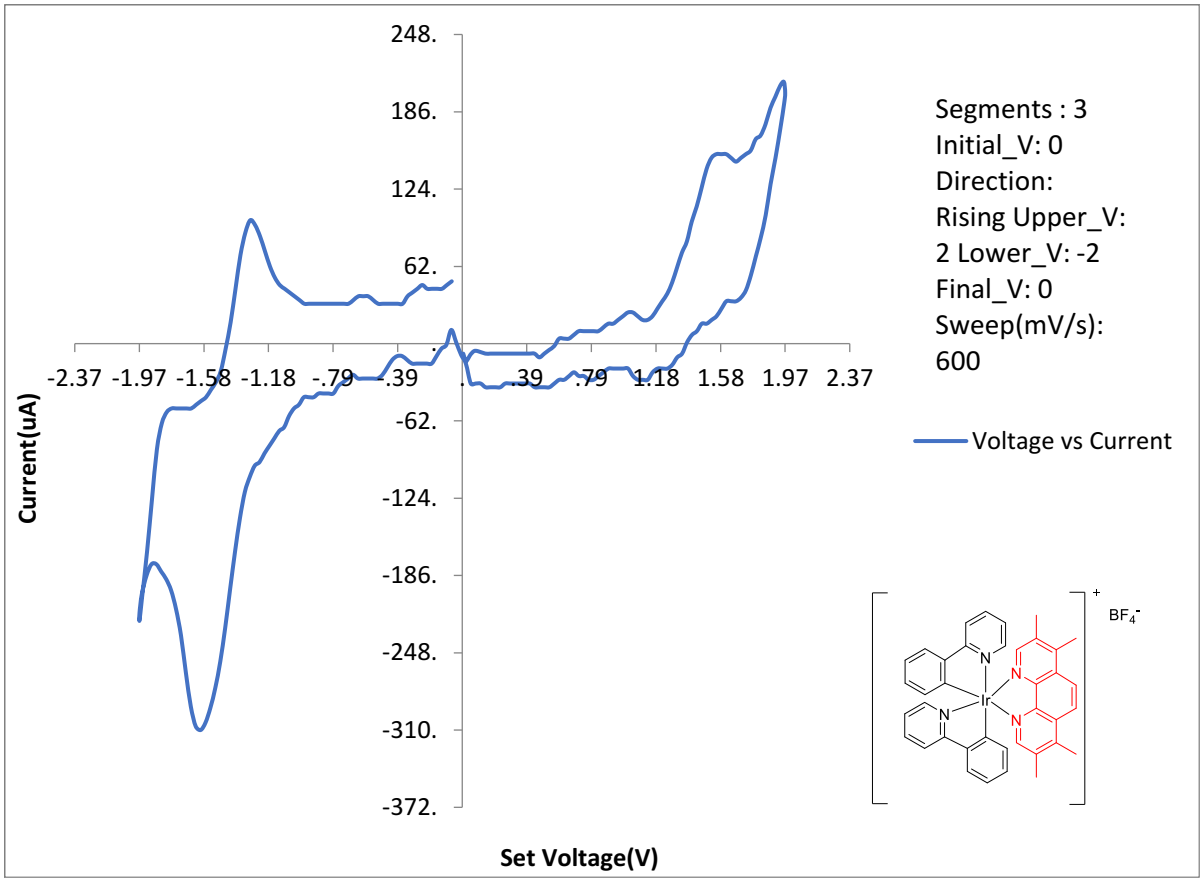

Ered (V vs Ag/AgCl)	-1.44
***Ered (V vs Ag/AgCl)**	1.23
Eox (V vs Ag/AgCl)	1.34
***Eox (V vs Ag/AgCl)**	-1.33

Synthesis of new bis-phosphine allenes and their use as metallic ligands

4.1 Introduction: Allenes and axial chirality

Allenes are organic compounds in which one carbon atom has a double bond with each of its two adjacent carbon centers. The C1 and C3 carbons of an allene are sp^2-hybridized, whereas the central C2 carbon is sp-hybridized (Figure 25).

Notably, when two different substituents on each of the two carbon atoms are present, the non-free rotation of the double bonds grants to allenes an interesting property: axial chirality (C2-simmetry). This is due to the fact that there are no longer observable mirror planes.

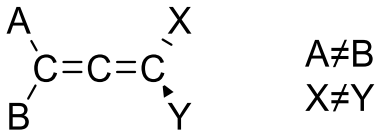

Figure 25: General structure of chiral allenes.

Axial chirality is a fundamental concept in organic chemistry that arises when a molecule contains an axis of chirality, which means it can exist in two or more non-superimposable mirror image forms. This type of chirality is distinct from the more commonly known point chirality, where stereocenters are involved.

An example of a molecule displaying axial chirality is BINAP, which stands for 2,2'-bis(diphenylphosphino)-1,1'-binaphthyl (Figure 26). BINAP is a widely used chiral ligand in asymmetric synthesis and catalysis.

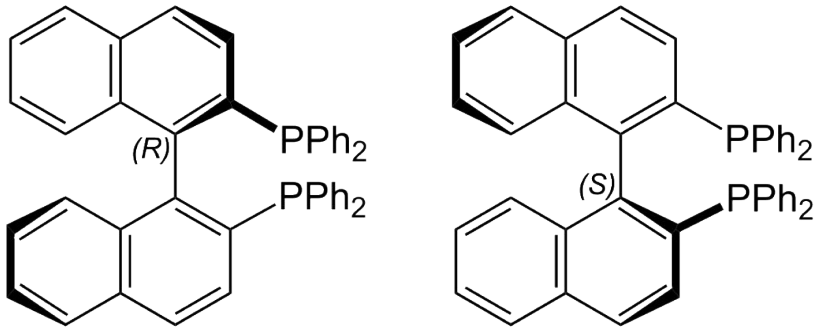

Figure26: Structure of (R) and (S) – BINAP.

The axial chirality in BINAP arises from the restricted rotation around the C-C bond which connects the two naphthyl units. Due to this restricted rotation, BINAP can exist as two distinct enantiomers (R and S), which cannot be superimposed on each other, just like left and right hands. This property makes BINAP a valuable tool in asymmetric catalysis, where

the specific orientation of the ligand's chirality can control the outcome of chemical reactions, leading to the formation of chiral products with high enantiomeric purity.

In the same way, allenes are considered valuable ligands in asymmetric catalysis, thanks to this unique property. Nonetheless, the number of allene-derived ligands involved in metallic coordination complexes is very limited.[67]

4.2 Introduction: Bis-phosphine allene ligands

The group of prof. Fensterbank first reported in 2016 the synthesis of 1,3-bis(diphenylphosphino)-1,3-diphenylallene.[67]

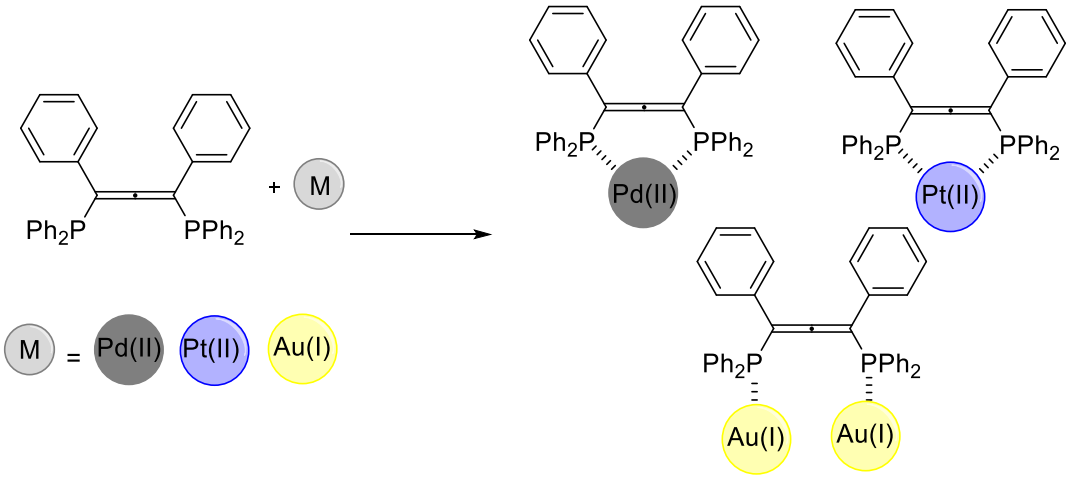

Figure 27: Coordination complexes of 1,3-bis(diphenylphosphino)-1,3-diphenylallene with transition metals.

The unexplored coordination properties of this ligand were studied, soon discovering that it could give rise to interesting coordination complexes with palladium, platinum and gold metals (Figure 27).

Mononuclear palladium(II) and platinum(II) complexes were obtained treating the ligand with bis(acetonitrile)dichloropalladium or bis(acetonitrile)dichloroplatinum in toluene at 80°C. The bis-phospine allene act as a bidentate ligand.

In the case of gold metal instead, the formation of a polymeric gold complex was observed when trying to obtain the mononuclear complex. On the other hand, the formation of the reported dinuclear complex occurred easily and its structure was confirmed by XRD analysis. Moreover, the just mentioned dinuclear complex was used in a series of diagnostic catalytic reactions and gave promising preliminary results in asymmetric catalysis.

4.3 Results and discussion

Starting from alkyne **11**, we easily obtained the desired allene **12** after treatment with two equivalents of butyl lithium followed by two equivalents of chlorodiphenyl phosphine, as already described by Fensterbank and co-workers (Scheme 32).[67]

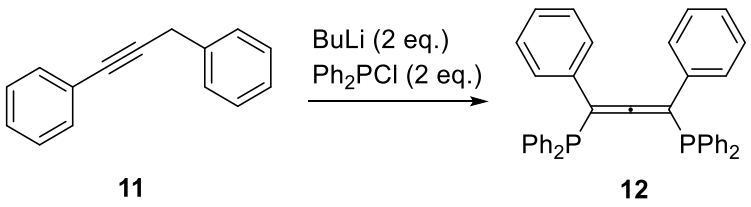

*Scheme 32: Synthesis of bis-phosphine allene **12**.*

Then, following the indications first reported in Dr. Fen Zhao's PhD thesis, free bis-phosphine **12** was directly treated in situ with two equivalents of borane dimethyl sulfide, in order to avoid the undesired oxidation of the bis-phosphine. Intermediate **13** was obtained in this way (Scheme 33). **13** is completely stable to oxidation in atmospheric conditions and, moreover, it can be purified by flash chromatography and stored for long periods without decomposition occurring.

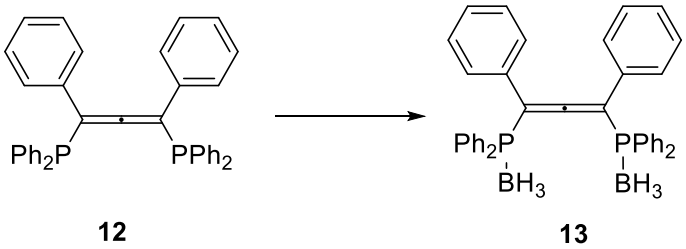

*Scheme 33: Synthesis of protected bis-phosphine allene **13**.*

Exploiting this impressive stability, the two enantiomers of **13** can be separated by HPLC resolution on chiral column (Figure 28).

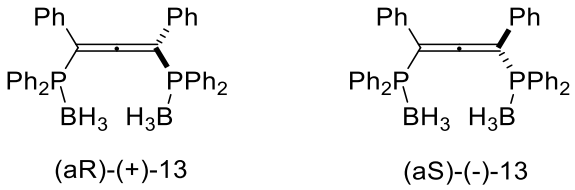

*Figure 28: Structure of (R) and (S) enantiomers of **13**.*

Knowing that heating **13** at reflux in a 1/1 solution of toluene and ethanol leads to the complete deprotection from the borane groups, re-forming free bis-phosphine **12**, we decided

instead to try to selectively mono-deprotect **13** thoroughly controlling the equivalents of EtOH added. In this way we successfully obtained the partially protected bis-phosphine **14** (Scheme 34).

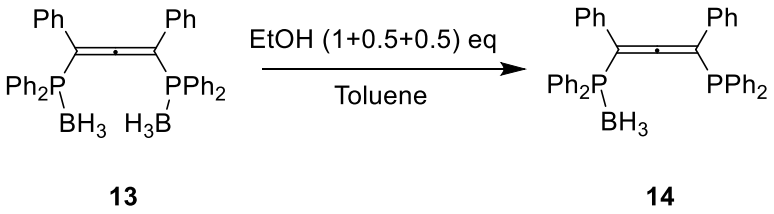

13 **14**

*Scheme 34: Synthesis of mono-protected bis-phosphine allene **14**.*

The optimal quantity of EtOH needed to perform this reaction was investigated. The molar ratio between **13**, **14** and **12** was calculated by NMR integration (Figure 29) after each addition:

1 eq of EtOH: 72% **13**, 28% **14**, 1% **12**

1.5 eq of EtOH: 63% **13**, 35% **14**, 2% **12**

2 eq of EtOH: 55% **13**, 42% **14**, 3% **12**

2.5 eq of EtOH: 46% **13**, 47% **14**, 7% **12**

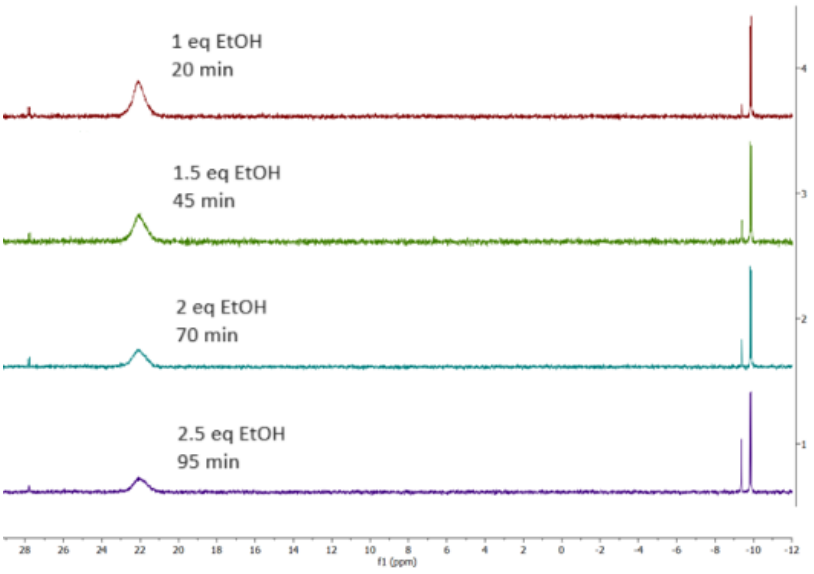

Figure 29: ^{31}P NMR spectra after each addition of EtOH.

After each addition, the formation of the desired product **14** increases together with the formation of the side-product **12**, which is very challenging to remove from the mixture. It is easier instead to remove the starting material **13,** through re-crystallization. For this reason, with the idea to minimize the formation of **12**, we established 1.5 eq of EtOH as standard conditions, without pushing further.

The free phosphine of **14** does not undergo oxidation, even when bubbling air inside a solution of this derivative. This is contrary to the normal behaviour of similar, electron-rich and sterically accessible phosphines. A possible explanation to this behaviour is reported hereafter: every BH_3 group could bridge two phosphines forming a totally stable chain structure (Figure 30).

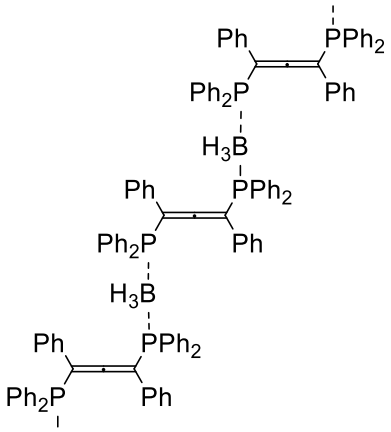

*Figure 30: Proposed conformation of **14** to rationalize the stability to oxidation.*

Exploiting the air stability of this unusual ligand, we successfully obtained a single crystal for XRD analysis and ^{31}P NMR characterization (Figure 31). The broad singlet at 22 ppm correspond to the P-BH_3 signal, while the sharp doublet at -10 ppm comes from the free phosphine. The small singlet at -9 ppm is the signal of the fully deprotected phosphine, which is present in traces.

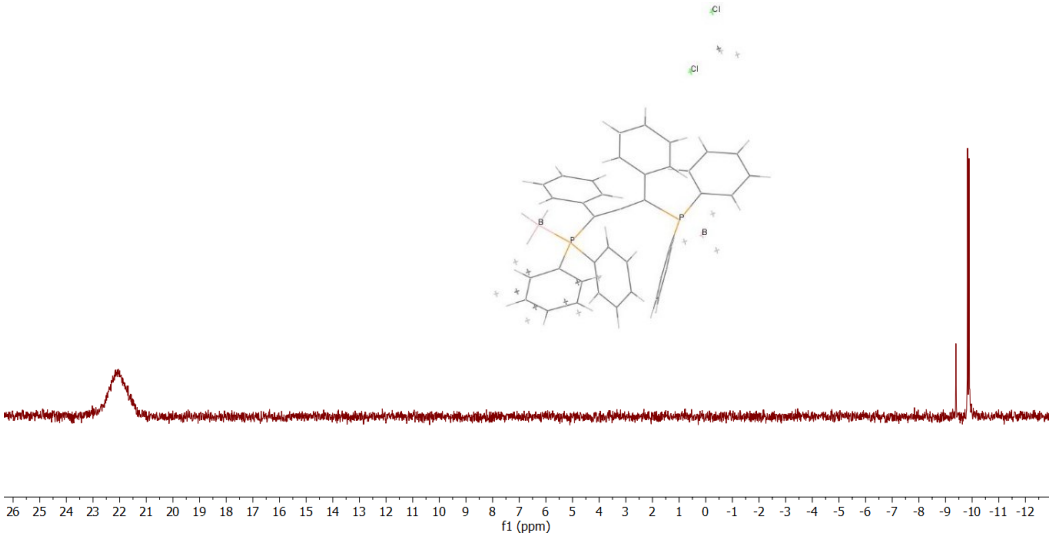

*Figure 31: ^{31}P NMR spectrum and XRD of **14**.*

Then, treating **14** with one equivalent of an Au(I) salt we obtain gold complex **15** (Scheme 35).

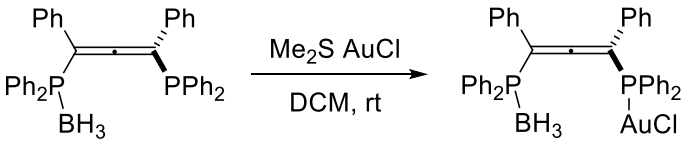

14 **15**

*Scheme 35: Synthesis of gold complex **15**.*

This complex was characterized by X-Ray Diffraction and by ^{31}P NMR (Figure 32). The broad singlet at 23.5 ppm correspond to the P-BH_3 signal, while the doublet at 29 ppm is the signal of P-Au unit. Finally, the singlet at 29.5 ppm testify the presence of traces of the symmetric dinuclear gold complex.

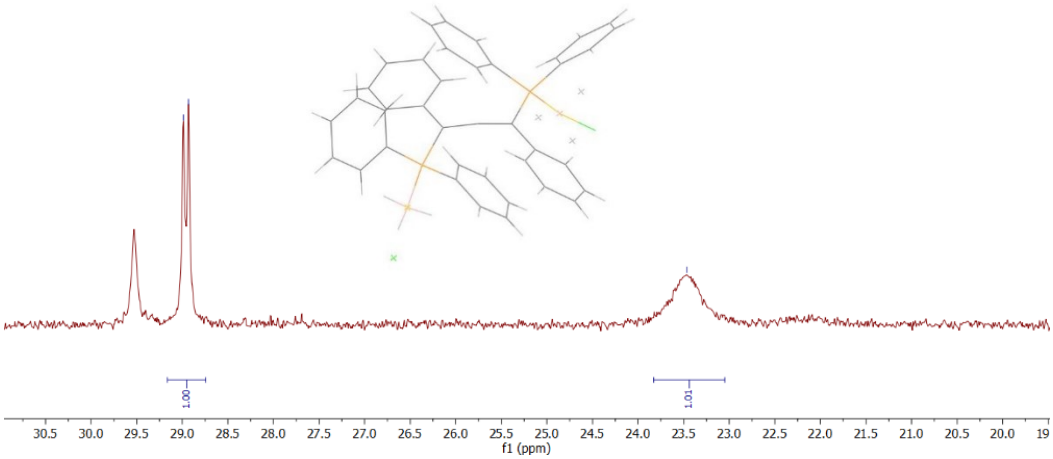

*Figure 32: ^{31}P NMR spectrum and XRD of gold complex **15**.*

Normally, gold complexes are activated by the use of a Ag(I) co-catalyst. This is possible for **15** too: the silver salt can capture the chloride anion and promote the formation of the active cationic gold species. However, for gold complex **15,** this is not the only possibility: we found an alternative method for the formation of the cationic gold species, without involving the silver salt. This alternative method implies the use of a source of trityl cation to abstract a hydrogen from the BH_3 group. Then, the positive charged B atom captures the chloride anion finally forming the active cationic gold species (Scheme 36).

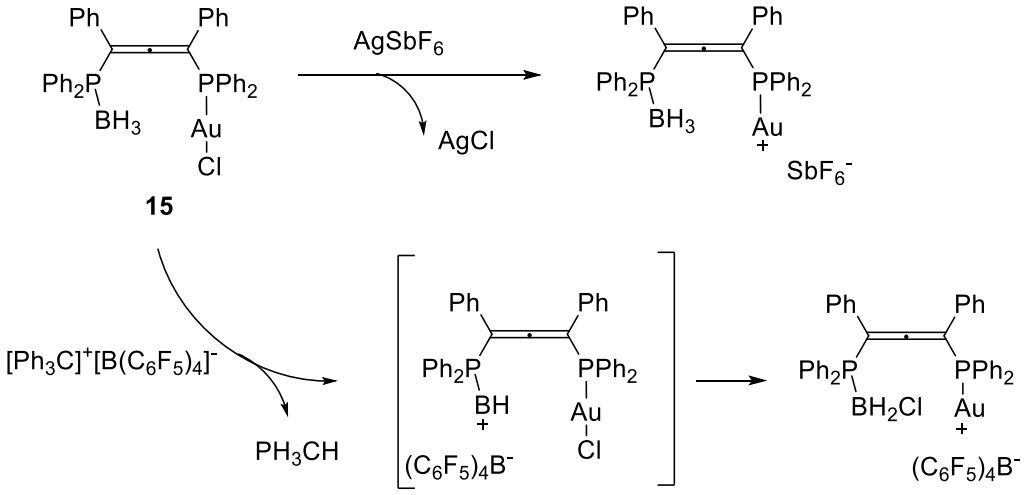

*Scheme 36: Different ways of activating gold complex **15**.*

The counter anion is different in the two cases, probably resulting in a different catalytic behaviour of the cationic Au(I) species. Even if this was not the case, the alternative method for the activation of the gold complex may be useful in those cases in which the substrates

are not inert towards silver salts (e.g. see the first chapter of this thesis). Moreover, AgX species are often not photostable, so normally incompatible with photocatalysis.

After this result, inspired by the work of Hahn's group,[68] we decided to prepare a second gold complex adorned with the bis-phosphine allene functionality. Hahn reported the synthesis of various mono-oxide gold complexes from 1,2-bis-phosphine benzenes. We decided to adapt this reactivity to bis-phosphine allenes. First, **13** was completely deprotected from the BH_3 groups refluxing in a mixture of ethanol and toluene. Free bis-phosphine allene **12** was obtained in this way. Then, **12** reacted with sodium tetrachloroaureate in a mixture of acetonitrile and water to give the desired product **16** (Scheme 37).

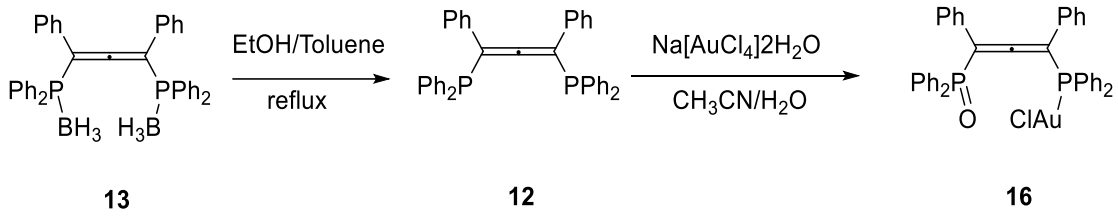

13 **12** **16**

*Scheme 37: Synthesis of gold complex **16**.*

Gold complex **16** is another potential interesting catalyst for asymmetric catalysis. The newly synthetized complex was characterized by XRD and ^{31}P NMR (Figure 33). The phosphorus NMR shows two doublets with the same coupling constant (12 Hz): the doublet at 29.5 ppm corresponds to P-Au, while the doublet at 28 ppm corresponds to P=O.

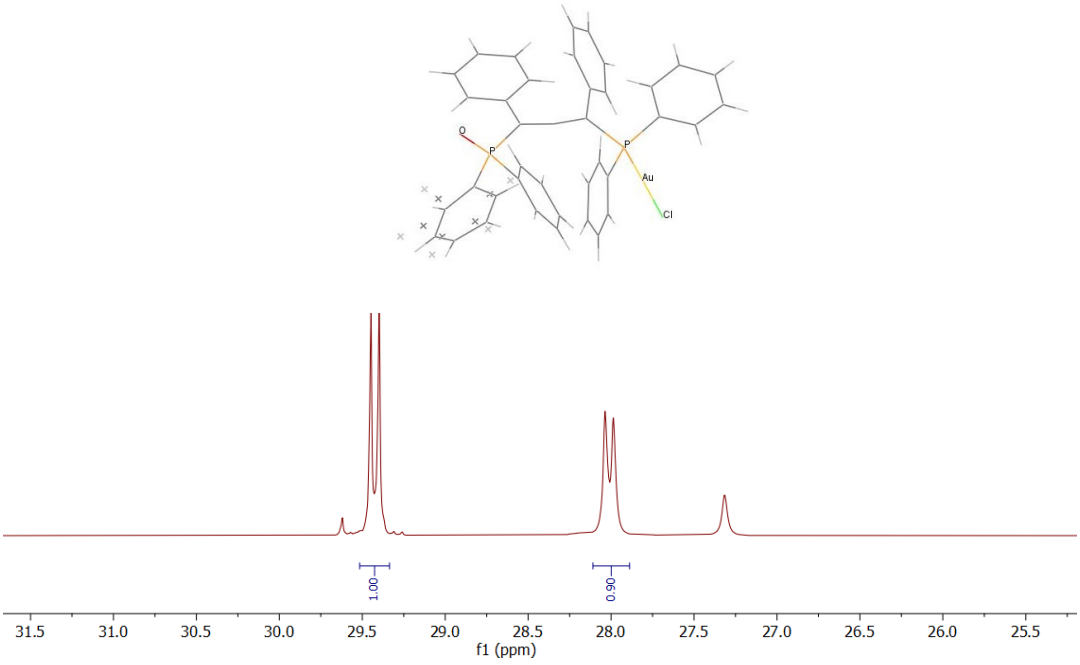

*Figure 33: ^{31}P NMR spectrum and XRD of gold complex **16**.*

4.4 Conclusion

In conclusion, we synthetized bis-phosphine allene ligands **12**, **13** and **14**. Mono-protected ligand **14** has an unreported structure, which unexpectedly granted stability to the oxidation of the free phosphine in atmospheric conditions. Then, two new gold complexes **15** and **16** were prepared and thoroughly characterized. These complexes hold great potential as catalysts in asymmetric reactions.

4.5 Experimental section

General Remarks

All reactions were performed under argon atmosphere, in flame dried glassware with magnetic stirring using standard Schlenk techniques, unless otherwise mentioned. All solvents were freshly distilled prior to use: Et_2O and THF over sodium and benzophenone; CH_2Cl_2 and toluene over CaH_2. DMF and DMSO were dried and degassed before using. Technical grade solvents for extraction and chromatography were used without distillation.All other reagents were purchased from commercial sources (Sigma-Aldrich, Alfa Aesar, Fluorochem, Strem Chemicals) and were used without purification, unless otherwise noted. Column chromatography was performed on Merck Geduran SI 60 A silica gel (35-70 mm). Analytical Thin-layer chromatography (TLC) was performed on Merck 60 F254 silica gel and visualized either with a UV lamp (254 nm), or using solutions of para-anisaldehyde-sulfuric acid-acetic acid in EtOH or $KMnO_4$-K_2CO_3 in water followed by heating. ^{1}H NMR and ^{13}C NMR spectra were recorded at room temperature unless otherwise required on a Bruker Avance 300 MHz or a Bruker Avance 400 MHz spectrometer. ^{31}P NMR spectra were recorded at 122 MHz or 162 MHz and data are reported as follows: chemical shift in ppm with an internal probe of H_3PO_4 (85% in H_2O, δ 0.0). Shifts (δ) are given in parts per million (ppm) and coupling constants (J) are given in Hertz (Hz). High resolution mass spectra (HRMS) were obtained using a mass spectrometer MicroTOF from Bruker with an electron spray ion source (ESI) and a TOF detector at Institut Parisien de Chimie Moléculaire.

Synthesis and carachterization

Synthesis of 13 (through 12)

To a solution of 1,3-diphenyl-1-propyne **1** (1.50 g, 7.80 mmol, 1 equiv) in THF (80 mL) was added *n*-BuLi (6.24 mL of 2.5 M in hexane, 15.60 mmol, 2 equiv) at –78 °C. The solution of chlorodiphenylphosphine (2.9 mL, 15.60 mmol, 2 equiv) in THF (10 mL) was slowly added into the mixture at the same temperature. The mixture was slowly warmed to room temperature for 15 h and concentrated under reduced pressure with an Argon balloon attached to the rotavapor's vent.

Then, the crude mixture was dissolved in 50 mL Et_2O and BH_3 Me_2S (2 eq.) was slowly added at 0 °C. The mixture was gradually warmed to rt for 1h and then extracted with CH_2Cl_2 (20 mL) and washed with water. The aqueous solution was extracted again with CH_2Cl_2 (2x 20 mL). The combined organic layers were washed with brine (10 mL), dried over anhydrous $MgSO_4$, filtered and concentrated under reduced pressure. Purification by chromatography on silica gel using DCM/pentane (1/2) as eluent to afford the desired product **13** (3.9 g, 85% yield) as a yellow solid.

Characterization of 13

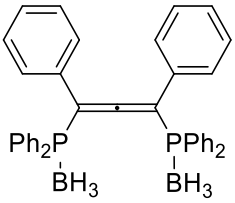

13

^{1}H NMR (400 MHz, $CDCl_3$) δ 7.64 - 7.14 (m, 30H), 1.29 (s, 6H).

The NMR data are consistent with previously reported spectra in Dr. Fen Zhao's PhD Thesis.

Synthesis of 14

A degassed solution of **13** (1 eq.) in Toluene (0.2 M) was flushed with Argon and then heated to 100°C using an oil bath. Small quantities of absolute EtOH (1 eq. + 0.5 eq. + 0.5 eq.) were added in portions every 20 minutes. After 20 minutes from the last addition, the oil bath was removed and the solution was left stirring until it got back to r.t. under Argon atmosphere. The solvents were removed through a Schlenk line giving the crude desired product **14**.

Characterization of 14

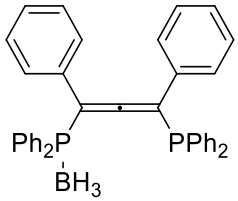

14

^{31}P NMR (162 MHz, $CDCl_3$) δ 22.06 (bs, 1P), -9.86 (d, J= 6.6 Hz, 1P).

MS calcd. for $C_{39}H_{33}BP_2$ ([M + Na]+) 574.2 found 597.2

Synthesis of 15

AuCl SMe_2 (0.6 eq, considering a maximum 60% conversion of **13** to **14**) is added to a flask containing crude **14**. Then, degassed DCM (0.1 M final concentration) is added and the mixture is stirred for 1h at r.t. under Argon atmosphere. The solvent is then evaporated under reduced pressure.

Purification: **15** can be isolated by slow evaporation crystals growth from a solution of Hexane and DCM (using the minimum possible quantity of DCM necessary to dissolve the crude).

Characterization of 15

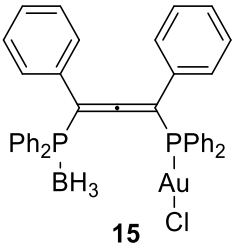

15

^{1}H NMR (400 MHz, $CDCl_3$) δ 7.61 - 7.22 (m, 30H), 1.29 (bs, 3H).

^{13}C NMR (100 MHz, $CDCl_3$) δ **213.1 – 213.0** (m, central carbon allene), 135.2 (d, J = 14.8 Hz), 135.0 (d, J = 14.9 Hz), 134.0 (d, J = 14.2 Hz), 133.9 (d, J = 14.0 Hz), 133.5 (d, J = 9.8 Hz), 133.4, 132.9 (d, J = 9.5 Hz), 132.8, 132.6 (d, J = 2.8 Hz), 132.4 (dd, J = 8.6, 2.5 Hz), 132.2 (d, J = 2.6 Hz), 130.7 (dd, J = 9.9, 4.0 Hz), 130.4 (dd, J = 9.3, 4.5 Hz), 129.8 – 129.4 (m), 129.4 – 129.0 (m), 128.9 – 128.8 (m), 128.4 (d, J = 3.9 Hz), 127.9 – 127.6 (m), 127.6, 127.5, 127.3, 127.2, 126.8, 126.4, **104.6** (dd, terminal carbon 1 allene, J = 46.0, 10.7 Hz), **101.7** (dd, terminal carbon 2 allene, J = 56.1, 9.1 Hz).

^{31}P NMR (162 MHz, $CDCl_3$) δ 28.96 (d, J= 9.1 Hz, 1P), 23.47 (bs, 1P).
(ESI)-HRMS calcd for $C_{34}H_{36}O_2$ $[M + Na]^+$ 829.1403, found 829.1404.

Synthesis of 16

13 (1 eq) was placed in a sealed flask, flushed with Argon and then dissolved in a degassed mixture of Toluene and EtOH (1/1, 0.1 M). The solution is stirred for 20 minutes at 100°C and then it is slowly cooled to r.t., under Argon atmosphere. The solvents are removed under reduced pressure through a Schlenk line. $Na[AuCl_4]2H_2O$ was quickly added to the flask, maintaining the Argon atmosphere. A degassed solution of CH_3CN/H_2O (10/1, 0.06 M) was cooled to 0°C and added. The mixture was stirred at r.t. for 40 minutes. After 20 minutes of rest, the desired product (precipitated) was separated from the solution and then further purified through a short pad of silica (from DCM only to DCM/AcOEt 1/1).

Characterization of 16

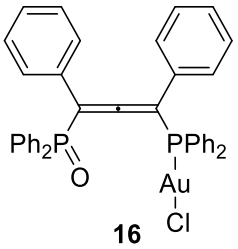

16

^{1}H NMR (400 MHz, $CDCl_3$) δ 7.62 - 7.22 (m, 30H).
^{13}C NMR (100 MHz, $CDCl_3$) δ **213.3 – 213.2** (m, central carbon allene), 135.0 (d, J = 15.1 Hz), 134.1 (d, J = 14.2 Hz), 132.9 (d, J = 2.9 Hz), 132.7 (d, J = 2.8 Hz), 132.6 (d, J = 2.7 Hz), 132.2 (d, J = 2.8 Hz), 132.1, 132.0, 131.9 – 131.8 (m), 131.7 (d, J = 9.8 Hz), 131.4 (d, J = 10.0 Hz), 131.2, 131.0, 130.9 – 130.8 (m), 130.4 – 130.2 (m), 129.3 (d, J = 3.8 Hz), 129.2 (d, J = 3.6 Hz), 129.2, 129.0, 128.9 – 128.7 (m), 128.2 (d, J = 4.4 Hz), 127.9 (d, J = 7.2 Hz), 127.6, 127.4, 127.2, 127.0, **106.5** (dd, terminal carbon 1 allene, J = 92.3, 10.4 Hz), **101.6** (dd, terminal carbon 2 allene J = 55.6, 12.0 Hz).
^{31}P NMR (162 MHz, $CDCl_3$) δ 29.42 (d, J= 11.9 Hz, 1P), 28.01 (d, J= 12.2 Hz, 1P).

References

1 X. Bi and C. J. Li, *ChemCatChem*, 2021, **13**, 3200–3201.

2 Y. C. Wu, Y. T. Xiao, Y. Z. Yang, R. J. Song and J. H. Li, *ChemCatChem*, 2020, **12**, 5312–5329.

3 M. Neetha, T. Aneeja, C. M. A. Afsina and G. Anilkumar, *ChemCatChem*, 2020, **12**, 5330–5358.

4 X. Y. Liu, S. J. Zhai, F. F. Feng, F. G. Zhang and J. A. Ma, *ChemCatChem*, 2020, **12**, 5623–5626.

5 M. Li, W. Wu and H. Jiang, *ChemCatChem*, 2020, **12**, 5034–5050.

6 S. Zhu, R. Liang, H. Jiang and W. Wu, *Angewandte Chemie*, 2012, **124**, 11019–11023.

7 G. Mo, Z. Tian, J. Li, G. Wen and X. Yang, *Appl Organomet Chem*, 2015, **29**, 231–233.

8 A. Venkanna, O. W. Kwon, S. Afzal, C. Jang, K. H. Cho, D. K. Yadav, K. Kim, H. G. Park, K. H. Chun, S. Y. Kim and M. H. Kim, *Scientific Reports 2017 7:1*, 2017, **7**, 1–17.

9 S. Pajk, M. Živec, R. Šink, I. Sosič, M. Neu, C. W. Chung, M. Martínez-Hoyos, E. Pérez-Herrán, D. Álvarez-Gómez, E. Álvarez-Ruíz, A. Mendoza-Losana, J. Castro-Pichel, D. Barros, L. Ballell-Pages, R. J. Young, M. A. Convery, L. Encinas and S. Gobec, *Eur J Med Chem*, 2016, **112**, 252–257.

10 F. Colobert, R. Des Mazery, G. Solladié and M. C. Carreño, *Org Lett*, 2002, **4**, 1723–1725.

11 H. Fuwa, S. Naito, T. Goto and M. Sasaki, *Angew Chem Int Ed Engl*, 2008, **47**, 4737–4739.

12 E. A. Crane and K. A. Scheidt, *Angew Chem Int Ed Engl*, 2010, **49**, 8316.

13 H. Fuwa, *Mar Drugs*, 2016, **14**, 65.

14 Z. Zhang, H. Xie, H. Li, L. Gao and Z. Song, *Org Lett*, 2015, **17**, 4706–4709.

15 Q. Su and J. S. Panek, *J Am Chem Soc*, 2004, **126**, 2425–2430.

16 A. K. Ghosh, K. A. Shurrush and Z. L. Dawson, *Org Biomol Chem*, 2013, **11**, 7768–7777.

17 T. Ollevier, *Org Biomol Chem*, 2013, **11**, 2740–2755.

18 A. H. Hoveyda and A. R. Zhugralin, *Nature*, 2007, **450**, 243–251.

19 C. F. Nising and S. Brase, *Chem Soc Rev*, 2012, **41**, 988–999.

20 L. Wang, P. Li and D. Menche, *Angewandte Chemie International Edition*, 2010, **49**, 9270–9273.

21 M. F. Semmelhack, C. Kim, N. Zhang, C. Bodurow, M. Sanner, W. Dobler and M. Meier, *Pure and Applied Chemistry*, 1990, **62**, 2035–2040.

22 M. Dehghany and J. M. Schomaker, *Curr. Opin. Green Sustain.Chem*., 2021, **30**, 100483.

23 P. J. Pérez, *Angewandte Chemie International Edition*, 2010, **49**, 9040–9040.

24 X. Bi and C. J. Li, *ChemCatChem*, 2021, **13**, 3200–3201.

25 A. Serafino, D. Balestri, L. Marchiò, M. Malacria, E. Derat and G. Maestri, *Org Lett*, 2020, **22**, 6354–6359.

26 A. Serafino, N. Camedda, M. Lanzi, N. Della Ca', G. Cera and G. Maestri, *Journal of Organic Chemistry*, 2021, **86**, 15433–15452.

27 D. Tanaka, Y. Sato and M. Mori, *J Am Chem Soc*, 2007, **129**, 7730–7731.

28 D. C. Nonhebel, *Chem Soc Rev*, 1993, **22**, 347–359.

29 G. Benoit and A. B. Charette, *J. Am. Chem. Soc*, 2017, **139**, 1364–1367.

30 M. Bakos, Á. Gyömöre, A. Domján and T. Soós, *Angewandte Chemie*, 2017, **129**, 5301–5305.

31 S. Kumar, S. Joyasawal, B. V. S. Reddy, P. Chakravarthy, A. D. Krishna and J. S. Yadav, *Indian J Chem*, 2005, **44b**, 1686–1682.

32 Zoua Pa Vang, Albert Reyes, Reilly E. Sonstrom, Martin S. Holdren, Samantha E. Sloane, Isabella Y. Alansari, Justin L. Neill, Brooks H. Pate and Joseph R. Clark*, *J. Am. Chem. Soc.*, 2021, **143**, 7707–7718.

33 D. Ruggeri, E. Motti, N. Della Ca' and G. Maestri, *Org Biomol Chem*, 2022, **20**, 9287–9291.

34 M. Lanzi, V. Santacroce, D. Balestri, L. Marchiò, F. Bigi, R. Maggi, M. Malacria and G. Maestri, *Angewandte Chemie*, 2019, **131**, 6775–6779.

35 J. Young Buckanan, *J. Chem. Soc.*, 1926, **129**, 993–1050.

36 G. Büchi, C. G. Inman and E. S. Lipinsky, *J Am Chem Soc*, 1954, **76**, 4327–4331.

37 J. M. Herrmann, J. Disdier, M. N. Mozzanega and P. Pichat, *J Catal*, 1979, **60**, 369–377.

38 C. Kormann, D. W. Bahnemann and M. R. Hoffmann, *Environ Sci Technol*, 1988, **22**, 798–806.

39 J. W. Verhoeven, *Pure and Applied Chemistry*, 1996, **68**, 2223–2286.

40 F. Strieth-Kalthoff, M. J. James, M. Teders, L. Pitzer and F. Glorius, *Chem Soc Rev*, 2018, **47**, 7190–7202.

41 C. Michelin and N. Hoffmann, *ACS Catal*, 2018, **8**, 12046–12055.

42 L. Marzo, S. K. Pagire, O. Reiser and B. König, *Angewandte Chemie International Edition*, 2018, **57**, 10034–10072.

43 F. Glaser, C. Kerzig and O. S. Wenger, *Angewandte Chemie International Edition*, 2020, **59**, 10266–10284.

44 M. Lepori, S. Schmid and J. P. Barham, *Beilstein Journal of Organic Chemistry*, 2023, **19**, 1055–1145.

45 M. Marchini, G. Bergamini, P. G. Cozzi, P. Ceroni and V. Balzani, *Angewandte Chemie International Edition*, 2017, **56**, 12820–12821.

46 A. Chatterjee and B. König, *Angewandte Chemie International Edition*, 2019, **58**, 14289–14294.

47 A. Serafino, *PhD Thesis, Visible light promoted polycyclizations of enynes and enallenes*, Parma, 2021.

48 D. B. Huple, B. D. Mokar and R. Liu, *Angewandte Chemie*, 2015, **127**, 15137–15141.

49 C. Cecchini, M. Lanzi, G. Cera, M. Malacria and G. Maestri, *Synthesis (Germany)*, 2019, **51**, 1216–1224.

50 J. C. Bawden, P. S. Francis, S. DiLuzio, D. J. Hayne, E. H. Doeven, J. Truong, R. Alexander, L. C. Henderson, D. E. Gómez, M. Massi, B. I. Armstrong, F. A. Draper, S. Bernhard and T. U. Connell, *J Am Chem Soc*, 2022, **144**, 11189–11202.

51 S. Diluzio, T. U. Connell, V. Mdluli, J. F. Kowalewski and S. Bernhard, *J Am Chem Soc*, 2022, **144**, 1431–1444.

52 J. He, Z. Q. Bai, P. F. Yuan, L. Z. Wu and Q. Liu, *ACS Catal*, 2021, **11**, 446–455.

53 J. H. Shon, D. Kim, M. D. Rathnayake, S. Sittel, J. Weaver and T. S. Teets, *Chem Sci*, 2021, **12**, 4069–4078.

54 S. Diluzio, V. Mdluli, T. U. Connell, J. Lewis, V. Vanbenschoten and S. Bernhard, *J Am Chem Soc*, 2021, **143**, 1179–1194.

55 M. Chiminelli, A. Serafino, D. Ruggeri, L. Marchiò, F. Bigi, R. Maggi, M. Malacria, G. Maestri, M. Chiminelli, A. Serafino, D. Ruggeri, L. Marchiò, F. Bigi, R. Maggi, G. Maestri and M. Malacria, *Angewandte Chemie International Edition*, 2023, **62**, e202216817.

56 J. Struwe, K. Korvorapun, A. Zangarelli and L. Ackermann, *Chemistry - A European Journal*, 2021, **27**, 16237–16241.

57 A. Singh, K. Teegardin, M. Kelly, K. S. Prasad, S. Krishnan and J. D. Weaver, *J Organomet Chem*, 2015, **776**, 51–59.

58 Z. Lu, T. P. Yoon, [Z Lu and T. P. Yoon, *Angewandte Chemie International Edition*, 2012, **51**, 10329–10332.

59 H. J. Bolink, L. Cappelli, S. Cheylan, E. Coronado, R. D. Costa, N. Lardiés, M. K. Nazeeruddin and E. Ortí, , *J. Mater. Chem*., 2007,**17**, 5032-5041

60 C. D. Sunesh, M. Chandran, G. Mathai and Y. Choe, *Opt Mater (Amst)*, 2013, **35**, 407–413.

61 Z. Li, H. Li, B. J. Gifford, W. D. N. Peiris, S. Kilina and W. Sun, *RSC Adv*, 2016, **6**, 41214–41218.

62 E. Sauvageot, P. Lafite, E. Duverger, R. Marion, M. Hamel, S. Gaillard, J. L. Renaud and R. Daniellou, *J Organomet Chem*, 2016, **808**, 122–127.

63 Y. Xing, C. Liu, J. H. Xiu and J. Y. Li, *Inorg Chem*, 2015, **54**, 7783–7790.

64 M. Hitt and A. N. Vedernikov, *Org Lett*, 2022, **24**, 7737–7741.

65 K. Li, M. L. Li, Q. Zhang, S. F. Zhu and Q. L. Zhou, *J Am Chem Soc*, 2018, **140**, 7458–7461.

66 W. E. Jones and M. A. Fox, *J Phys Chem*, 1994, **98**, 5095–5099.

67 A. Vanitcha, C. Damelincourt, G. Gontard, N. Vanthuyne, V. Mouriès-Mansuy and L. Fensterbank, *Chem Commun,* 2016, **52**, 6785–6788.

68 C. Hahn, L. Cruz, A. Villalobos, L. Garza and S. Adeosun, *Dalton Transactions*, 2014, **43**, 16300–16309.